

Interaction of water with oxide glass structures

Von der Naturwissenschaftlichen Fakultät der

Gottfried Wilhelm Leibniz Universität Hannover

zur Erlangung des Grades

Doktor der Naturwissenschaften (Dr. rer. nat.)

genehmigte Dissertation

von

Robert Balzer, M. Sc.

[2019]

Referent: Prof. Dr. Harald Behrens
Korreferent: Prof. Dr. Joachim Deubener
Tag der Promotion: 05.09.2019

Schlagwörter: Wasserhaltige Gläser, Hochdruck, Spektroskopische Untersuchung, Phosphat-Gläser, Silicoborat Gläser, Aluminosilikat Gläser

Keywords: hydrous glasses, high pressure, spectroscopic analyses, phosphate glasses, silicoborate glasses, aluminosilicate glasses

Danksagung

Es versteht sich von selbst, dass diese Arbeit ohne die Hilfe und Unterstützung vieler Menschen nicht möglich gewesen wäre.

Zunächst möchte ich mich bei Harald Behrens danken, der mir diese Arbeit ermöglicht hat, aber auch für seine Unterstützung und die hilfreichen Diskussionen während der Arbeit und unseren Publikationen. Mein Dank gilt weiterhin auch Joachim Deubener und Stefan Dultz. Auch dem übrigen Projektteam Ralf Müller Stefan Reinsch, Philippe Kiefer und Tina Waurischk gilt mein Dank für die gute Zusammenarbeit im Rahmen des Projektes von der diese Arbeit profitiert. Hierzu gehört auch Philipp Beckmann, der mich durch seine Hilfsbereitschaft, Proben zu messen, enorm entlastet hat.

Danke auch an Stephan Schuth, Ingo Horn sowie Michael Fechtelkord für ihre Unterstützung bei den La-ICP-MS bzw. MAS NMR Analysen, sowie an Claus Rüscher, der immer ein offenes Ohr für meine Fragen hatte. Ein großes Dankeschön möchte ich an dieser Stelle auch dem Werkstatteam Ulli Kroll, Andreas Reimer aussprechen, ohne deren Unterstützung die IHPV wohl nicht so zuverlässig funktioniert hätte. Weiterhin möchte ich mich bei Julian Feige für die zahlreichen Proben bedanken, die er in den letzten Jahren mich präpariert hat.

Danken möchte ich auch Anna-Maria, die mir während meiner Anfangszeit enorm viel beigebracht hat und mich auch jetzt, wo sie am anderen Ende der Welt lebt, immer unterstützt hat.

Ein ganz besonderer Dank gilt den GneisBoys (Marius Stranghöner, Lennart Fischer, Stefan Linsler und Dominik M. Mock). Ohne eure Unterstützung, Tipps, Ratschläge, nicht wissenschaftliche Diskussionen (und manches Gefecht in den Mittagspausen), besonders in den letzten Monaten, wäre es eine harte Zeit geworden. Danken möchte ich auch Florian Kiesel, der immer ein offenes Ohr und aufmunternde Worte gefunden, auch wenn es mal nicht um Gläser ging. Danke Buddy.

Ein riesiges Dankeschön geht an meine Familie sowie Andrea und Jörg Lukas, die mich während meines gesamten Studiums immer unterstützt und motiviert haben. Ganz besonders jedoch, möchte ich mich bei meiner Freundin Jannike bedanken, die immer an mich geglaubt und mir den Rückhalt gegeben hat, der nötig war!

Letztendlich möchte ich der Deutschen Forschungsgemeinschaft (DFG) für die finanzielle Unterstützung dieses Projektes (SPP 1594).

Abstract

The aim of this thesis is to investigate the influence of different network converters on different glass structures. A special focus lies hereby on the incorporation of water regarding its corrosive behavior on the glass network. This in turn improves the understanding of water-related material fatigue and subcritical crack growth in technical glasses. For this purpose, two lithium-magnesium aluminophosphate glasses ($30\text{Li}_2\text{O} \ 20\text{-xMgO} \ \text{xAl}_2\text{O}_3 \ 50\text{P}_2\text{O}_5$ with $x = 0$ and 5), 4 silicoborate glasses ($15\text{-xNa}_2\text{O} \ \text{xCaO} \ 15\text{SiO}_2 \ 70\text{B}_2\text{O}_3$ with $x = 0; 7.5$ and 10 , as well as $10\text{Na}_2\text{O} \ 15\text{SiO}_2$ and $75\text{B}_2\text{O}_3$) and three aluminosilicate glasses ($22.5\text{-xNa}_2\text{O} \ \text{xK}_2\text{O} \ 22.5 \ \text{Al}_2\text{O}_3 \ 55\text{SiO}_2$ with $x = 0; 7.5; 11.25$) were prepared. Water bearing glasses between 0-8 wt% H_2O were synthesized at 500 MPa using an Internally Heated Pressure Vessel (IHPV) at temperatures between 1473 – 1873 K. With respect to the structure and water speciation in the glasses, anhydrous and hydrous glasses have been analyzed using MAS-NMR (Magic Angle Spinning Nuclear Magnetic Resonance) and infrared-spectroscopy (IR). The glass transition temperature (T_g) was determined by Differential Thermal Analysis (DTA). IR spectroscopy on phosphate glasses reveal that OH groups are the dominating water species. A similar trend was observed in silicoborates. The incorporation of water results in a dominance of hydroxyl groups, here too. A dominance of OH groups was also observed in aluminum-containing phosphates. However, the proportion of molecular water is higher compared to aluminum-free phosphates. In aluminosilicates, on the other hand, the incorporated water is present in molecular form at water contents above 3 % wt%. The decrease in T_g upon hydration is similarly continuous for phosphates and silica borates, while a dramatic decrease has been observed for aluminosilicates. This indicates that the incorporation of OH groups has a significantly weaker effect on structural relaxation in phosphate and borate systems than in silicate dominated glasses. The depolymerization of the glass network during hydration varies depending on the glass system. The incorporation of water has a very strong depolymerizing effect on the phosphate structure, as more and more Q^1 and even Q^0 species are formed at the expense of Q^3 and Q^2 species as the water content increases. ^{11}B MAS NMR in silicoborates reveals that the BO_4 species depends mainly on the alkali and alkaline earth content and that water plays only a minor role in the formation of the BO_4 species. However, the efficiency for the formation of BO_4 units in silicoborates is higher than in pure borate glasses. ^{27}Al MAS NMR spectra of aluminosilicates reveal that aluminum is exclusively present in the form of AlO_4 tetrahedra in both dry and hydrous glasses. The incorporation of water causes the relaxation of highly distorted Q^4 species by forming slightly depolymerized Q^3 species.

Zusammenfassung

Ziel dieser Arbeit ist es den Einfluss verschiedener Netzwerkänderer auf unterschiedliche Glasstrukturen zu untersuchen. Ein besonderer Fokus liegt dabei auf dem Einbau von Wasser hinsichtlich seines korrosiven Verhaltens auf das Glasnetzwerk. Dies wiederum verbessert das Verständnis von wasserbedingter Materialermüdung und dem subkritischen Risswachstum in technischen Gläsern. Hierfür wurden zwei Lithium-Magnesium-Aluminophosphate ($30\text{Li}_2\text{O} \cdot 20-x\text{MgO} \cdot x\text{Al}_2\text{O}_3 \cdot 50\text{P}_2\text{O}_5$ mit $x = 0$ und 5), vier Silicoborat Gläser ($15-x\text{Na}_2\text{O} \cdot x\text{CaO} \cdot 15\text{SiO}_2 \cdot 70\text{B}_2\text{O}_3$ mit $x = 0; 7,5$ und 10 , sowie $10\text{Na}_2\text{O} \cdot 15\text{SiO}_2$ und $75\text{B}_2\text{O}_3$) und drei Aluminosilikat Gläser ($22,5-x\text{Na}_2\text{O} \cdot x\text{K}_2\text{O} \cdot 22,5 \text{Al}_2\text{O}_3 \cdot 55\text{SiO}_2$ mit $x = 0; 7,5; 11,25$) hergestellt. Die wasserhaltigen Gläser zwischen 0-8 Gew.% H_2O wurden bei 500 MPa in einer intern beheizten Gasdruckanlage (IHPV) bei Temperaturen zwischen 1473 – 1873 K hergestellt. Die Struktur der trockenen und wasserhaltigen Gläser wurde hinsichtlich der Netzwerkstruktur und Wasserspeziation mittels MAS-NMR- (Magic Angle Spinning Nuclear Magnetic Resonance) und Infrarot-Spektroskopie (IR) untersucht. Die Glasübergangstemperatur (T_g) wurde mittels Differentieller Thermischer Analyse (DTA) bestimmt. Die IR-Spektroskopie an Phosphaten zeigt, dass OH Gruppen die dominierende Wasserspezies sind. Ein ähnlicher Trend wurde in Silicoboraten beobachtet. Auch dort resultiert der Einbau von Wasser in einer Dominanz von Hydroxylgruppen. In aluminiumhaltigen Phosphaten wurde ebenfalls eine Dominanz von OH Gruppen beobachtet. Allerdings ist der Anteil von molekularem Wasser im Vergleich zu den aluminiumfreien Phosphaten größer. In Aluminiumsilikaten hingegen, liegt das eingebaute Wasser ab Wassergehalten von ca. 3 Gew.% in molekularer Form vor. Die im Zuge des Wassereinbaus abnehmende T_g läuft für Phosphate und Silicoborate ähnlich kontinuierlich ab, während ein dramatischer Abfall für Aluminosilikaten beobachtet wurde. Das deutet darauf hin, dass der Einbau von OH Gruppen einen deutlich schwächeren Effekt auf die strukturelle Relaxation in Phosphat- und Borat Systemen, hat als in Silikat dominierten Gläsern. Die Depolymerisierung des Glasnetzwerks, im Zuge der Hydratisierung, ist abhängig vom Glassystem unterschiedlich stark ausgeprägt. So wirkt sich der Einbau von Wasser auf die Phosphatstruktur sehr stark depolymerisierend aus, indem mit steigendem Wassergehalt mehr und mehr Q^1 und sogar Q^0 Spezies auf Kosten von Q^3 und Q^2 Spezies gebildet werden. ^{11}B MAS NMR in Silicoboraten zeigt, dass die BO_4 Spezies hauptsächlich vom Alkali und Erdalkali Gehalt abhängt und Wasser nur eine untergeordnete Rolle für die Bildung der BO_4 Spezies spielt. Allerdings ist die Effizienz zur Bildung von BO_4 Einheiten in Silicoboraten größer als in reinen Boraten. ^{27}Al MAS NMR Spektren von Aluminosilikaten zeigen, dass Aluminium sowohl in trockenen als

auch in hydratisierten Gläsern ausschließlich in Form von AlO_4 Tetraedern vorliegt. Der Einbau von Wasser bewirkt die Entspannung von stark verzerrten Q^4 Spezies indem leicht depolymerisierte Q^3 Spezies gebildet werden.

Inhaltsverzeichnis

Schlagwörter:.....	III
Keywords:	III
Danksagung.....	IV
Abstract	V
Zusammenfassung.....	VI
General Introduction.....	1
Short structural overview of the investigated glass structures	4
Phosphate glasses	4
Borate glasses.....	4
Aluminosilicate glasses	5
Structural investigation of hydrous phosphate glasses.....	7
1.1 Introduction	8
1.2 Experimental and analytical methods.....	9
1.2.1 Starting materials.....	9
1.2.2 Hydrous and compacted glasses.....	10
1.2.3 Karl-Fischer titration	10
1.2.4 Differential thermal analysis	12
1.2.5 IR spectroscopy	12
1.2.6 ^{27}Al and ^{31}P MAS NMR spectroscopy	13
1.3 Results	13
1.3.1 Water distribution in the glass.....	13
1.3.2 Density.....	14
1.3.3 MIR spectroscopy.....	15
1.3.4 NIR spectroscopy	18
1.3.5 NMR spectroscopy	22
1.4 Discussion	24
1.4.1 Structural overview of phosphate glass network.....	24
1.4.2 Depolymerization by H_2O	27
1.5 Conclusionss.....	30
The influence of H_2O and SiO_2 on the structure of silicoborate glasses	32
2.1. Introduction	33
2.2 Experimental and Analytical Methods	35
2.2.1 Starting Materials	35
2.2.2 Hydrous and compressed glasses	36
2.2.3 Karl-Fischer Titration.....	37
2.2.4 Differential thermal analyses.....	40
2.2.5 IR Spectroscopy	40

2.2.6 ^{11}B MAS-NMR Experiments.....	41
2.3. Results	41
2.3.1 Water distribution in the glasses.....	41
2.3.2 Density.....	42
2.3.3 MIR Spectroscopy	43
2.3.4 NIR Spectroscopy.....	48
2.3.5 NMR Spectroscopy	53
2.4. Discussion	55
4.1 Water species in silicoborate glasses.....	55
2.4.2 Influence of water on boron speciation	58
2.4.3 Compositional effects on the glass transition temperature	59
2.5. Conclusion.....	61
Chapter 3	62
Water in alkali aluminosilicate glasses.....	62
3.1. Introduction	63
3.2. Experimental and Analytical Methods	65
3.2.1 Starting Materials	65
3.2.2 Hydrous and compressed glasses	66
3.2.3 Karl Fischer Titration	67
3.2.4 Differential thermal analysis	70
3.2.5 IR spectroscopy	70
3.2.6 ^{27}Al MAS-NMR spectroscopy.....	71
3.3. Results	71
3.3.1 Water distribution in the glasses.....	71
3.3.2 Density.....	72
3.3.3 MIR spectroscopy.....	73
3.3.4 NIR spectroscopy	79
3.3.5 ^{27}Al NMR Spectroscopy	84
3.3.6 Tg/DTA	86
3.4. Discussion	88
3.4.1 Structure of aluminosilicate glasses	88
3.4.2 Water speciation in aluminosilicate glasses	92
3.4.3 Effect of water on the glass fictive temperature	95
3.5. Conclusion.....	96
General conclusions	97
References	99
Appendix	110
Curriculum Vitae.....	110

List of Publications.....	111
Conference Abstracts	111

General Introduction

Glasses are ubiquitous in nature and in our daily lives [1]. For thousands of years glasses have been part of our daily lives and during this time have found a wide range of applications ranging from window glass, windscreens, container glass and light bulbs to liquid crystal displays and fiber optic cables in telecommunication networks [2].

In applications like this, glasses are subject to far-field tensile stress, and failure usually occurs by the extension of a crack from the surface [2]. The crack grows slowly until a critical size is reached. At this point, unstable crack growth causes brittle fractures [2]. Of particular importance here is the strength of the glasses which has significant influences on its durability. The strength of a glass can be distinguished by the theoretical and the practical strength [3-5]. The theoretical (or intrinsic) strength is defined as the strength of the chemical bonds and the energy required to break these bonds. Pavelchek et al. [6] determined the intrinsic strength of a SiO₂ network, based on molecular bonding, to be in the order of 14 GPa. The practical strength of a glass is, however, affected by material failures (e.g. surface damages) which increases the strain in the glass body [3]. Lower et al. [7] experimentally determined the practical strength of a silica glass to be in the order of only 10 GPa. Hence, the practical strength is several orders of magnitudes lower compared to the theoretical strength [3].

The differences between intrinsic and practical strength represents an important challenge to the glass industry, since brittle fracture of glasses is often preceded by delayed fatigue, resulting in a time dependence of strength and known as subcritical crack growth (SCCG) [2, 8-10]. Delayed fatigue can occur without warning weeks or even months after the first application of load [11-13]. It is known, that delayed fatigue is a combined effect of stress and water from the atmosphere (environment), which causes surface cracks in the glass to grow slowly [2, 9]. The first systematic studies on SCCG were carried out by Wiederhorn et al. [9] in which he measured the crack extension as a function of the applied force at different humidity conditions [2]. In his famous diagram the crack velocity is plotted against the stress intensity factor K_I (which depends on the geometry, the crack length and the force of the applied stress) [9] (Fig. 1). He showed that three regions (I, II, III) exist in which the SCCG in glasses is influenced by different complex process. In region I, an exponential crack growth with the applied force is observed, whereby the crack velocities increase with increasing humidity [9]. This indicates that region I is controlled by a stress-enhanced chemical reaction between water vapor and the Si-O bonds at the crack tip [2, 9]. In region II, the crack velocity is completely independent from the applied force, but increases with increasing water vapor content. This

behavior implies that the crack velocity is controlled by water diffusion to the crack tip [14, 15]. Thus, both region I and II are assigned to stress corrosion by the environment influences. In region III a stronger dependency of the crack velocity on the applied load is observed compared to region I and II. This implies that with increasing crack velocity the surrounding reactive medium (e.g. water) cannot follow the rapidly advancing crack tip. Thus, the motion is independent from environmental conditions, but strongly related to inert conditions (e.g. glass composition) [3].

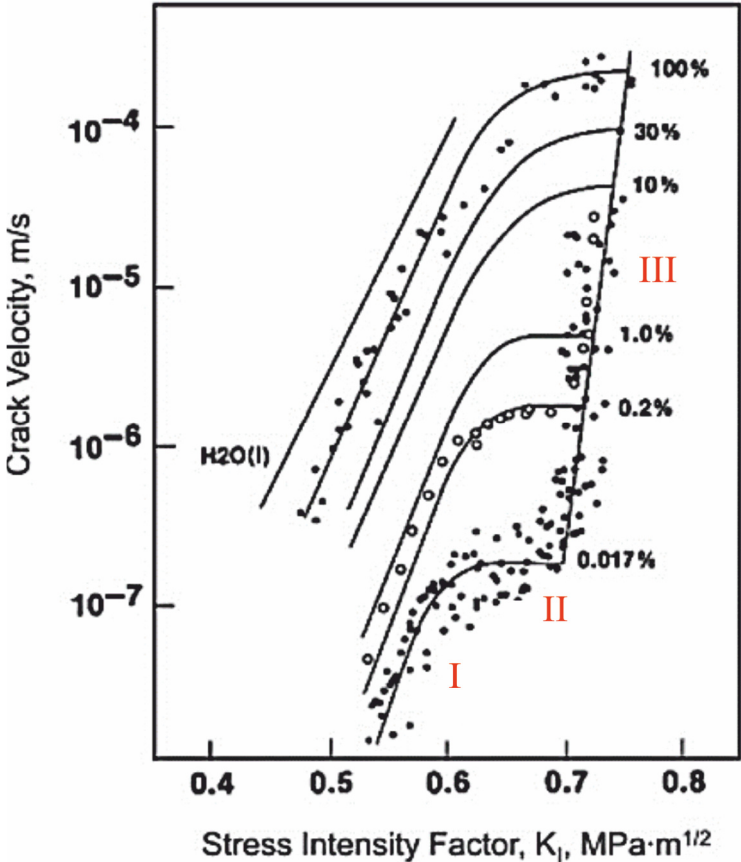


Figure 1: Dependence of crack velocity on applied force. The percent relative humidity is given on the right-hand side of the diagram. Roman numerals identify the different regions of crack propagation Based on Wiederhorn et al. [9], but with slight modifications (red roman numerals) for better visibility of these regions.

Based on the studies of Wiederhorn, there have been many further investigations to improve the understanding of basic mechanisms and effects of glass topology on SCCG [16-19]. However, it is difficult to draw a general conclusion on SCCG, as there are indications that stress corrosion is not only influenced by the simple reaction of SiO₂ and H₂O, where Si-O-Si bonds are ruptured, as described by Michalske et al. [3, 20-22]. Rather, it seems to be a

matter of mutually influencing effects. For instance, the crack tip geometry as well as the structure near the crack tip can be influenced by the interplay e.g. of hydration, hydrolysis, condensation, ion exchange, stress enhanced water diffusion, glass dissolution and alkali diffusion [23-26].

Furthermore, region III indicates that SCCG is also affected by entry of water into the glass structure, accelerated by tensile stress at the crack tip [25, 27, 28]. This results in local changes of mechanical relaxation and elastic moduli [27, 29]. For instance, diffusion coefficients under tensile stress, which prevail at a crack, are significantly higher than under compressive stress, so that hydration occurs around the crack and the crack tip. Thus, the incorporated water leads to a direct reduction of the local strength (weaker bonding strength) and the crack can grow more easily [21, 27]. In this context, changes in glass chemistry or environmental conditions are of particular importance as they can reduce or intensify the subcritical crack growth.

Since these local phenomena are difficult to measure in situ, studies on hydrous oxide glasses were used to mimic this relaxation mechanism [27]. Hence, for a comprehensive understanding of the mechanical properties with special attention to the SCCG on oxide glasses, detailed investigations of structural properties of water-containing glasses is essential.

This study aims to investigate the structural properties of different glass network structures (phosphate glasses, silicoborate glasses and aluminosilicate glasses) in dependence on different network-modifier types and contents. The bond strengths of these different glasses between the network forming tetrahedra (P-O-P, B-O-B, B-O-Si, Al-O-Si and Si-O-Si) are supposed to behave different, especially towards SGGC. Incorporation of different network modifying cations is also of great importance, since they can either enhance the strength of the glass and thus, the resistance to the SCCG, or they can reduce the strength and favor the SCCG. Special attention is thereby paid to the effect of water on the glass structure and the formation of different water species which are known to effect the glass network differently.

For this purpose, this study is divided into three parts in which each deals with a different glass network. Results of this study may help to improve the understanding of the SCCG, particularly in region III.

Short structural overview of the investigated glass structures

Phosphate glasses

Most of our present understanding of the phosphate glass structure comes from the study by Van Wazer [30] but was significantly improved in more modern times with the development of NMR spectroscopy. The basic structural building unit in phosphate glass is a PO_4^{3+} tetrahedron comprising four oxygens oriented around a centrally-positioned P^{5+} atom. Three of the P-O bonds within the tetrahedron are hybridized while the remaining P-charge is balanced through double-bonding with a single oxygen. This oxygen represents a terminal oxygen and it does not actively participate in bridging between the tetrahedral units within the glass network. Within the PO_4^{3+} tetrahedron the bond between P and the terminal oxygen is shorter than those with the remaining oxygens as evidenced by neutron diffraction studies of phosphate glasses [31, 32].

The glass network is to a large degree randomly built via non-terminal oxygens shared between individual phosphate tetrahedra [33, 34]. A single tetrahedron can have all three non-terminal oxygens shared with adjacent PO_4^{3+} tetrahedra, thus forming Q^3 species [33] as found in vitreous P_2O_5 . Q^2 and Q^1 species are defined by two and three underbonded non-terminal oxygens, respectively, while Q^0 has all four tetrahedral oxygens partially bonded with P [33, 35]. The predominance of a specific Q -species depends on the O/P ratio whereby 2.5 for vitreous P_2O_5 is the lowest value for stable phosphate glass compositions. Our investigated glasses have O/P ratios between 3.06 and 3.17 which puts them on the boundary between the meta- and poly-phosphate compositions [33].

Borate glasses

According to Warren and Bisco [36, 37], pure B_2O_3 glasses consist of a random network of three-dimensional linked BO_3 units. Based on XRD analysis, Richter et al [37, 38] concluded later that a single BO_3 unit is not in a planar structure configuration, and the boron ion is moved somewhat out of the plane and in this way a planar BO_3 tetrahedron is formed. With this being said, a much higher structural order is assumed in the BO_3 glass network. In a SiO_2 glass a continuous change in properties can be observed with increasing alkali contents. Incorporation of alkalis into a B_2O_3 glass, on the other hand, leads to an anomalous change in the glass properties, e.g. the expansion coefficient of the glass does not increase, but decreases instead which is in contrast to general expectations. Only at higher alkali contents (> 16 mol%) the

trend changes and proceeds as it is known from alkali silicate glasses. This behavior is also known as boron-anomaly.

Based on XRD measurements, Warren and Bischoff [36] proposed that addition of network modifiers up to about 16 mol% does not result in a rupture of the BO_3 network and, thus, formation non-bridging oxygens. Instead, a change from BO_3 units to BO_4 tetrahedra takes place. The incorporation of alkaline components in the glass structure results in the transformation of two BO_3 groups each into a BO_4 tetrahedron, which then three-dimensionally cross-link the glass network [4]. An increase of the alkaline content above 16 mol%, however, leads to the formation of BO_3 units and non-bridging oxygens and a break-up of the network structure. Unlike the incorporation of boron in silicon-rich glasses, the incorporation of SiO_2 in boron-dominated glasses is poorly investigated. However, considering that SiO_2 serves as network former, a reinforcing effect of SiO_2 on the boron dominated structure is expected.

Aluminosilicate glasses

The structure of aluminosilicate melts and glasses is sensitive to compositional changes [39]. In general, the main components forming the aluminosilicate glass structure are silicon and aluminum. Si^{4+} serves as a network former and is almost exclusively tetrahedrally coordinated forming SiO_4 units [4, 40]. Evidence for a higher Si coordination was only observed in pure Si-O glasses at extremely high pressures (> 15 GPa) [41].

Al is predominantly found in 4-fold coordination as AlO_4 tetrahedra that serve as network formers. However, 5- and 6-fold coordinated Al is also present forming AlO_5 and AlO_6 units, respectively, that serve as network modifiers. Al coordination in glass network depends on the ratio of Al^{3+} relative to alkali metals (e.g. Na^+ , K^+) or alkali earth (e.g. Mg^{2+} , Ca^{2+}) as this controls how Al^{3+} in tetrahedral coordination is charge-balanced [39].

For instance, in peralkaline melts ($\text{Na}/\text{Al} > 1$), Na^+ compensates the negative charge of the Al unit. The excess Na cations that do not charge compensate Al units form non-bridging oxygens and thus depolymerizes the structure. Merzbacher et al. [42] observed the preference of Al for fully polymerized AlO_4 tetrahedra (also expressed as Q^4 units) in peralkaline aluminosilicate glasses [42-44]. A higher $\text{Al}/(\text{Al}+\text{Si})$ ratio favors the formation of Q^4 sites but minor abundance of depolymerized units (e.g. Q^3 and Q^2) was also observed [39].

The opposite of peralkaline melts are so called peraluminous melts where Al^{3+} exceeds the charge compensating capacity of alkalis and alkaline earths ($\text{Na}/\text{Al} < 1$) [39, 45]. The excess of Al that is not charge compensated goes in higher coordination forming AlO_5 and AlO_6 units

[44, 46, 47]. A further possibility how Al^{3+} in peraluminous melts can be incorporated into the network is the formation of so-called triclusters first suggested by Lacy et al. [48]. He assumed that triclusters in the $\text{Na}_2\text{O}-\text{Al}_2\text{O}_3-\text{SiO}_2$ system can consist either of one silicate and two aluminum tetrahedra or the other way round [48, 49]. The idea of triclusters is still controversially discussed, since it would imply that the Al-O-Al avoidance (Loewenstein' rule) is not strictly maintained in glasses, since AlO_4 tetrahedra are linked via one oxygen atom [42]. In recent years, many studies on various aluminosilicate compositions e.g. NAS, KAS, CAS and MAS [42, 45-47, 50] have confirmed the assumption that tricluster occur in peraluminous melts. Toplis et al. [45] observed that tricluster can also occur in peralkaline melts, but their minor abundance does not significantly influence the physical properties of the melts.

Chapter 1

Structural investigation of hydrous phosphate glasses

Robert Balzer^{a,b}, Harald Behrens^{a,b*}, Stefan Reinsch^c, Michael Fechtelkord^d

^a Leibniz Universität Hannover, Institute of Mineralogy, Callinstr. 3, 30167 Hannover, Germany

^b ZFM – Center for Solid State Chemistry and New Materials, Leibniz Universität Hannover, Germany

^c Federal Institute for Materials Research and Testing (BAM), 12489 Berlin, Germany

^d Ruhr Universität Bochum, Institute of Geology, Mineralogy und Geophysics, 44780 Bochum, Germany

This chapter was published in Phys. Chem. Glasses: Eur. J. Glass Sci Technol. B, April 2019, 60(2), 49-61. DOI:10.13036/17533562.60.2.041

Abstract

Dissolved water has major impact on physical and chemical properties of phosphate glasses. In the present study we have investigated the structural response to water incorporation for glasses in the system $\text{Li}_2\text{O-MgO-Al}_2\text{O}_3\text{-P}_2\text{O}_5$. Glasses containing 0 – 8 wt% H_2O were synthesized at 500 MPa confining pressure in internally heated gas pressure vessels at 1323 K (LMP, Al-poor glass) and 1423 K (LMAP, Al-enriched glass). Water contents of glasses were determined by pyrolysis and subsequent Karl-Fischer titration (KFT) and/or by infrared spectroscopy. Density varies non-linearly with water content implying large structural changes when adding up to 2 wt% H_2O to the dry glass. Glass transition temperatures measured by differential thermal analysis (DTA) continuously decrease with water content. The trend can be explained by depolymerization of the phosphate network. Near-infrared spectroscopy shows that even in Al-poor glasses only a minority of dissolved water is present as H_2O molecules, but the largest amount is present as OH groups formed by hydrolysis of P-O-P bonds. The network is stabilized by aluminum which is predominantly 6-coordinated in these glasses as shown by ^{27}Al MAS NMR spectroscopy. With increase of Al in the glasses, breaking up of the phosphate network through hydrolysis is depressed, i.e. much lower OH contents are formed at same total water content. Network depolymerization upon addition of H_2O is evident also from ^{31}P MAS NMR spectroscopy. While phosphate tetrahedra are cross-linked by two to three bridging oxygen in dry glasses, diphosphate groups are dominant in glasses containing 8 wt% H_2O .

1.1 Introduction

Phosphate-based glasses have been of scientific interest since several decades due to the broad spectrum of possible applications. Due to high refractive indices, low dispersion and high transparency for ultraviolet light, phosphate glasses are indispensable as optical components [33]. Some phosphate glass compositions exhibit large rare-earth stimulated emission cross sections and low thermo-optical coefficients, making them very useful for high power laser applications [51, 52]. Chemical durability and low processing temperature makes iron-containing phosphate glasses into promising materials for nuclear waste encapsulation [53]. Due to high expansion coefficients and low processing temperatures, phosphate glasses are useful as hermetic seals [54]. High cation mobility makes alkali aluminophosphate glasses suitable for thermally-triggered fast ion conductors and for glass-ceramic cation exchange [55]. However, the largest field of application of phosphate glasses in recent years is in bioactive and biomedical implementation [56, 57].

A key feature of phosphate glasses is often an easy reaction with water, an advantage for bioapplications [58] but a disadvantage for use e.g. in optical devices [59]. The affinity of phosphate to water is also the reason that traces of dissolved water are practically unavoidable in phosphate glasses. As known from literature, water can dramatically affect mechanical and physical properties of oxide glasses such as viscosity, hardness, crack growth and crack propagation. But little is known about how structurally bonded water affects these properties in phosphate glasses.

In the present study we have systematically investigated the structural role of water in phosphate glasses in the system $\text{Li}_2\text{O-MgO-Al}_2\text{O}_3\text{-P}_2\text{O}_5$. Variation of water contents over a wide range of 0 - 8 wt% can be achieved by high pressure - high temperature synthesis. This allows analyzing water-induced changes in network topology as well as in coordination of cations. Here, aluminum is of particular interest because it can act as network former as well as network modifier in oxide glasses. Additionally, comparison of the high pressure glasses with those produced at ambient pressure give insights to compaction mechanisms in the glasses. Nuclear magnetic resonance (NMR) spectroscopy and Fourier transform infrared (FTIR) spectroscopy were applied to analyze the structural response to water incorporation and compaction of the glass. Density measurement and determination of the glass transition temperature (T_g) via differential thermal analyses (DTA) provide further information on interaction between the phosphate network and hydrous species in the glass. The findings of

these studies have implications for understanding corrosion mechanisms of glasses as well as crack propagation mechanisms.

1.2 Experimental and analytical methods

1.2.1 Starting materials

For the purpose of this study, two lithium magnesium phosphate glass compositions were produced, one comprised 30 mol% Li₂O, 20 mol% MgO and 50 mol% P₂O₅ (LMP) and the other 30 mol% Li₂O, 15 mol% MgO, 5 mol% Al₂O₃ and 50 mol% P₂O₅ (LMAP). Considering the nominal O/P ratio of 3.0 and 3.1, respectively, the composition of the glasses can be classified as close to metaphosphate.

For each glass composition, high purity Li₂CO₃, MgO, Al₂O₃ and NH₄H₂PO₄ powders were carefully mixed and then loaded in corundum crucibles (Degussitt AL23) held at 673 K in a chamber furnace. Stepwise loading of the powder was required due to excessive degassing by decomposition of ammonium dihydrogen phosphate. After that, degassing temperature was increased to 1373 K in the case of LMP and to 1523 K in the case of LMAP. After heating for 1 h melts were quenched by pouring on a brass plate. Glasses were crushed and re-melted under the same conditions to improve chemical homogeneity. Clear and bubble-free glasses without any signs of crystallization were obtained by this procedure.

Bulk composition was analyzed using inductively coupled plasma optical emission spectrometry, ICP-OES (715-ES Varian/Agilent). 30-50 mg of glass was dissolved in 10 % HCl for each analysis. Samples were taken from three different regions of the glass body to check material homogeneity (Tab. 1.1). Analyses revealed that both glasses are homogenous and compositions are close to the nominal values except for aluminum. Contamination by 2.5 mol% Al₂O₃ from the corundum crucible has to be acknowledged.

Table 1.1: Nominal and measured composition of starting materials in mol% normalized to 100.

	Li ₂ O	MgO	Al ₂ O ₃	P ₂ O ₅	O/P	
LMP	30	20	0	50	3.00	nominal
	28.88 ± 0.17	19.32 ± 0.11	2.53 ± 0.08	49.26 ± 0.11	3.06	OES
LMAP	30	15	5	50	3.10	nominal
	29.33 ± 0.21	14.44 ± 0.07	7.48 ± 0.19	48.74 ± 0.1	3.17	OES

Notes. Errors represent one standard deviation.

1.2.2 Hydrated and compacted glasses

Hydrated glasses with water contents up to 8 wt% were prepared in noble metal capsules. For the LMP series Au was chosen as the capsule material, while Au₉₀-Pt₁₀ was used for the LMAP series due to higher experimental temperature required for these glasses. In order to achieve a homogeneous initial water distribution, glass powder and distilled water were alternately added to the capsule. The powder-water mixture was compacted with a steel piston between loading steps to minimize air bubble inclusions. After loading, capsules were sealed by arc-welding. Weld seams of capsules were tested for leakage by heating in a drying oven at 373 K for at least one hour.

Syntheses were performed in an internally heated pressure vessel (IHPV) at 500 MPa and 1323 K for LMP and 1423 K for LMAP for 15 h, using Argon as pressure medium. In each run, two capsules were placed in the hot zone of a normal quench sample holder (controlled by a K-type thermocouple), pressurized and heated up to the desired p-T conditions. Detailed description of apparatus and procedures are given by Berndt et al. [60].

Samples were isobarically quenched to preserve pressure-induced structural changes and to avoid water loss from the hydrated glasses. The produced glasses had cylindrical shape with a length of 30 mm and a diameter of 6 mm. All glass cylinders were transparent and contained neither bubbles nor crystals. For further measurements, ~5 mm thick slices were cut out from both ends of the cylinders, to check for homogeneity of water distribution within the glass samples. Due to a lack of material, no additional chemical analyses were performed on hydrated glasses. However, because the capsule represents a closed system, no significant change in bulk composition is expected.

1.2.3 Karl-Fischer titration

The total water content of hydrated glasses was determined by pyrolysis and subsequent Karl-Fischer titration (KFT). For this purpose, ca. 15 mg of each glass were filled into small platinum containers and were heated up rapidly to 1573 K within 4 minutes. To prevent explosive release of H₂O during heating, the upper end of the Pt container has been folded down. A detailed description of the KFT is given in Behrens et al. [61]. Results are shown in Tab. 1.2. Note that 0.1 wt% H₂O is added to the measured water content to account for unextracted water during analyses [62].

Table 1.2: Sample characterization and spectroscopic data of NIR measurements.

	CH ₂ O, KFT [wt%]	T_f [K]	T_g [K]	ρ [g/l]	d [mm]	Peak position [cm ⁻¹]		A ₅₂₀₀ [mm ⁻¹]	A ₄₅₀₀ [mm ⁻¹]
LMP _{start}	n.a.	677	676	2486 ± 2					
LMP _{dry}	0.059*	683	677	2544 ± 2		/			
LMP1-I	1.24 ± 0.05	626	625	2539 ± 2	0.265	/	4445	0	0.018
LMP1-II	0.97 ± 0.04				0.270	/	4445	0	0.022
LMP2-I	2.63 ± 0.04	588	587	2530 ± 3	0.275	/	4445	0	0.015
LMP2-II	2.74 ± 0.04				0.275	/	4445	0	0.034
LMP4-I	3.55 ± 0.05	539	539	2506 ± 2	0.267		4441	0.003	0.066
LMP4-II	4.14 ± 0.05				0.264	/	4441	0	0.045
LMP6-I	5.85 ± 0.05	503	499	2474 ± 3	0.260	5208	4443	0.005	0.043
LMP6-II	5.64 ± 0.05				0.257	5208	4443	0.006	0.051
LMP8-I	7.94 ± 0.07	459	459	2432 ± 2	0.250	5208	4448	0.011	0.063
LMP8-II	8.08 ± 0.07				0.253	5208	4448	0.011	0.061
LMAP _{start}	n.a.	694	695	2500 ± 2					
LMAP _{dry}	0.047*	695	685	2578 ± 3		/			
LMAP1-I	0.90 ± 0.05	638	638	2579 ± 2	0.296	/	4461	0	0.019
LMAP1-II	0.89 ± 0.05				0.298	/	4461	0	0.019
LMAP2-I	1.77 ± 0.05	606	603	2584 ± 2	0.298	/	4458	0	0.038
LMAP2-II	2.36 ± 0.06				0.301	/	4458	0	0.044
LMAP4-I	3.61 ± 0.07	559	558	2564 ± 2	0.299	/	4445	0	0.036
LMAP4-II	4.50 ± 0.04				0.304	5206	4445	0.002	0.041
LMAP6-I	4.89 ± 0.06	514	513	2523 ± 2	0.295	5206	4448	0.006	0.054
LMAP6-II	5.86 ± 0.06				0.294	5206	4448	0.011	0.052
LMAP8-I	7.70 ± 0.07	470	467	2479 ± 2	0.307	5196	4458	0.023	0.081
LMAP8-II	8.10 ± 0.08				0.300	5196	4458	0.028	0.074

Notes. I and II in the sample name refer to pieces cut from both ends of the synthesized glass body. Subscript “start” indicate the glass melted at ambient pressure, subscript “dry” refers to the glass after high pressure synthesis. The number in the sample name indicates the nominal water content. Water contents were measured by KFT, except for data marked by * based on MIR spectroscopy using the calibration presented in this paper. Fictive temperatures T_f of glasses were determined by the first upscan of DTA and glass transition temperatures T_g are averages from three following upscans of DTA. Uncertainties are ± 2 K. Peak positions (± 5 cm⁻¹) and absorbances (± 0.002) of NIR combination bands were determined after linear baseline corrections, see text for details.

1.2.4 Differential thermal analysis

The glass transition temperature, T_g , was determined by differential thermal analysis in air using 15 – 20 mg of glass pieces or powdered glass placed in Pt-crucibles (thermobalance TAG 24, Setaram, Caluire, France). The same measurement routine and data evaluation was applied to hydrous borate glasses, and T_g values were found to be in perfect agreement with isokom temperatures (T_{12}) at which viscosity equals 10^{12} Pa·s [63]. For each sample four heating and cooling cycles with 10 K min^{-1} were applied. The maximum temperature did not exceed T_g by more than 50 K. The first cycle represents the fictive temperature T_f of the glasses, since the cooling history of the samples reflects the status of quenching after IHPV synthesis. The following three cycles were used for the determination of T_g . Definition of T_f and T_g is based on the onset of the endothermic step in the DTA curve according to Mazurin [64, 65]. The average T_g values for all investigated glasses are included in Tab. 1.2. Both, LMP and LMAP show a continuous decrease of T_g with increasing water content, similar to borate glasses but less pronounced as found for silicate and aluminosilicate glasses [66-68].

1.2.5 IR spectroscopy

IR spectra were measured on both-side polished sections using a FTIR spectrometer Bruker IFS 88. The spectrometer is coupled with an IR microscope Bruker IR scope II, equipped with a mercury-cadmium-tellurium (MCT) detector. Absorption spectra in the mid-infrared (MIR) were recorded to investigate fundamental OH stretching vibrations. In these measurements a KBr beam splitter and a globar light source were used. Spectra were recorded from 600 to 6000 cm^{-1} with a spectral resolution of 2 cm^{-1} . For each sample and background (air) measurement 50 scans were accumulated.

In addition, MIR spectra of KBr pressed pellets (2 mg glass powder + 198 mg KBr) of LMP were collected in the range of $370 - 4000 \text{ cm}^{-1}$ using a FTIR spectrometer (Bruker Vertex 80v) with a globar light source, a KBr beam splitter and a pyroelectric deuterated L-alanine doped triglycerine sulfate (DLaTGS) detector. A pure KBr pellet was used as reference. The spectral resolution was 2 cm^{-1} and 32 scans for each spectrum were accumulated.

Near-infrared (NIR) spectra were recorded to study water speciation in the glasses using the same set-up as for MIR measurements on polished sections, but with a tungsten light source and a CaF₂ beam splitter. The spectral resolution was 4 cm⁻¹. For each spectrum 100 scans were accumulated. On each sample at least three spectra were recorded to check reproducibility and water distribution in the glass. The thickness of the samples was determined by a digital micrometer (Mitutoyo Absolute) with a precision of ± 2 μm.

1.2.6 ²⁷Al and ³¹P MAS NMR spectroscopy

MAS-NMR spectra were recorded on a Bruker ASX 400WB spectrometer at room temperature. Measurements were collected at 104.27 MHz (²⁷Al) and 161.97 MHz (³¹P) respectively, using a standard Bruker 4 mm probe with rotor speed of 12.5 kHz. Na₂HPO₄ (diso. = 1.4 ppm) for ³¹P and AlCl₃ (1M) for ²⁷Al were processed as reference standards. For the ²⁷Al MAS-NMR spectra a single pulse duration of 0.6 μsec was applied to ensure homogenous excitation. For ³¹P a pulse duration of 4 μsec was chosen. The recycle delay was 0.1 sec (²⁷Al) and 480 sec (³¹P), respectively. 16000 scans were accumulated for ²⁷Al spectra and 24 scans for ³¹P.

1.3 Results

1.3.1 Water distribution in the glass

In most cases determination of water contents by KFT from both ends of the synthesized glass body are in good agreement (Tab. 1.2). Some water-rich samples (LMP4, LMAP4, LMAP6) show noticeable disagreement, significantly larger than the analytical error. But the average water content matches closely the loaded water in the capsules. This implies that water was initially concentrated on one end of the capsule, and synthesis conditions were insufficient to homogenize water in the melt. In following we refer to the average of KFT data for analytical bulk methods (density, NMR), being aware that the water content has relative large error. For local methods (IR) we used KFT measurements on pieces taken just next to the analysis points.

The water content of dry pressurized glasses was measured by MIR spectroscopy using the calibration described below. Both glasses are homogeneous with 0.059 wt% H₂O (LMP) and 0.047 wt% H₂O (LMAP). The relatively low water content confirms that both compositions show low

reactivity against atmospheric water, i.e. little water was adsorbed on the glass powder before loading in the capsule.

1.3.2 Density

Densities were determined by the buoyancy method, measuring the samples weight in air and in ethanol. Results are shown in Fig. 1.1a. Pressurization at 500 MPa increased the density of dry glasses by 2.3 % (LMP) and 3.1 % (LMAP), respectively. The compactability is higher than for silicates and aluminosilicates (ca. 1 %) [69, 70] but lower than for soda lime borates (up to 4.1 wt%) [63].

The effect of water on glass density is non-linear. Addition of 2-3 wt% H₂O has only weak effect, while higher water contents result in a pronounced density decrease. These trends indicate large structural changes in the glasses, i.e. denser packing, when some water is added to the dry phosphate glasses. The roughly linear behavior at high water content is consistent with ideal mixing of oxide glass and water, as also found for silicate glasses [71]. Fig. 1.1b show the molar volumes of phosphate glasses. According to [71, 72] we directly obtained the partial molar volume of water as the intercept of tangents fitted to data at low and high water contents, respectively, with the axis at mol fractions of H₂O of 1. Compared to silica glasses the partial molar volumes of H₂O in our phosphate glasses is not constant over the studied range of water content. Partial molar volumes of H₂O in phosphate glasses with molar fraction > 0.11 (LMP: $12.3 \pm 0.3 \text{ cm}^3/\text{mol}$; LMAP: $13.0 \pm 0.5 \text{ cm}^3/\text{mol}$) are in a good agreement with those of silicate glasses ($\sim 11.5 - 12.5 \text{ cm}^3/\text{mol}$) [71]. However, partial molar volumes of H₂O at low water contents is much lower in phosphate glasses (LMP: $8.6 \pm 0.2 \text{ cm}^3/\text{mol}$; LMAP: $6.2 \pm 0.2 \text{ cm}^3/\text{mol}$). These results indicate large structural changes upon hydration in particular for water-poor glasses.

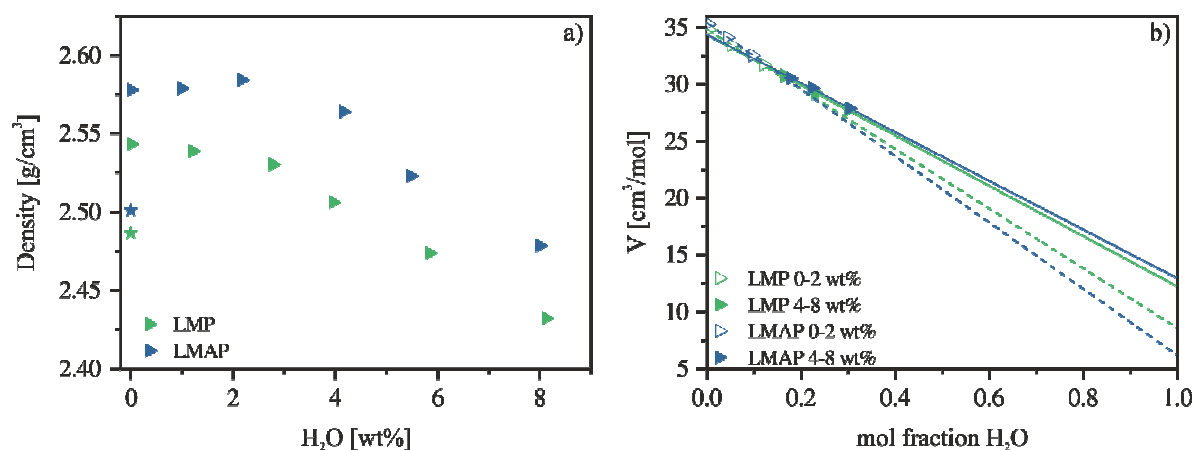


Figure 1.1: Density of LMP and LMAP glasses. Error bars are smaller than symbols (a). Molar volume of hydrous glasses (b).

1.3.3 MIR spectroscopy

MIR spectra of LMP glasses in the frequency of 400 and 4000 cm⁻¹ are shown in Fig. 1.2. Network vibration bands are visible in the region between 900 and 1500 cm⁻¹. Band assignment follows [73-75]. The IR band recorded at ~ 490 cm⁻¹ is attributed to the bending vibration of P-O-P modes of PO₂⁻ - chains. The band at 730 cm⁻¹ can be assigned to symmetric stretching vibrations of P-O-P rings. The peak at ~904 cm⁻¹ represents the asymmetric stretching vibration of P-O-P linked groups with linear metaphosphate chains, and the band at 1140 cm⁻¹ is due to asymmetric modes of PO₃²⁻ of nonbridging oxygens. The band at 1265 cm⁻¹ is due to asymmetric modes of PO₂⁻ nonbridging oxygens [76]. Although some minor changes in band position and

intensity about hydration can be noticed, the effect of water on network vibrations is in general weak.

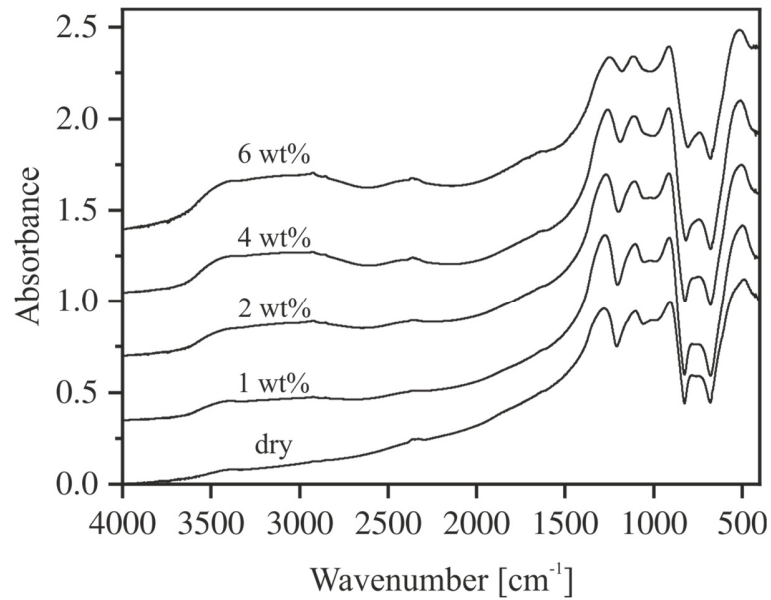


Figure 1.2: MIR spectra of KBR pressed pellets of LMP. Spectra were normalized to the asymmetric stretching vibration band P-O-P (~ 904 cm⁻¹) and shifted vertically for clarity. Nominal water contents are indicated.

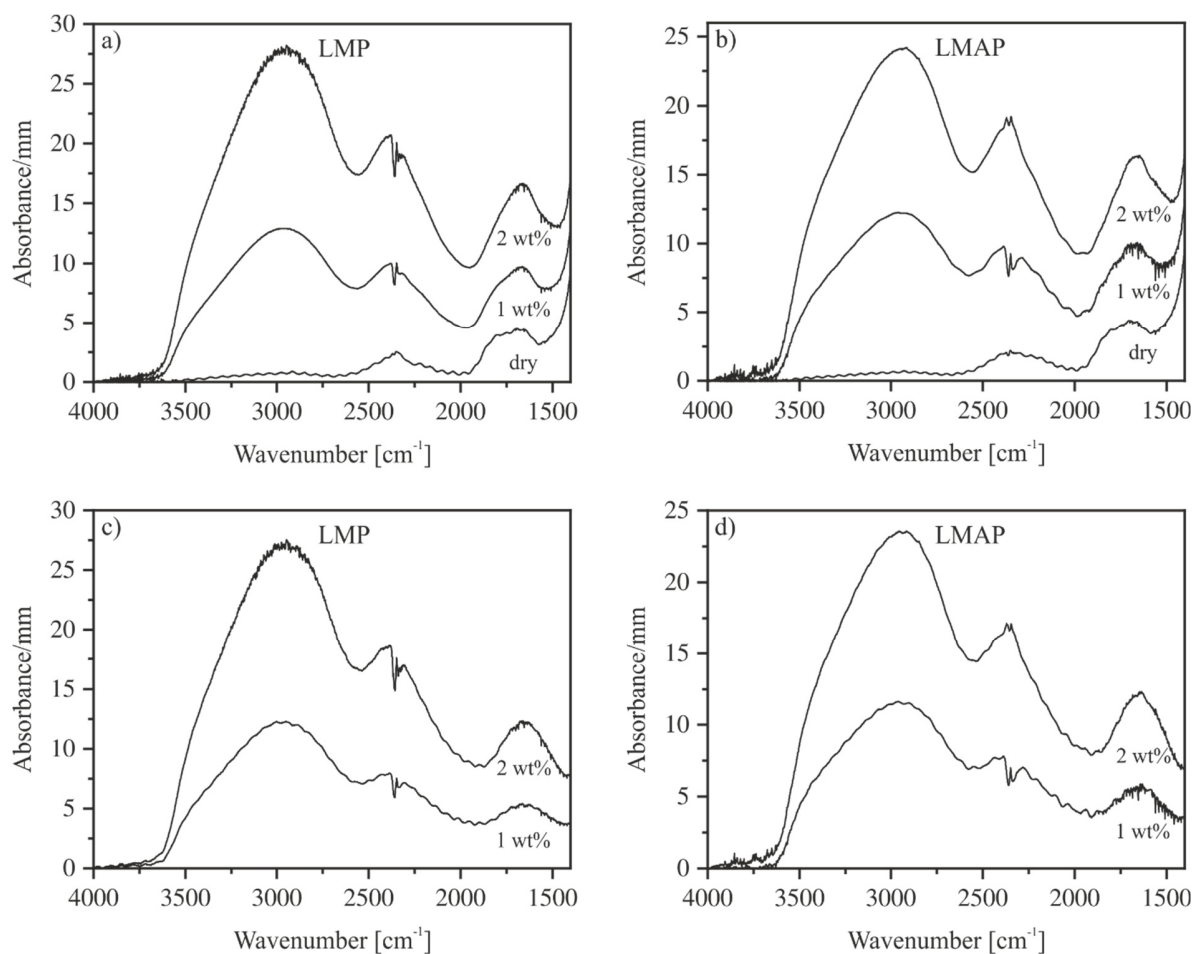


Figure 1.3: Measured MIR spectra of thin sections of LMP (a) and LMAP (b) containing 0-2 wt% H₂O. Irregularities at 2350 cm⁻¹ are due to differences in CO₂ during background and sample measurements. Subtraction spectra (hydrated-dry glass) demonstrate for both LMP (c) and LMAP glasses (d) that the three main bands are caused by OH stretching vibrations. Spectra were normalized to sample thickness.

The high frequency region between 1600 and 3600 cm⁻¹ is characterized by broad OH vibration bands. When using KBr pressed pellets, contributions of H₂O in potassium bromide and water adsorbed on glass powder cannot be completely separated from water dissolved in the glasses. Therefore, MIR spectra of thin sections were recorded to get more detailed information on structural incorporation of water in the glasses (Fig. 1.3). In order to separate water-related peaks from network vibrations, spectra of nominally dry glasses were subtracted from those of hydrous glasses (Fig. 1.3c, d). The main absorption band has its maximum near 2950 cm⁻¹ and only a weak shoulder near 3500 cm⁻¹, indicating that most hydrous species are involved in strong hydrogen bonding [77-79]. The intensity of the bands at 2340 cm⁻¹ and 1660 cm⁻¹ is correlated to the band at 2950 cm⁻¹, implying that these bands are caused by the same hydrous species. Thus, the three bands

do not represent different species but only different vibrations of similar species. This interpretation is consistent with findings of Zarubin for silicate glasses [80].

In order to quantify water contents of nominally dry glasses, practical absorption coefficients were determined for the band at 2950 cm^{-1} . In doing so, the absorbance at the maximum was related to the total water content measured by KFT. This procedure is justified since the intensity ratio of the water-related bands is roughly constant. Then the total water content $c_{\text{H}_2\text{O}_t}$ is given as

$$c_{\text{H}_2\text{O}_t} = \frac{1802 \cdot A_{2950}}{\rho \cdot d \cdot \varepsilon_{2950}} \quad (1.1)$$

where A_i refers to the absorbance of band i , ρ to the density [g/cm^3], and d to the sample thickness [cm]. The derived values of the linear molar absorption coefficient ε_{2950} for glasses containing ca. 1 wt% H_2O are $91.1 \pm 5.1 \text{ L} \cdot \text{mol}^{-1} \cdot \text{cm}^{-1}$ for LMP and $97.1 \pm 6.7 \text{ L} \cdot \text{mol}^{-1} \cdot \text{cm}^{-1}$ for LMAP. It is noteworthy that the calculated absorption coefficients from this study are in good agreement with those reported for other phosphate glasses [81].

1.3.4 NIR spectroscopy

The NIR spectra of LMP and LMAP containing up to 8 wt% H_2O are shown in Fig. 1.4. In accordance with literature on water-bearing glasses two main absorbance bands are observed in the range of 6000 - 3500 cm^{-1} [77, 82-84]. Analogue to silicate glasses the band at 5200 cm^{-1} is assigned to the combination of stretching and bending modes of H_2O molecules [83-86]. Absorption bands near 4450 cm^{-1} are assigned to the combination of stretching and bending of structurally bonded OH groups [63, 84, 86]. In both glass series molecular water is first measurable at total water contents above 4 wt% H_2O . In general, peak intensities of both bands increase with total water content. No distinct peak shift related to the water content occurs in both glasses (Tab. 1.2).

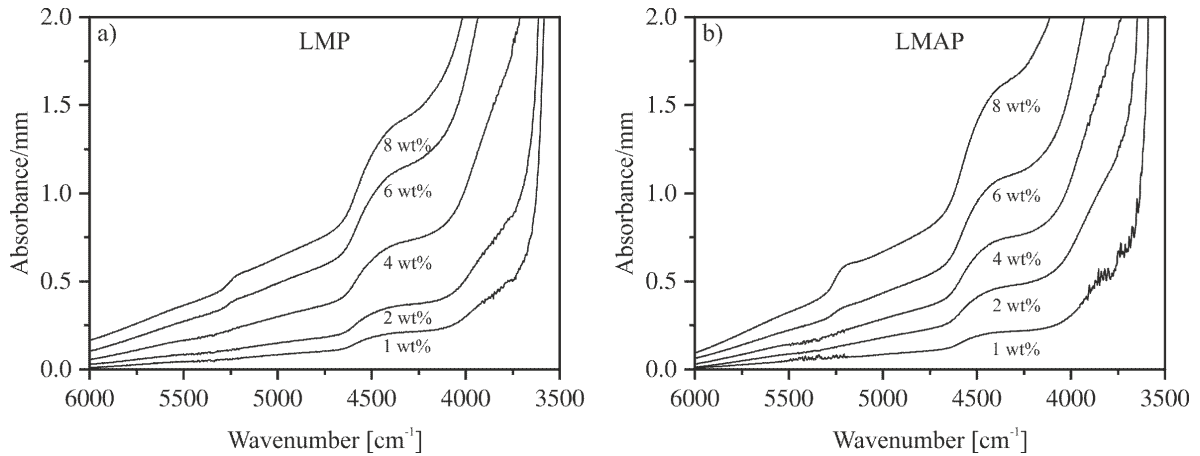


Figure 1.4: NIR spectra of LMP (a) and LMAP (b) containing 1-8 wt% H_2O . Spectra are vertically shifted for clarity. Nominal water contents are indicated.

A problem in the quantification of the NIR bands is their overlap with the tail of the fundamental OH stretching vibration bands centred in the MIR. Different types of baseline corrections have been tested for aluminosilicate glasses to separate the combination bands. The highest reproducibility was found for tangential baselines [87]. We followed that approach, and spectra were corrected as illustrated in Fig. 1.5. The resulting spectra are displayed in Fig. 1.6.

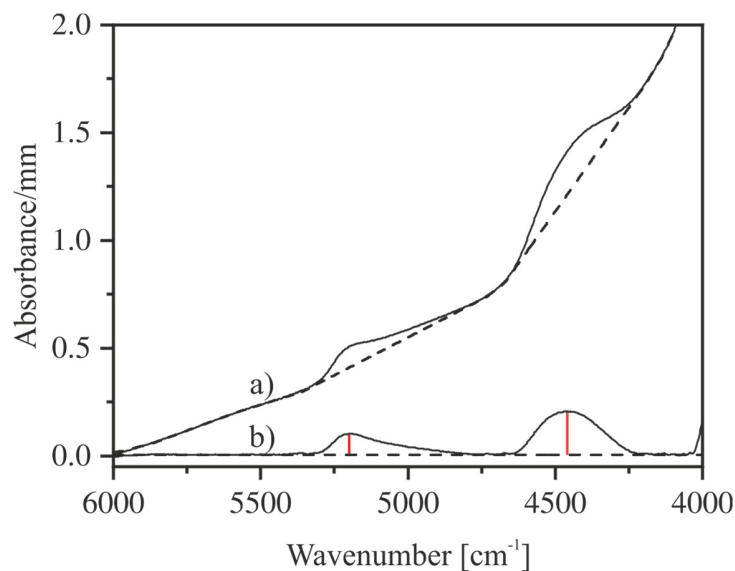


Figure 1.5: Measured NIR spectrum of LMAP8-I (a) and the corrected spectrum after subtraction of linear baselines (b). Resulting absorbances are illustrated by vertical lines.

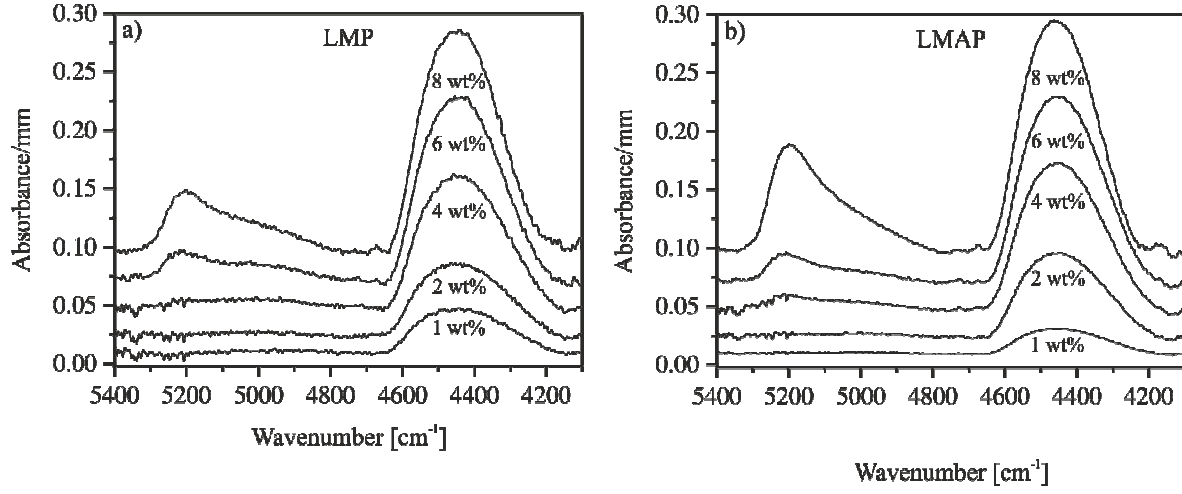


Figure 1.6: Baseline corrected NIR spectra of LMP (a) and LMAP (b) glasses. Spectra are vertically shifted for clarity. Nominal water contents are indicated.

Assuming that the total water content is represented by the combination bands and that the absorption coefficients are independent on water content, a simple calibration can be performed to determine the absorption coefficients for both bands [87]:

$$c_{H_2O_t} = c_{OH} + c_{H_2O} \quad (1.2)$$

$$c_{OH} = \frac{1802 \cdot A_{4450}}{\rho \cdot d \cdot \epsilon_{4450}} \quad (1.3)$$

$$c_{H_2O} = \frac{1802 \cdot A_{5200}}{\rho \cdot d \cdot \epsilon_{5200}} \quad (1.4)$$

where c_{OH} denotes the content of water dissolved as OH groups and c_{H_2O} the content of molecular H_2O . The linear molar absorption coefficients ϵ can be derived by combining Eqs. 1.2-1.4:

$$\frac{1802 \cdot A_{5200}}{d \cdot \rho \cdot c_{H_2O_t}} = \epsilon_{5200} - \frac{\epsilon_{5200}}{\epsilon_{4450}} \cdot \frac{1802 \cdot A_{4450}}{d \cdot \rho \cdot c_{H_2O_t}} \quad (1.5)$$

Following this approach, the linear molar absorption coefficient of the NIR absorption bands can be determined by a regression analysis as the intercepts with the axis (Fig. 1.7). This method was successfully applied to various silicate and borate glasses, examples are shown in Fig. 1.7b. In the case of the phosphate glasses, absorbances of the NIR bands are very low and have high uncertainty. Thus, an unambiguous determination of ϵ values by regression of data in Fig. 1.7a was not possible.

Since molecular water is only measurable above 4 wt% total H₂O, we can estimate the absorption coefficients in two steps. First, ϵ_{4450} is determined for glasses with up to 4 wt% H₂O by fitting the data to Eq. 1.1. When plotting $A_{4450}/(d \cdot \rho)$ vs. the total water content, the slope represents ϵ_{4450} (Fig. 1.8). The derived values of ϵ_{4450} are $0.29 \pm 0.04 \text{ L} \cdot \text{mol}^{-1} \cdot \text{cm}^{-1}$ for LMP and $0.42 \pm 0.03 \text{ L} \cdot \text{mol}^{-1} \cdot \text{cm}^{-1}$ for LMAP. Next, the data in Fig. 1.7a were fitted to Eq. (1.5) using the ϵ_{4450} values determined in the first step as a constraint. Thus, we obtained values of ϵ_{5200} of $0.14 \pm 0.05 \text{ L} \cdot \text{mol}^{-1} \cdot \text{cm}^{-1}$ for LMP and $0.15 \pm 0.06 \text{ L} \cdot \text{mol}^{-1} \cdot \text{cm}^{-1}$ for LMAP.

Low absorption coefficients of the NIR bands are consistent with the statement of Zarubin that the NIR bands represent only hydrous species with weak hydrogen bonding [80]. Nevertheless, a quantification of total OH groups and molecular H₂O is possible, since the shape of IR bands and, hence, the relative abundance of subspecies does not depend on water content.

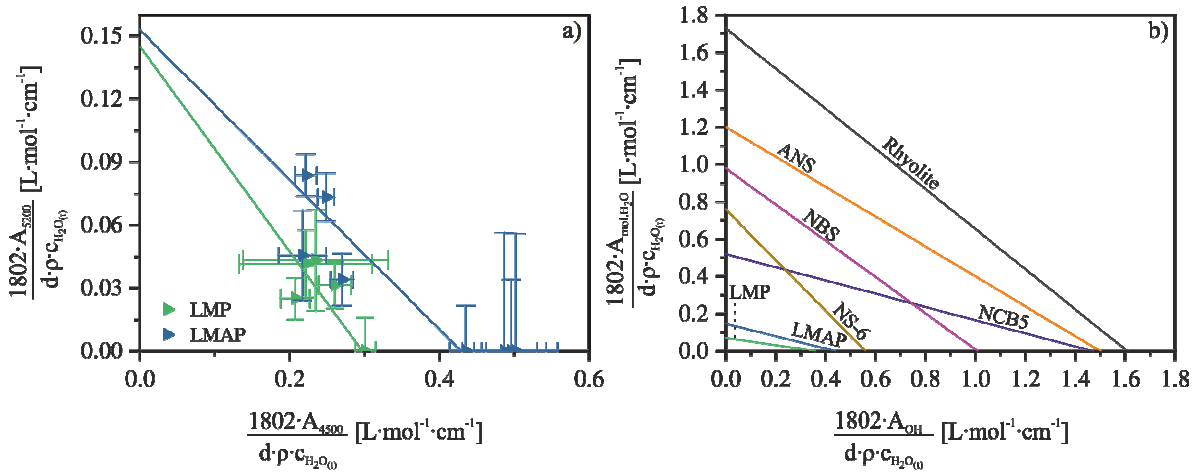


Figure 1.7: Calibration plot for the determination of the linear molar absorption coefficient of the NIR absorption bands 5200 and 4500 cm^{-1} (a). Comparison of LMP and LMAP glasses with selected other compositions (b). Data sources: rhyolite [88], ANS (anorthite-silica) [88], NBS (sodium borosilicate) [89], NCB5 (soda-lime-borate) [63], NS-6 (sodium hexasilicate) [90]. The absorption coefficients ϵ for each composition are given by the intercepts with the axis.

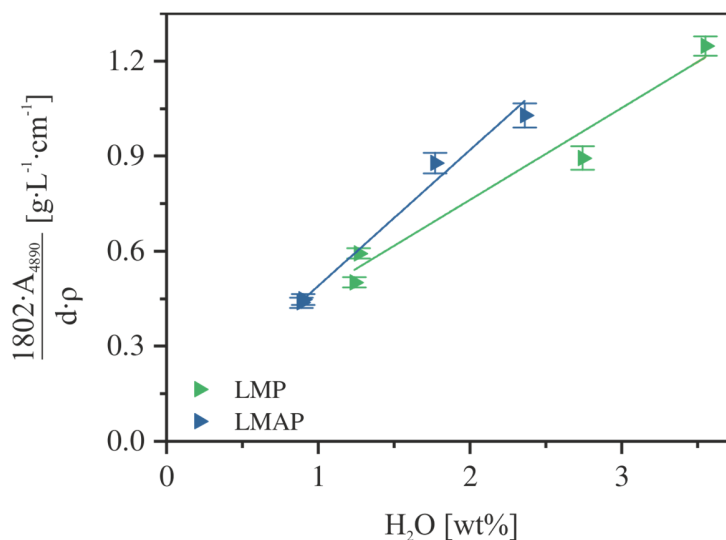


Figure 1.8: Absorbance of the 4500 cm^{-1} band normalized to density (ρ) and sample thickness (d) as a function of H_2O content determined by KFT. Regression lines for low water contents were used to estimate the absorption coefficient ε_{4500} , see text for details.

1.3.5 NMR spectroscopy

^{31}P MAS-NMR spectra of LMP and LMAP (Fig. 1.9) exhibit similar features. The main resonance in spectra of nominally dry LMP glasses is located at -29 ppm with a small shoulder at ~ -16 ppm, independent on the compaction state of the glasses (Fig. 1.9a). With increasing water content the shoulder evolves to the main resonance in glasses containing 6 and 8 wt% H_2O , whereas the peak at -29 ppm disappears (see Fig. 1.13 for more details of the main resonance evolution). The spinning sidebands of the main resonance are located at 124, 46, -107 and -184 ppm. The spectra for LMAP (Fig. 1.9b) show the same behaviour. The difference in shape between the LMP and LMAP can be explained by different Al_2O_3 content in the glasses.

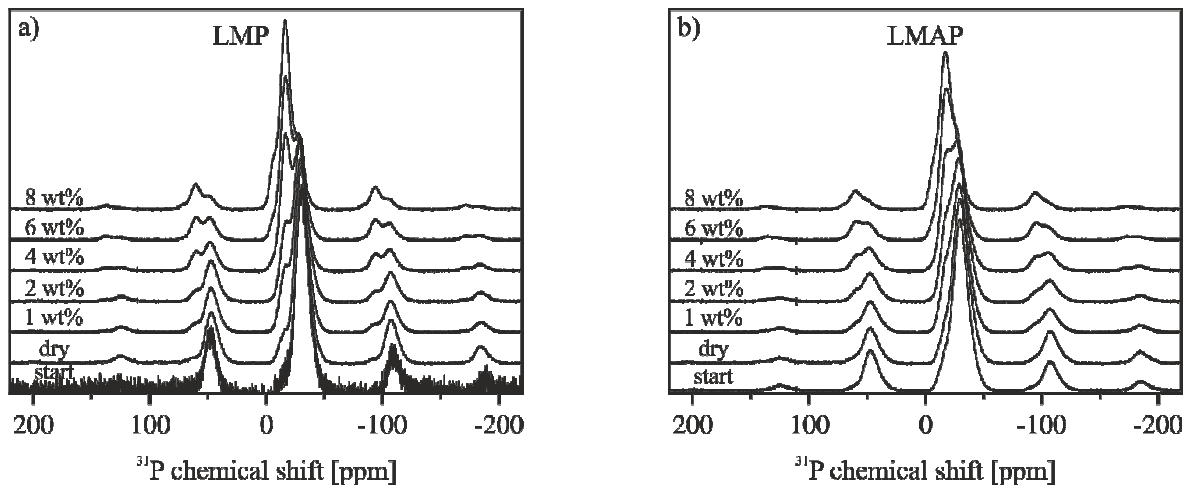


Figure 1.9: ^{31}P MAS-NMR spectra of LMP (a) and LMAP (b). For comparison spectra are scaled to same area of the central signal. Spectra are vertically shifted for clarity. Nominal water contents are indicated. Large scatter of the spectrum $\text{LMP}_{\text{start}}$ is due to low intensity of the measured spectrum.

^{27}Al MAS-NMR spectra were recorded on the Al-rich glass composition LMAP (Fig. 1.10). Dry glasses exhibit a dominating resonance at -16 ppm which is caused by octahedrally coordinated aluminium, (Al^{VI}) [91]. With increasing water content, this resonance is slightly shifted to -15 ppm. Additional resonances at 6 ppm and 36 ppm correspond to 5-coordinated aluminium (Al^{V}) and 4-coordinated aluminium (Al^{IV}), respectively [91]. Both resonances are strongly reduced after addition of 1 wt% H_2O .

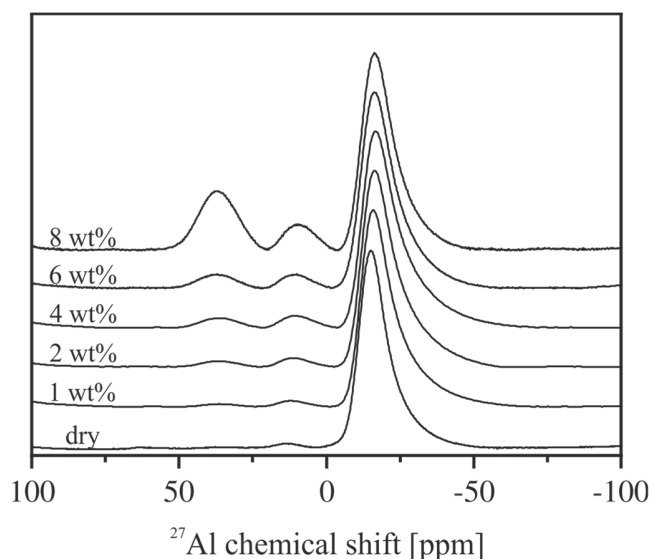


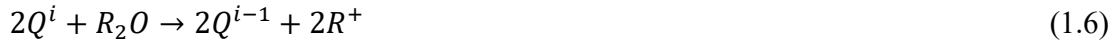
Figure 1.10: ^{27}Al MAS-NMR for LMAP. Spectra are shifted and normalized to the Al(VI) peak at ~ -16 ppm for clarity. Nominal water contents are indicated.

1.4 Discussion

1.4.1 Structural overview of phosphate glass network

Most of our basic understanding of phosphate glass structure comes from the study of Van Wazer [30] but was significantly improved in modern times with the development of NMR techniques. Basic structural unit in phosphate glass is a PO_4^{3-} tetrahedron. Three of the P-O bonds within the tetrahedron are hybridized while the remaining charge on the phosphate is balanced by double-bonding to one oxygen atom in metaphosphate glasses. This terminal oxygen is not actively engaged in bridging tetrahedral units within the glass network. The special character of the terminal oxygen is supported by neutron diffraction studies showing that bond lengths to terminal oxygens are shorter than those to the other oxygens [31, 32].

The network topology of phosphate glasses is determined by the connection of tetrahedra through bridging oxygens [33, 34]. Different Q^i species are characterized by the number of bridging oxygens i . The maximum of i is 3 (Q^3 species) as found in vitreous P_2O_5 . Addition of alkali oxides, R_2O , causes breaking the polymerization of the network, introducing non-bridging oxygens and changing the distribution of the Q -species by the reaction:



The average chain length, as suggested by Van Wazer, depends on the alkali content, i.e. the higher the alkali content the shorter the chains [30]. The dry phosphate glasses considered in this study are close to meta-phosphate compositions, and the structure is composed mainly by phosphate chains. Chain lengths can reach several hundred to thousand phosphate units [92]. However, the spatial arrangement of phosphate units strongly depends on the type of the modifying cation in the structure. Neutron diffraction studies by Hoppe and co-workers have indicated a decrease in the mean P-O bond length with the increasing modifier cation field strength [48].

The combination of three cations (Li, Mg, Al) in our glass compositions is expected to result in a complex network topology with phosphate chains as main feature. In following we review the structural role of the different cations based on findings reported in literature.

The main cation in our glasses is lithium, a high ionic field strength ion. Theoretical modelling by Uchino and Yoko [93] has indicated that Li cations are coordinated by negative potentials of both bridged and non-bridged oxygens. Based on results of early X-ray photoelectron spectroscopic studies, a partial transfer of charge from the double-bonded terminal oxygen to a non-bridged oxygen is suggested to balance the difference between the terminal negative potentials. NMR studies by Alam and co-workers [55, 94-96] have indicated that at low alkali concentrations, Li ions are randomly distributed within the phosphate glass network. Furthermore, it was found that the glass composition with 20 mol% of Li₂O represents the glass with the highest degree of depolymerisation of the network, and with the largest abundance of the 3-membered phosphate rings adjacent to Li-cations [94]. With further addition of alkali, the increase in Li-O bonds stabilizes larger rings which connect the chain-like phosphate domains. At Li₂O contents of 20 - 25 mol%, Li-cations are in average coordinated by four or five oxygens. This is considered as a critical threshold for a number of structural and physical properties, including such as density and T_g .

Mg²⁺ is also a high ionic field strength cation. It has a tendency towards coordination higher than 4, involving partly non-bridging and partly terminal oxygens [33]. Mg-phosphates exhibit an anomalous discontinuity of composition-property dependence in the metaphosphate field mainly triggered by the tendency of Mg towards coordination number of 6 [33].

Presence of Al in the phosphate network modifies the structural design in its own way, predominantly strengthening the network. As a consequence, chemical durability and glass transition temperature are increased, and the thermal expansion coefficient and residual OH content in glasses are reduced [97, 98]. ^{27}Al NMR studies indicate that Al can be present in different coordinations (4, 5 and 6), depending on glass composition. Higher coordination is preferred in metaphosphates [99] and lower coordination in glasses with $\text{O/P} > 3$ [97].

The NMR spectrum of the dry LMAP glass is consistent with this trend, i.e. Al(VI) is strongly dominating. However, the effect of water on aluminium speciation is different to that of alkali oxides. As shown in Fig. 1.11, addition of water even increases the fraction of octahedrally coordinated aluminium. Addition of 8 wt% H_2O to dry LMAP corresponds to an increase of the O/P ratio from 3.17 to 3.63. The findings demonstrate clearly that aluminium plays the role of a network modifier in these phosphate glasses.

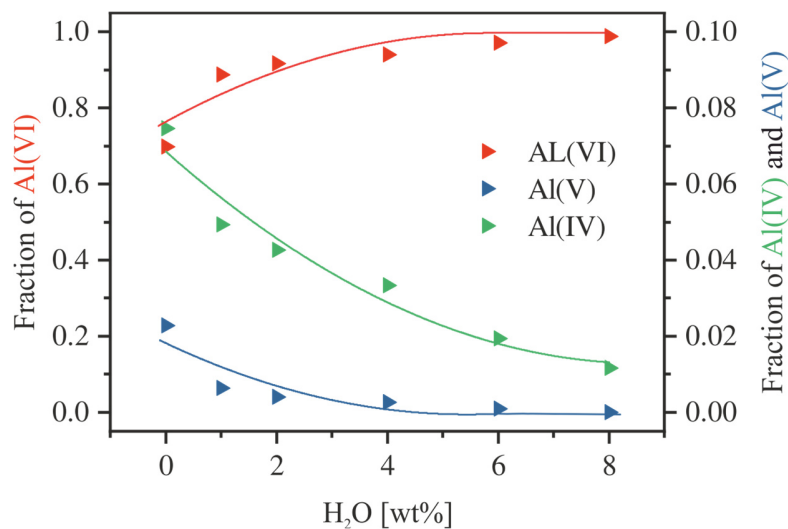


Figure 1.11: Fraction of Al species in LMAP glasses with increasing water content. Fractions of the species were determined by integrating the corresponding peak in Fig. 1.10 and subsequent division by the total area. Minima between the peaks were used as boundaries for integration.

1.4.2 Depolymerization by H₂O

As already known from the literature, the incorporation of water in a glass weakens the structure through depolymerization of the glass network [4]. Our data confirm these trends. Clear indication for structural changes is given by the density-water content relationships. The density of both glass series remains constant between 0 and 2 wt% H₂O (Fig. 1.1) but strongly decreases at higher water contents. This can be explained by depolymerization of the network with first addition of water and denser packing of structural units. Densification is limited up to about 3 wt% H₂O, then incorporation of the light component H₂O dominates the density trend.

Water speciation data show a continuous increase of OH contents even up to 8 wt% H₂O (Fig. 1.12). Thus, depolymerization proceeds also at high water content. The evolution of water speciation in the LMP glasses resembles the trend observed for soda lime borate glasses [63] in that the relative abundance of H₂O molecules remains low even at the highest water contents. These trends confirm that both P-O-P and B-O-B bridges are easily broken by reaction with water. Hydrolysis of the network is suppressed by incorporation of aluminium in the structure. At 8 wt% total water 50 % of dissolved water is present in molecular form in LMAP glasses but only 30 % in LMP glasses. These differences cannot be explained by different fictive temperatures of the glasses because T_f is very similar (LMP8: 459 K; LMAP: 470 K).

Accounting for the water that enters the glass structure as -OH groups, the approximate molar composition of the LMP8 glass is 23H₂O-22Li₂O-15MgO-2Al₂O₃-38P₂O₅ and the approximate molar composition of the LMAP8 glass is 17H₂O-25Li₂O-12MgO-6Al₂O₃-40P₂O₅.; the latter glass contains about twice as much molecular water as the former. The O/P ratios of both glasses are about 3.4, meaning that in both compositions, there remain P-O-P bonds in the structure that resist hydrolysis. This ratio is close to the pyrophosphate stoichiometry (O/P=3.5) and so consistent with the ³¹P observation of significant fractions of Q¹ species in the glasses containing 8 wt% water (see below).

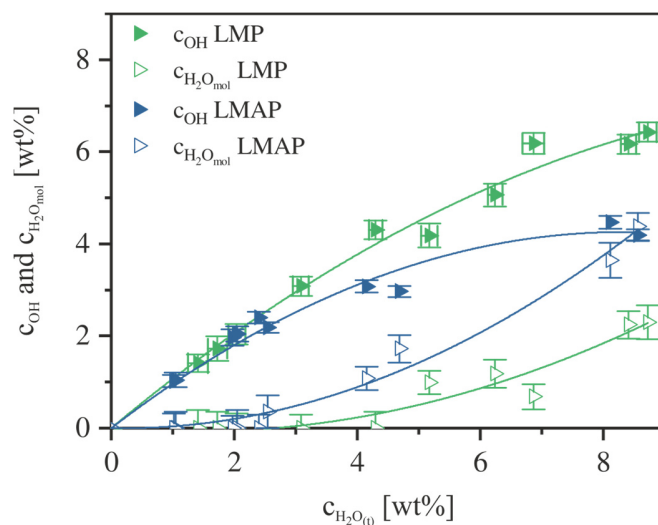


Figure 1.12: Water species concentration in LMP and LMAP glasses in function of total water content.

A more detailed view on the changes in network topology upon hydration can be obtained by quantitative evaluation of the ^{31}P MAS NMR spectra. To determine the relative abundance of Q species the central resonance and the spinning sidebands have to be considered. Fitting of the spectra follows [33]. Examples of deconvolution of the central resonance are shown in Fig. 1.13. Sidebands are fitted simultaneously using the DmFit 2010 program, and areas of each Q species are added together. Finally, these accumulated areas are normalized by the total area.

The ^{31}P spectra clearly show that water depolymerizes the phosphate network, consistent with previous studies. For instance, Brow et al. [100] show that water depolymerizes phosphate structures in a manner similar to Na_2O , at least up to the metaphosphate structure. Under the assumption that all H_2O depolymerizes the phosphate network, they suggest that the Q species distribution in their phosphate glasses can be quantitatively explained by the $[\text{Na}+\text{H}]/\text{P}$ ratio. Our glasses show a similar trend, at least up to the limit where the concentration of molecular water becomes significant. Fits of spectra shown in Fig. 1.13 indicate that the cross-linked aluminophosphate network is replaced by one with smaller phosphate anions as water is incorporated into the glass network. However, one should be aware that the glass structure is much more complex than assumed in the simple fit model.

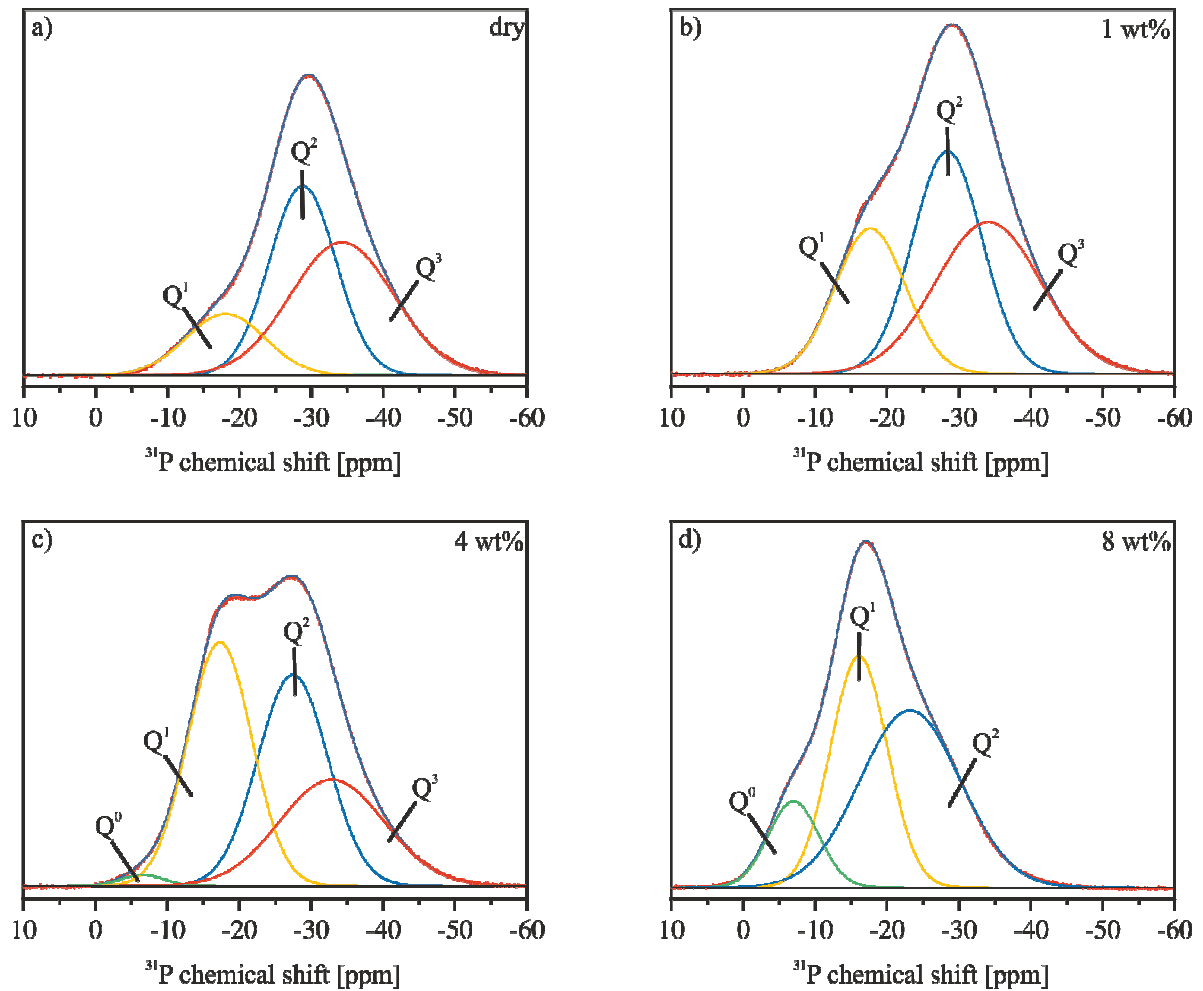


Figure 1.13: Fit of the main resonance of LMAP glasses with different water contents. Nominal water contents are indicated.

Fit results for Q species are represented in Fig. 1.14. In dry glasses Q² and Q³ species are dominating. The abundance of Q³ is slightly higher in the Al-rich composition, suggesting that Al supports three-dimensional connection of phosphate groups. Pressurization to 500 MPa has only minor effect on Q species distribution in dry LMAP glasses (Fig. 1.14b). The spectrum of the air-melted LMP glass shown in Fig. 1.9a was too noisy for reliable fitting and, thus, this statement cannot be extended to Al-poor glasses.

With increasing water content in particular Q¹ strongly increases on expense of Q² and Q³. While the decrease of both species is similar at low water addition, Q³ is much more affected than Q² at high water contents. Above 4 wt% H₂O Q¹ becomes the dominant species. This suggests that

diphosphate groups are favored in strongly hydrated glasses. Single phosphate groups (Q^0) only reaches a measurable extent in glasses containing 6 wt% H_2O or more. Q^3 species are absent in glasses containing 8 wt% H_2O .

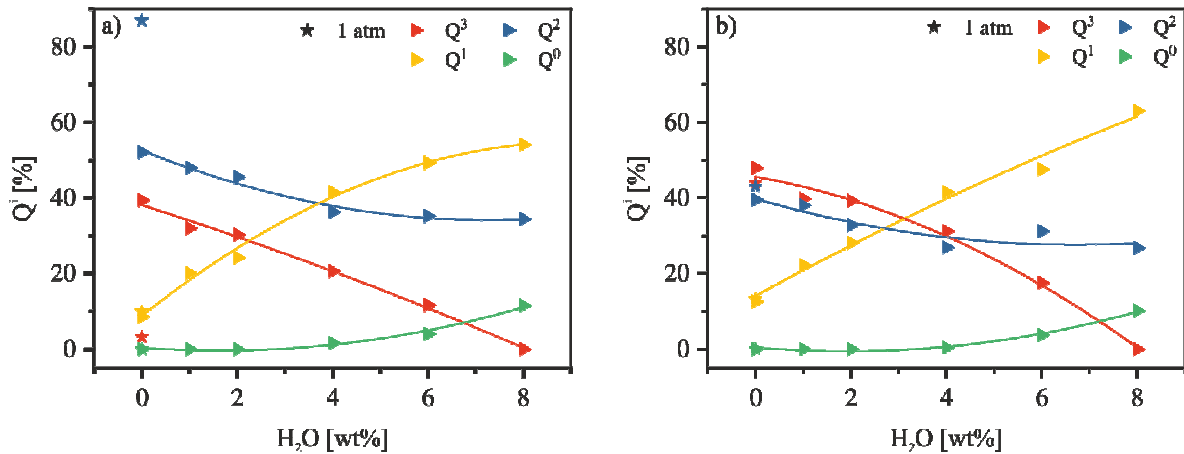


Figure 1.14: Q-species distribution in LMP (a) and LMAP (b) glasses with increasing water content. The stars in same colour represent data of glass melted at 1 atm.

1.5 Conclusionss

High pressure syntheses demonstrate that several weight percent H_2O can be incorporated in lithium magnesium phosphate glasses. IR and NMR spectroscopy gives evidence that water incorporation is associated with depolymerisation of the network and diphosphate groups become dominate species in water-rich glasses. However, it needs to be stressed that despite of the network degradation induced by water incorporation, the hydrous glasses have high mechanical stability and high durability. No visible changes of the glasses were observed after storage at ambient conditions for several months. This implies that the reinforcing effect of the cations Li, Mg and Al dominates over the reduction of network connectivity by hydrolysis of P-O-P bonds.

It has to be emphasized that these findings cannot be simply transferred to understand dissolution of phosphate glasses in water at ambient temperatures. Kinetics of hydrolysis of P-O-P bonds is slow at low temperatures while bonds to alkali and alkaline earth cations are more easily broken [33]. Thus, larger phosphate units can be expelled from glasses and are suitable for analysis, e.g. by chromatography. In the glasses of our study water was incorporated in the melt at high temperature. Under these conditions thermodynamics control the speciation in the system. At high

T, breaking of P-O-P bonds is thermodynamically preferred to complexation of cations by hydrous species.

Chapter 2

The influence of H₂O and SiO₂ on the structure of silicoborate glasses

Robert Balzer^{a,b}, Harald Behrens^{a,b}, Stephan Schuth^a, Tina Waurischk^c, Stefan Reinsch^c, Ralf Müller^c, Michael Fechtelkord^d, Joachim Deubener^e

^a Leibniz Universität Hannover, Institute of Mineralogy, Callinstr.3, 30167 Hannover, Germany

^b ZFM-Center for Solid State Chemistry and New Materials, Leibniz Universität Hannover, Germany

^c Federal Institute for Materials and Testing (BAM), 12489 Berlin, Germany

^d Ruhr-Universität Bochum, Institute of Geology, Mineralogy and Geophysics, 44780 Bochum, Germany

^e Clausthal University of Technology, Institute of Non-Metallic Materials, 38678 Clausthal-Zellerfeld, Germany

This chapter was published in the Journal of Non-Crystalline Solids (2019) 119454. DOI: 10.1016/j.jnoncrysol.2019.05.030

Abstract

To understand the impact of dissolved water on structure and properties, four boron-rich glasses of molar compositions 15-x Na₂O x CaO 15 SiO₂ 70 B₂O₃ (with x = 0, 7.5, 10) and 10 Na₂O 15 SiO₂ 75 B₂O₃ were prepared and subsequently hydrated (up to 8 wt% H₂O). Density measurements show a non-linear trend upon hydration implying large structural changes in particular at water contents < 2 wt%. Near-infrared spectroscopy shows hydroxyl groups are the dominant species in all glasses upon the entire range of water content. Molecular H₂O is detectable only at total water contents >2 wt%. ¹¹B MAS NMR spectra show that the abundance of BO₄ species is mainly controlled by ratio of (Na₂O+CaO)/B₂O₃ while incorporation of water plays a minor role. Compared to borate glasses, the efficiency of formation of BO₄ tetrahedra is favored by crosslinking of the network by SiO₄-units. The glass transition temperatures, determined by differential thermal analysis, decreases continuously with water content due to breakage of B-O-B bonds by hydrolysis. However, compared to silicates and aluminosilicates, the effect of dissolved water is less pronounced which can be explained by weaker B-O-B bonds in comparison to Si-O-Si bonds.

2.1. Introduction

First detailed investigations on water in glasses were carried out by Scholze et al. in the late 1950s [101]. Since then, numerous studies were published, dealing with the influence of water on various glass systems, such as silicates [71, 78, 102-104], aluminosilicates [61, 105, 106], borosilicates [27, 89, 107], borates [63, 108] and phosphates [19, 79, 109, 110].

Spectroscopic methods give evidence, that water can occur in form of two species in glasses, i.e. as hydroxyl groups and as molecular water [78, 83, 101, 111]. In the melt, the two hydrous species interconvert through the following reaction:



Assuming an ideal mixing of H₂O, O and OH, the equilibrium constant K for Eq. 1 is:

$$K = \frac{[OH]^2}{[H_2O] \cdot [O]} \quad (2.2)$$

where square brackets indicate mole fractions calculated on a single oxygen basis [77, 78, 83, 112]. As a basic assumption, the measured speciation in glasses at room temperature corresponds to the equilibrium water speciation in the melt, frozen-in at the fictive temperature upon cooling [63, 112, 113].

In recent years, the interest in boron-bearing glasses has steadily increased, as the incorporation of boron can significantly influence the chemical and physical properties of glasses. For instance, boron-bearing glasses are used for encapsulation of radioactive waste, chemically resistant sealing glasses and as fast ionic conductors in solid-state lithium batteries [75, 114-116].

A special feature of boron-bearing glasses is the so-called boron anomaly, which describes the property of boron to change its coordination number from 3 to 4 and back again to 3 surrounding oxygens. This behavior is a response to the addition of network modifiers in form of alkali and alkaline earth oxides and was first reported by Warren and Bischoe [36]. The trend reflects the preservation of a completely interconnected framework at low contents of network modifiers, and the formation of non-bridging oxygens (NBO) at high network modifier contents through [63, 117, 118]:



The effects of temperature, pressure and network modifiers on boron coordination are widely studied. Michaelis et al. [119] observed that the increase of the fraction of tetrahedral coordinated boron in binary borate glasses depends on the type of cation. For example, lithium is more efficient in charge compensation of the BO_4 units than other alkalis, due to its small ion radius. In hydrous soda-lime borate glasses Bauer et al. [63] observed that protons are less suitable for stabilization of BO_4 groups than alkali cations. In borosilicates, i.e. in a glass structure dominated by Si-O-Si bonds, the incorporated boron is forced into a 4-fold coordination; only a small fraction of boron remains in trigonal coordination. The addition of 3 wt% H_2O results in a complete conversion to tetrahedrally coordinated boron in these glasses.

While there are some studies dealing with water and its role on the boron speciation in borosilicate glasses [63, 120], no such studies exist to the best of our knowledge on silicoborate glasses. Fundamental questions are (i) whether silica has a similar stabilizing effect on BO_4 species in a boron dominated glass structure as observed in borosilicate glasses, and (ii) does the incorporation of water affects the glass structure in the same way as alkali oxides do.

Regarding these questions, we have systematically investigated the structural role of water in silicoborate glass of molar compositions $15-x \text{ Na}_2\text{O} \ x \ \text{CaO} \ 15 \ \text{SiO}_2 \ 70 \ \text{B}_2\text{O}_3$ (with $x = 0, 7.5, 10$) and $10 \ \text{Na}_2\text{O} \ 15 \ \text{SiO}_2 \ 75 \ \text{B}_2\text{O}_3$. Modifications of alkali and alkaline earth oxide contents are used to explore their influence on the boron speciation. Variation of water contents over a wide range of up to 8 wt% were achieved by high pressure – high temperature synthesis. This allows analyzing water-induced changes in network topology as well as in coordination of boron. Additionally, comparison of high-pressure melted glasses with those produced at ambient pressure give insights to compaction mechanisms in the glasses. Fourier transformed infrared (FTIR) spectroscopy and nuclear magnetic resonance (NMR) spectroscopy were applied to analyze the structural response to water incorporation and compaction of the glasses. Density data and glass transition temperatures (T_g) derived from differential thermal analyses (DTA) provide further information about the interaction between the silicoborate network and hydrous species. Furthermore, the influence of SiO_2 on the influence of boron coordination is discussed, as well as the effect on T_g . These findings have implications for understanding corrosion mechanisms of glasses as well as crack propagation mechanisms.

2.2 Experimental and Analytical Methods

2.2.1 Starting Materials

Four silicoborate glasses (Tab. 2.1) were prepared using Na_2CO_3 , CaCO_3 , SiO_2 and H_3BO_3 powders. These powders were carefully mixed by hand, filled stepwise into a platinum crucible at 1473 K in a chamber furnace. After heating for 1 h the melt was quenched by pouring onto a brass plate. To achieve a good homogeneity, the glasses were crushed and re-melted under the same conditions. Clear and bubble free glasses were obtained by this method.

The bulk compositions were analyzed using laser ablation inductively coupled plasma mass spectrometry (LA-ICP-MS). The laser ablation system is based on a 100 femtosecond (fs) Ti-sapphire regenerative amplifier system (Solstice-System, Spectra Physics, USA) operating at a fundamental wavelength of 775 nm in the infrared spectra (IR). The laser system produces a pulse energy of 70-90 μJ in the fourth harmonic. This ultra-short pulsed laser generates a soft ablation with high control and avoids elemental fractionation at the sample site.

The laser ablation cell was coupled to a Thermo-Scientific Element XR fast-scanning sector field ICP mass spectrometer. For analysis, isotopes of ^{11}B , ^{23}Na , ^{27}Al , ^{29}Si , ^{39}K and ^{43}Ca were selected.

A detailed description of the laser ablation system used at the Institute for Mineralogy (University of Hannover) is given by e.g. Oeser et al. [121, 122] and Lazarov et al. [123]. For our glasses, a plasma energy of 1235 W was applied for the sample ablation and Ni H-Type skimmer cones were used. The measurements were performed in low resolution mode. The NIST 610 standard glass [124] was measured as reference material. Raster analysis were performed five times at different spots on each glass with a spot size of 50 - 60 μm , whereby the sample material was ablated for 60 seconds. The instrumental background was collected for 40 seconds (without laser ablation). A repetition rate of 100 Hz for the samples and 10 Hz for the NIST standard glass was used. In order to separate the instrumental background from the sample measurements, the background was subtracted from the sample measurements. Analyses were processed using ICPMSDataCal [125] and revealed that all glasses are homogeneous, and compositions are close to the nominal values (Tab. 2.1).

Table 2.1: Nominal and measured composition of starting materials in mol%.

	Na ₂ O	CaO	SiO ₂	B ₂ O ₃	
NSB10	10.00	-	15.00	75.00	nominal
	10.43 ± 0.06	-	11.23 ± 0.09	78.28 ± 0.11	La-ICP-MS
NSB15	15.00	-	15.00	70.00	nominal
	15.91 ± 0.08	-	14.10 ± 0.06	69.99 ± 0.09	La-ICP-MS
NCSB15(1:1)	7.50	7.50	15.00	70.00	nominal
	7.95 ± 0.08	7.65 ± 0.29	12.21 ± 0.53	72.16 ± 0.26	La-ICP-MS
NCSB15(1:2)	5.00	10.00	15.00	70.00	nominal
	5.21 ± 0.04	10.01 ± 0.12	13.02 ± 0.25	71.75 ± 0.17	La-ICP-MS
NIST610	14.00	12.00	72.00	0.10	nominal
	13.44 ± 0.03	12.75 ± 0.14	72.43 ± 0.21	0.10 ± 0.01	La-ICP-MS

2.2.2 Hydrus and compressed glasses

Hydrated glasses with water contents up to 8 wt% were prepared in platinum capsules. In order to achieve homogeneous initial water distribution, glass powder and distilled water were alternately added to the capsules. The powder-water mixture was compacted with a steel piston between loading steps to minimize air bubble inclusion. In order to obtain a cylindrical shape, the capsules were welded with platinum lids after loading. The capsules had a length of approx. 25 mm and an inner diameter of 6 mm. Capsules were tested for leakage by heating in a drying oven at 373 K for several hours.

Syntheses were performed in an internally heated pressure vessel (IHPV) at 500 MPa and 1473 K for 20 h using argon as pressure medium. In each run, three capsules have been placed in the hot zone of a normal quench sample holder (controlled by K-type thermocouples), pressurized and heated up to the desired p-T conditions. A detailed description of the vessel and procedures is given by Berndt et al [60]. Samples have been quenched isobarically to avoid pressure induced structural changes and to prevent water loss from hydrated glasses. The cooling rates in the regime of T_g was approx. 7-8 K·s⁻¹ for dry glasses and approx. 3.5 K·s⁻¹ for glasses containing 8 wt% H₂O. All glass cylinders were transparent and contained neither bubbles nor crystals. To check for homogeneity of the water distribution in the glasses approx. 5 mm thick slices have been cut from both ends of the cylinders.

2.2.3 Karl-Fischer Titration

The total water content of hydrous glasses was determined by pyrolysis and subsequent by Karl-Fischer Titration (KFT). For this, approx. 10-15 mg of each glass was filled into small platinum crucibles and heated up rapidly to 1573 K. To avoid an explosive release of H₂O during heating, the crucibles were tightly bended on the top. A detailed description of the method is given by [61, 86, 126]. Results are shown in Tab. 2.2a-b.

Table 2.2a: Sample characterization and spectroscopic data of NIR measurements on calcium free glasses.

	CH ₂ O ₂ , KFT [wt%]	T _r [K]	T _g [K]	ρ [g/l]	d [mm]	Peak position [cm ⁻¹]			A ₅₂₀₀ [mm ⁻¹]	A ₄₈₉₀ [mm ⁻¹]	A ₄₆₀₀ [mm ⁻¹]	COH [wt%]	CH ₂ O [wt%]	CH ₂ O ₂ , IR [wt%]
NSB10 _{start}	/	651	649	2109 ± 2	/	/	/	/	/	/	/	/	/	/
NSB10 _{dry} -I	0.28 ± 0.15*	649	647	2169 ± 2	0.296	/	4910	4588	/	0.003	0.012	0.22	/	0.22
NSB10 _{dry} -II									/	0.003	0.012	0.20	/	0.20
NSB10 1-I	2.81 ± 0.08	606	598	2162 ± 3	0.305	/	4911	4587	/	0.012	0.052	0.94	/	0.94
NSB10 1-II	2.78 ± 0.08				0.305				/	0.012	0.053	0.96	/	0.96
NSB10 2-I	2.35 ± 0.24	557	558	2158 ± 2	0.302	/	4909	4584	0.002	0.021	0.098	1.79	0.14	1.93
NSB10 2-II	3.19 ± 0.09				0.300				0.002	0.023	0.104	1.94	0.17	2.10
NSB10 4-I	6.37 ± 0.11	505	505	2150 ± 2	0.292	5220	4903	4581	0.007	0.039	0.170	3.24	0.48	3.72
NSB10 4-II	5.99 ± 0.08				0.283				0.009	0.041	0.180	3.57	0.62	4.19
NSB10 6-I	13.24 ± 0.14	470	471	2127 ± 3	0.282	5224	4902	4579	0.016	0.057	0.233	4.67	1.19	5.86
NSB10 6-II	8.46 ± 0.13				0.288				0.019	0.058	0.246	4.84	1.35	6.19
NSB10 8-I	11.89 ± 0.14	442	441	2099 ± 2	0.296	5218	4903	4575	0.033	0.074	0.301	5.84	2.32	8.15
NSB10 8-II	11.97 ± 0.13				0.300				0.033	0.075	0.308	5.91	2.299	8.20
NSB15 _{start}	/	704	703	2167 ± 2	/	/	/	/	/	/	/	/	/	/
NSB15 _{dry} -I	0.34 ± 0.09*	698	698	2271 ± 2	0.295	/	/	4590	/	0.002	0.005	0.13	/	0.13
NSB15 _{dry} -II									/	0.003	0.005	0.45	/	0.45
NSB15 1-I	1.16 ± 0.05	649	647	2246 ± 3	0.290	/	4916	4585	/	0.009	0.044	0.92	/	0.92
NSB15 1-II	1.18 ± 0.05				0.288				/	0.010	0.047	0.96	/	0.96
NSB15 2-I	1.93 ± 0.07	593	593	2225 ± 3	0.286	/	4904	4581	0.005	0.019	0.079	1.66	0.23	1.89
NSB15 2-II	2.42 ± 0.06				0.283				0.008	0.021	0.095	2.02	0.35	2.37
NSB15 4-I	2.83 ± 0.07	524	524	2218 ± 3	0.281	5215	4906	4584	0.007	0.026	0.112	2.43	0.33	2.75
NSB15 4-II	5.15 ± 0.06				0.283				0.030	0.042	0.173	3.71	1.41	5.12
NSB15 5-I	4.90 ± 0.07	505	503	2209 ± 2	0.287	4219	4904	4578	0.027	0.041	0.177	3.79	1.29	5.07
NSB15 5-II	4.73 ± 0.06				0.280				0.022	0.042	0.170	3.65	1.03	4.68
NSB15 6-I	4.46 ± 0.07	486	483	2199 ± 2	0.281	5217	4910	4581	0.019	0.040	0.169	3.68	0.87	4.54
NSB15 6-II	7.30 ± 0.08				0.287				0.065	0.062	0.241	5.18	2.93	8.11
NSB15 8-I	7.55 ± 0.07	442	442	2166 ± 2	0.302	5218	4905	4573	0.050	0.064	0.244	5.04	2.26	7.30
NSB15 8-II	8.88 ± 0.08				0.315				0.079	0.069	0.268	5.22	3.30	8.53

Table 2.2b: Sample characterization and spectroscopic data of NIR measurements on calcium bearing glasses.

	CH_2O_t , KFT [wt%]	T_f [K]	T_g [K]	ρ [g/l]	d [mm]	Peak position [cm ⁻¹]			A_{5200} [mm ⁻¹]	A_{4890} [mm ⁻¹]	A_{4600} [mm ⁻¹]	COH [wt%]	CH_2O [wt%]	CH_2O_t , IR [wt%]
NCSB15(1:1) _{start}	/	729	722	2180 ± 2	/	/	/	/	/	/	/	/	/	/
NCSB15(1:1) _{dry} -I	0.13 ± 0.08*	734	731	2262 ± 3	0.294	/	/	4599	/	0.001	0.004	0.08	/	0.08
NCSB15(1:1) _{dry} -II									/	0.001	0.003	0.07	/	0.07
NCSB15(1:1)1-I	0.74 ± 0.07	666	666	2250 ± 2	0.287	/	4908	4590	/	0.007	0.039	0.96	/	0.96
NCSB15(1:1)1-II	1.08 ± 0.07				0.288				/	0.008	0.045	1.08	/	1.08
NCSB15(1:1)2-I	1.87 ± 0.06	652	639	2244 ± 3	0.280	/	4916	4588	0.002	0.013	0.070	1.73	0.05	1.79
NCSB15(1:1)2-II	1.85 ± 0.05				0.260				0.003	0.014	0.072	1.79	0.09	1.89
NCSB15(1:1)4-I	3.96 ± 0.05	590	560	2221 ± 3	0.278	5223	4912	4584	0.013	0.032	0.145	3.64	0.43	4.07
NCSB15(1:1)4-II	4.04 ± 0.05				0.283				0.014	0.030	0.143	3.53	0.47	4.00
NCSB15(1:1)6-I	6.16 ± 0.06	540	512	2196 ± 2	0.282	5217	4919	4581	0.032	0.047	0.202	5.01	1.06	6.07
NCSB15(1:1)6-II	6.07 ± 0.08				0.282				0.034	0.045	0.203	5.03	1.16	6.18
NCSB15(1:1)8-I	8.25 ± 0.09	476	471	2168 ± 2	0.285	5215	4909	4578	0.058	0.063	0.259	6.34	1.89	8.22
NCSB15(1:1)8-II	8.31 ± 0.08				0.282				0.058	0.063	0.256	6.42	1.95	8.38
NCSB15(1:2) _{start}		767	761	2186 ± 3					/	/	/	/	/	/
NCSB15(1:2) _{dry} -I	0.14 ± 0.07*	764	761	2285 ± 3	0.286	/	/	4593	/	/	0.003	0.06	/	0.06
NCSB15(1:2) _{dry} -II									/	/	0.004	0.06	/	0.06
NCSB15(1:2)1-I	1.34 ± 0.06	673	673	2268 ± 3	0.276	/	4929	4591	0.002	0.007	0.041	0.76	0.12	0.88
NCSB15(1:2)1-II	1.07 ± 0.04				0.276				0.002	0.009	0.045	0.82	0.12	0.94
NCSB15(1:2)2-I	1.98 ± 0.05	663	654	2259 ± 3	0.278	/	4915	4589	0.003	0.016	0.076	1.40	0.21	1.61
NCSB15(1:2)2-II	2.08 ± 0.08				0.282				0.003	0.015	0.072	1.34	0.17	1.51
NCSB15(1:2)4-I	3.88 ± 0.06	577	578	2218 ± 3	0.285	5213	4913	4585	0.016	0.034	0.151	2.77	1.02	3.80
NCSB15(1:2)4-II	3.91 ± 0.07				0.297				0.016	0.035	0.157	2.82	1.12	3.93
NCSB15(1:2)6-I	6.30 ± 0.06	513	509	2207 ± 3	0.295	5212	4912	4579	0.038	0.053	0.225	3.99	2.48	6.47
NCSB15(1:2)6-II	5.99 ± 0.07				0.289				0.030	0.048	0.207	3.76	2.02	5.78
NCSB15(1:2)8-I	8.26 ± 0.10	476	482	2180 ± 2	0.285	5211	4914	4578	0.059	0.063	0.256	4.82	4.10	8.92
NCSB15(1:2)8-II	8.02 ± 0.07				0.281				0.050	0.058	0.240	4.54	3.58	8.1

Notes: I and II in the sample name refer to pieces cut from both ends of the synthesized glass body. Subscripts “start” indicate the glass melted at ambient pressure, subscript “dry” refers to the nominally dry glass after high pressure synthesis. The last number in the sample indicates the nominal water content in wt%. Water contents are measured by KFT, except for data marked by *, which were obtained by MIR spectroscopy. Fictive temperatures T_f of glasses were determined by the first upscan of DTA and glass transition temperatures T_g are averages from three following upscans of DTA. Uncertainties are ± 2K. Peak positions (± 5 cm⁻¹) and absorbances (± 0.002) of NIR combination bands were determined after linear baseline corrections, see text for detail

2.2.4 Differential thermal analyses

The glass transition temperature, T_g , was determined by differential thermal analyses in air using 15-20 mg of glass pieces placed in Pt crucibles (thermobalance TAG 24 Setaram, Caluire, France). The same kind of measurement and data evaluation was applied to hydrous borate glasses, and T_g values were found to be in perfect agreement with the isokom temperature (T_{12}) at which viscosity equals 10^{12} Pa·s [108]. For each sample, four heating and cooling cycles at 10 K min^{-1} were applied. The maximum temperature did not exceed T_g by more than 50 K. The first cycle represents the fictive temperature T_f of the glasses, since the cooling history of the samples reflects the status of quenching after the IHPV synthesis. T_g was determined by the following three cycles. Definition of T_f and T_g is based on the onset of the endothermic step in the DTA curve according [64, 65]. The T_f -values and the average values of T_g are shown in Tab. 2.2a and 2.2b. In all samples, T_g decreases with increasing water content. This behavior is consistent with observations made on silicate, aluminosilicate, borosilicate and borate glasses [27, 63, 67, 108, 112, 127, 128].

2.2.5 IR Spectroscopy

In order to obtain information about the network structure of the glasses, MIR spectra of KBr pressed pellets in the range of $370\text{-}4000\text{ cm}^{-1}$ were collected using a Fourier Transform Infrared (FTIR) spectrometer (Bruker Vertex 80v). The spectrometer is equipped with a global light source, a KBr beam splitter and a pyroelectric deuterated, L-alanine doped triglycerine sulfate (DLATGS) detector. For this purpose, 1 mg glass powder and 199 mg KBr were mixed and pressed into a pellet at 100 kN. A pure KBr pellet was measured as reference to examine the contribution of contamination of KBr to the spectrum in the range of OH stretching vibrations.

Additionally, infrared spectra have been measured on double-polished glass sections using a FTIR spectrometer (Bruker IFS 88). The spectrometer is linked with an IR microscope Bruker IR scope II equipped with a mercury-cadmium-tellurium (MCT) detector. Absorption spectra in the mid-infrared (MIR) were recorded to investigate the fundamental OH stretching vibrations. The spectra were measured in a range of $600\text{ - }6000\text{ cm}^{-1}$ using a KBr beam splitter and a global light source with a spectral resolution of 2 cm^{-1} . For each sample and background (air) measurement 50 scans were accumulated.

Near-infrared (NIR) spectra were recorded to determine the water speciation in the glasses. Here, the same set-up was used as for MIR measurements on thin sections except that a tungsten light source and a CaF₂ beam splitter have been used. The spectral resolution was 4 cm⁻¹, and for each spectrum 100 scans were accumulated. In order to guarantee good reproducibility and homogeneous water distribution, pieces of each glass cylinder were cut off from the top and bottom, and each sample was analyzed at least three times at different positions. A digital micrometer (Mitutoyo Absolute) with a precision of ± 2 μm was used to determine the sample thickness.

2.2.6 ¹¹B MAS-NMR Experiments

¹¹B MAS-NMR spectra were acquired at room temperature using a Bruker ASX 400 WB spectrometer. Measurements were performed at a Larmor frequency of 128.38 MHz using a standard Bruker 4 mm probe with a sample spinning of 12.5 kHz. Solid NaBH₄ ($\delta_{\text{iso}} = -42.0$ ppm) was processed as secondary reference standard. A single pulse duration of 0.6 μs was applied to ensure homogeneous excitation of the central and all satellite transitions. The delay time was 1 s and 6400 scans were accumulated. ¹¹B MAS-NMR spectra were fitted with a quadrupolar lineshape using the DmFit 2015 program [129].

2.3. Results

2.3.1 Water distribution in the glasses

Tab. 2.2 summarizes total water contents measured by KFT, T_g , density, and water speciation data obtained by NIR spectroscopy. The first column lists total water content data measured by KFT on the end pieces of the samples (I and II). The respective average water contents of NSB15, NCSB15(1:1) and NCSB15(1:2) matches to the calculated water content indicated by the sample code. However, the deviation between the top and the bottom end pieces of the calcium oxide free samples is significant in some glasses with water contents > 3 wt% (Tab. 2.2a). One reason for this could be an initial inhomogeneous water distribution during capsule preparation. Water diffusion in oxide melts is too slow to achieve a homogenous water distribution over the entire glass body by diffusion within the applied synthesis duration [130]. The deviation of the calcium oxide bearing glasses is not significant and in the range of the analytical error.

It has to be mentioned that glasses of the NSB10 series were stored several months before the KFT analysis. The water contents of NSB10 glasses measured by KFT deviates significantly from their calculated values based on H₂O loaded into the capsules. Water contents are 80 % higher than expected for low water content glasses and ~ 50 % higher in glasses with high water content. Although, all glasses have been stored in the same desiccator, the other glass systems do not show such tendency. A possible reason for this is the lower content of network modifiers and the increased content of B₂O₃. Thus, the glasses of the NSB10 series are much more hygroscopic than glasses with a lower boron content. Taking this into account, the nominal water contents are used for further evaluations of the NSB10 glasses.

It is noteworthy that all nominally dry glasses processed at high pressure contain a certain amount of water (0.28 wt% in NSB10, 0.13 wt% in NSB15, 0.08 wt% in NCSB15(1:1) and 0.06 wt% in NCSB15(1:2)) as shown in Table 2.2a and 2.2b. This content originates from water absorbed on the glass powder before loading in the capsule. Similar water contents were reported for dry borate systems glasses by Bauer et al. and Reinsch et al. [63, 108].

In the following we refer to the average of KFT data for analytical bulk methods (density, NMR), being aware that the water content has relatively large errors for some samples. For local methods (IR) we used KFT measurements on pieces taken just next to the analysis points. For the evaluation of hydrous NSB10 glasses, the nominal water content is used.

2.3.2 Density

As shown in Fig. 2.1a, densities of water-poor glasses compacted at 500 MPa (triangles) are several percent higher compared to glasses melted at ambient pressure (stars). The effect is more pronounced for Ca-bearing glasses than for Ca-free glasses, i.e. densities of dry Ca-free glasses increase by 2.8 % (NSB10) and 2.9 % (NSB15), and for Ca-bearing glasses by 4.3 % (NCSB15(1:1) and 4.1 % NCSB15(1:2)), respectively. The density increase upon compression for these glasses is higher than reported for silicates and aluminosilicates [69, 70], but similar to soda-lime borate glasses [63]. Addition of up to 2 wt% water has only a weak effect on density, which might be explained by structural changes in the glasses.

The roughly linear behavior at water contents > 2 wt% is consistent with ideal mixing of oxide glass and water, as also found for silicate glasses [71]. Molar volumes of H₂O derived for water-rich glasses (NSB15: $12.6 \pm 0.2 \text{ cm}^3 \cdot \text{mol}^{-1}$; NCSB15(1:1): $12.6 \pm 0.3 \text{ cm}^3 \cdot \text{mol}^{-1}$; NCSB15(1:2): $11.0 \pm 0.2 \text{ cm}^3 \cdot \text{mol}^{-1}$) are in good agreement with values reported for silicate

and aluminosilicate glasses ($11.5\text{--}12.5\text{ cm}^3\cdot\text{mol}^{-1}$) [71]. The value for NSB10 is slightly higher ($13.2 \pm 0.4\text{ cm}^3\cdot\text{mol}^{-1}$). However, due to the hygroscopic behavior of the NSB10 glasses, the error of the molar volume is higher for this composition than given by the fitting error.

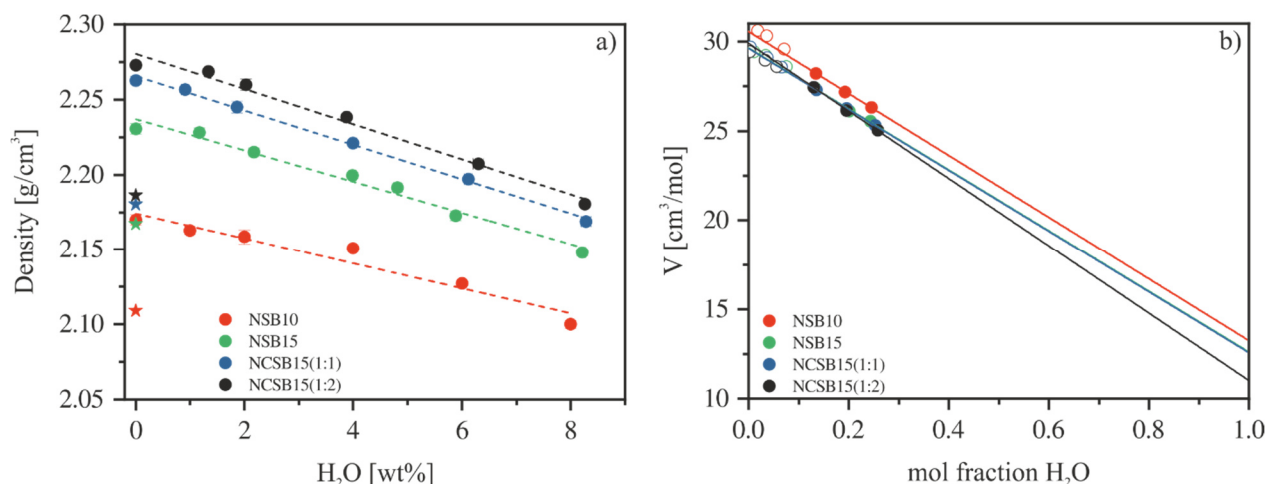


Figure 2.1: Density of silicoborate glasses. Densities of starting glasses (1 atm) are labeled as star. Compacted glasses (500 MPa) are marked as triangles (a). Molar volume of hydrous glasses. Open symbols represent mole fractions < 0.1. Filled symbols indicate mole fractions > 0.1 (b). Errors are smaller than symbol size.

2.3.3 MIR Spectroscopy

MIR spectra of silicoborate glasses in the frequency of $400\text{--}4000\text{ cm}^{-1}$ are shown in Fig. 2.2. The spectra can be divided into two areas. First, lattice vibrations in the range of $400\text{--}1500\text{ cm}^{-1}$ and second, the OH stretching vibrations in the range of $2800\text{--}3800\text{ cm}^{-1}$. The band assignment in the low wavenumber range follows Bauer et al. [63], Balachander et al. [131], Yiannopoulos et al. [118] and Kamitsos and Chryssikos [132]. The absorption bands between 750 and 1090 cm^{-1} are related to B-O stretching vibrations of BO_4 tetrahedra. Bands in the range of $1150\text{--}1400\text{ cm}^{-1}$ are due to stretching vibrations of B-O bands in BO_3 units.

A closer look at the band structures in this area reveals some differences in peak position and shape. These changes are caused by the different network modifier contents and by the differences in water content. For instance, the intensity of the BO_4 related vibrations (1000 cm^{-1}) in the anhydrous glasses increases significantly compared to that of BO_3 (1300 cm^{-1}) when the Na_2O content is increased by about 5 mol% (see e.g. NSB10 dry vs NSB15 dry). The addition of CaO has no significant effect on the intensity of these bands in dry glasses. Just the well resolved bands in the range of 1000 cm^{-1} merge with increasing CaO content. These observations are consistent with the ^{11}B MAS-NMR measurements (Fig. 2.12). The NMR data also show that the addition of 5 mol% Na_2O results in a significant increase of

BO₄ tetrahedra, while the substitution of CaO for Na₂O has only a weak effect on the formation of tetrahedral coordinated boron.

The addition of water also has a noticeable effect on the structure of the MIR bands. Spectra of dry NSB10 (Fig. 2.2a) show a double peak (1390 cm⁻¹ and 1248 cm⁻¹) in the range of BO₃ units. With increasing water content, peak positions shift to higher wavenumbers and merge together at water contents > 6 wt%. The bands related to BO₄ units show a similar behavior. The peak at 1059 cm⁻¹ (dry glass) shifts to 1098 cm⁻¹ with increasing water content. The band at 924 cm⁻¹, visible as a shoulder, becomes more pronounced with increasing water content. The intensity of the peak at 786 cm⁻¹ increases strongly with increasing water content. On the other hand, the peak at 698 cm⁻¹ does not change its shape and peak position.

Similar trends are visible for NSB15 glasses (Fig. 2.2b). The BO₃-related peaks at 1364 cm⁻¹ and 1239 cm⁻¹ shift to higher wavenumbers (1403 cm⁻¹ and 1280 cm⁻¹, respectively) upon hydration, and both peaks merge to a single peak at high water content. Bands in the range of BO₄ units show a similar trend as in NSB10 glasses. The band at 1029 cm⁻¹ (dry glass) shifts to 1064 cm⁻¹ and a small shoulder forms at 785 cm⁻¹ when the water content is increased to 8 wt%. The shoulder at 924 cm⁻¹ and the peak at 694 cm⁻¹ do not change the peak position.

Dry glasses of the NCSB15(1:1) (Fig. 2.2c) series also have this double peak (1373 cm⁻¹ and 1239 cm⁻¹) that becomes a single peak with a shoulder as the water content increases (Fig. 2.2c). The peak position shifts from 1373 cm⁻¹ (dry) to 1392 cm⁻¹ (8 wt%) and 1239 cm⁻¹ (dry) to 1269 cm⁻¹ (8 wt%), respectively. The peak at 1046 cm⁻¹ (dry) is shifted to 1070 cm⁻¹ (8 wt%). The peak positions of 917 cm⁻¹ and 694 cm⁻¹ do not change over the investigated range of water content.

In the NCSB15(1:2) glass series (Fig. 2.2d) the double peak in the range of the BO₃ units is not as pronounced as in the other glass series (Fig. 2.2a-c). The respective band structure looks more like a single peak (1377 cm⁻¹) with a shoulder at 1250 cm⁻¹ (dry). The peak shifts to higher wavenumbers (1388 cm⁻¹) with increasing water content (8 wt%), whereas the shoulder disappears at water contents > 4 wt%. In the range of BO₄ units the peak at 1059 cm⁻¹ (dry) is shifting to 1093 cm⁻¹ (8 wt%). The small shoulder at 767 cm⁻¹ and the peak at 694 cm⁻¹ do not change their position when the water content increases. Comparison of the integral intensities of BO₃- and BO₄ related bands shows no significant change in the ratios of these bands with increasing water content. Again, this indicates that addition of water has a minor effect on the abundance of BO₄, consistent with ¹¹B MAS NMR spectra (Fig. 2.12).

In the high wavenumber range, broad bands between 3230 cm^{-1} and 3500 cm^{-1} are visible in all glass series. According to Scholze et al. [101] and others, e.g. [77, 78], these bands are related to OH stretching vibrations of weakly to moderately H-bound hydrous species. This band is superimposed by artifacts, i.e. H_2O in potassium bromide and absorbed on glass powder. These contributions cannot be completely separated from water dissolved in the glasses, even when background spectra are recorded on pure KBr pellets. Especially glasses of the NSB10 series are very sensitive to H_2O adsorption. These glasses show a sharp peak at 3250 cm^{-1} , whose intensity increases significantly with increasing water content. Glasses with higher network modifier content do not show such feature. This indicates that glasses with network modifier content of 15 mol% are more stable compared to those with 10 mol%.

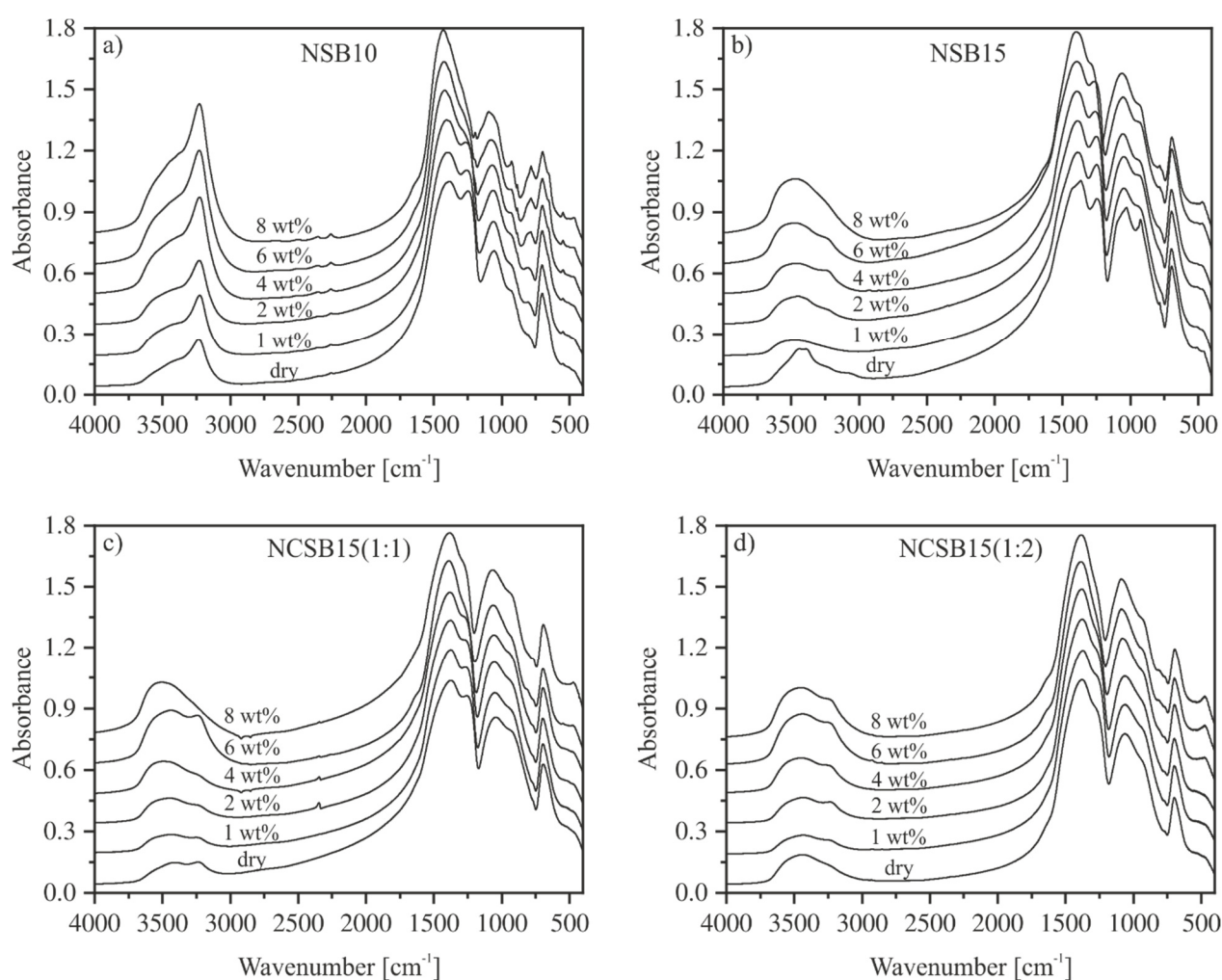


Figure 2.2: MIR spectra of KBr pressed pellets of NSB10 (a), NSB15 (b), NCSB15(1:1) (c) and NCSB15(1:2) (d). Spectra were normalized to the B-O stretching vibrations of trigonal BO_3 units ($\sim 1385\text{ cm}^{-1}$) and shifted vertically for clarity. Nominal water contents are indicated.

MIR spectra of thin sections (approx. 80 μm) for glasses containing < 2 wt% H_2O were recorded to get more detailed information of structural incorporation of water in the glass structure. Fig. 2.3 shows an example of these MIR measurements on the glasses with up to 2 wt% water.

The spectra of NSB15 show a main absorption peak at 3500 cm^{-1} that is attributed to OH stretching vibrations and a peak at 2700 cm^{-1} which is independent from the water content and probably corresponds to an overtone of the BO_3 band at 1350 cm^{-1} .

In order to separate the water-related peaks from the network vibration features, the spectrum of each dry glass was subtracted from the spectra of water bearing glasses, as shown in Fig. 2.4. After subtraction, only the water related band with its maximum at 3500 cm^{-1} and an asymmetric shoulder towards lower wavenumbers remains. This peak shape is very similar to that of aluminosilicate glasses and indicates that all hydrous species are weakly hydrogen bound to adjacent bridging oxygens [78, 101, 111, 133].

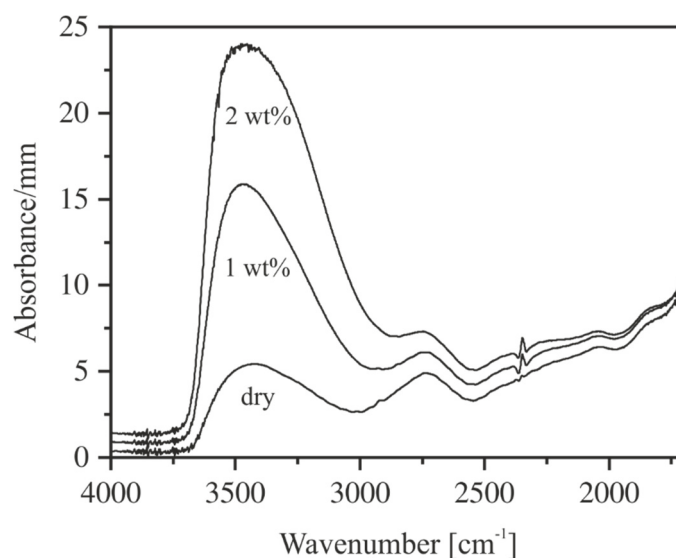


Figure 2.3: Measured MIR spectra of thin section of NSB15 containing 0-2 wt% H_2O . Irregularities at 2350 cm^{-1} are due to differences in CO_2 during background and sample measurements. Spectra are shifted for clarity. Nominal water contents are indicated.

The spectra of NCSB15(1:1) show a sharp peak at 2350 cm^{-1} which is absent in spectra of the other glass compositions. A weak doublet in that region is visible in some spectra, originating from difference in CO_2 content of the atmosphere during sample and background measurement. A single peak at 2350 cm^{-1} was observed in spectra of CO_2 -bearing rhyolitic glasses [134] and silica glasses [135]. It indicates incorporation of CO_2 molecules with hindered

rotation in the glass. No sources of CO₂ have been loaded into the capsule during preparation, but CO₂ may have been adsorbed on the glass powder used for synthesis. Such contamination has been observed by Behrens et al. in the synthesis of hydrous float glass [86]. However, in float glass CO₂ was incorporated as carbonate groups and not in molecular form.

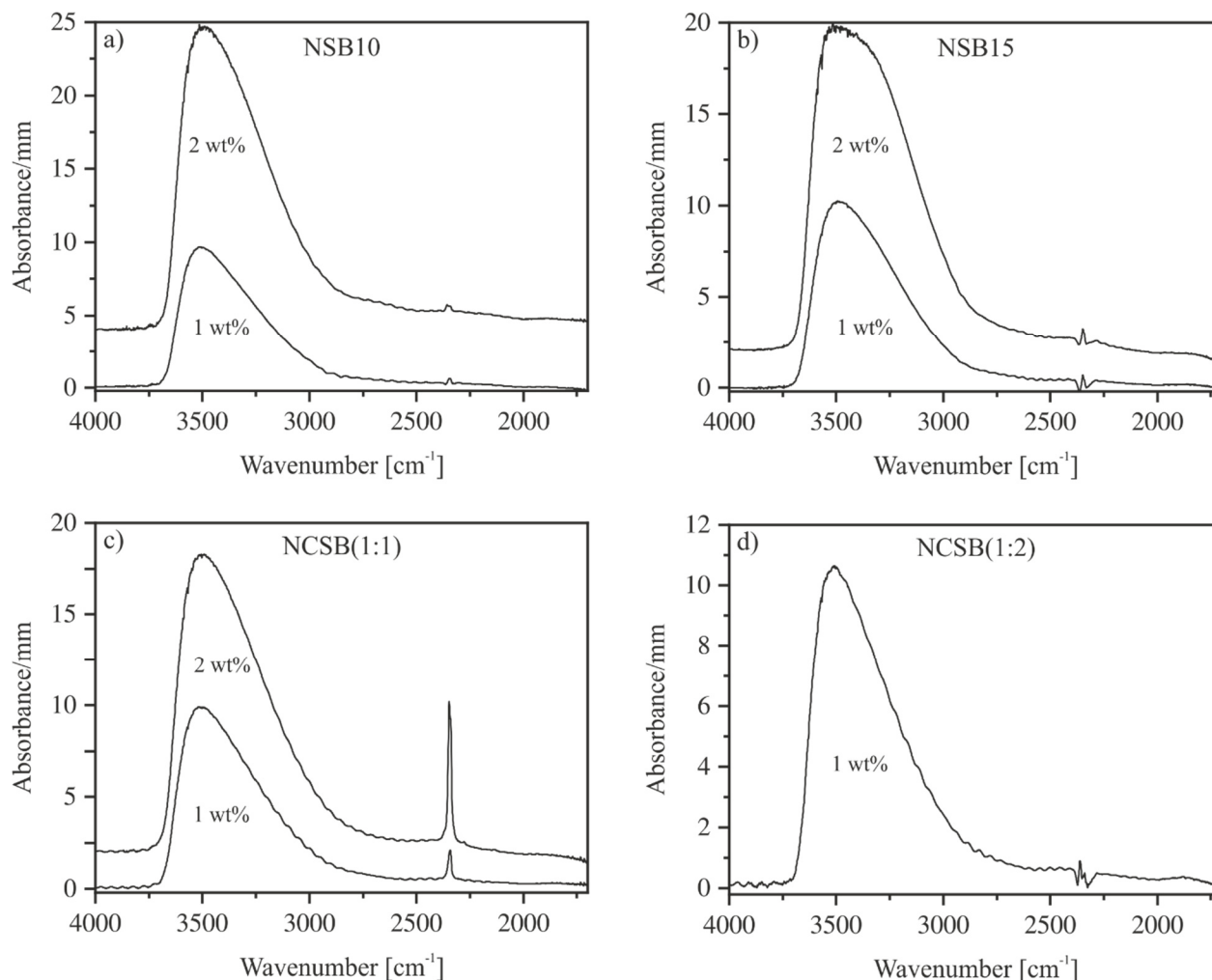


Figure 2.4: Subtraction spectra (hydrous - dry glass) demonstrate for NSB10 (a), NSB15 (b), NCSB15(1:1) (c) and NCSB15(1:2) (d) that the pronounced absorption band at 3500 cm⁻¹ is related to OH stretching vibrations.

The water contents of nominally dry glasses, shown in Tab. 2.2, were determined using the absorption coefficient of the band at 3500 cm⁻¹ which was determined using thin sections of glasses with water contents up to 2 wt%. In doing so, the absorbance at the peak maximum is related to the total water content measured by KFT. This approach is justified because the peak shape does not change significantly with increasing water content. The total water content $c_{H_2O_t}$ is given as

$$c_{H_2O_t} = \frac{1802 \cdot A_i}{\rho \cdot d \cdot \varepsilon} \quad (2.4)$$

where A_{3500} refers to the absorbance of the band at 3500 cm^{-1} , ρ to the density in $\text{g}\cdot\text{L}^{-1}$, and d to the sample thickness in cm. The derived values of the linear molar absorption coefficient ϵ_{3500} for samples containing approx. 1 wt% H_2O are given in Tab. 2.3. Addition of 5 mol% Na_2O (NSB10, NSB15) on expense of B_2O_3 decreases ϵ_{3500} by 14%. Substitution of CaO for Na_2O also leads to a systematic decrease of ϵ_{3500} . These trends are consistent with findings for hydrous borate glasses e.g. by Bauer et al. [63] and by Reinsch et al. [108].

Table 2.3: Average values of the linear molar absorption coefficient ϵ for water related bands in silicoborate glasses.

	MIR		NIR	
	ϵ_{3500} [$\text{L}\cdot\text{mol}^{-1}\cdot\text{cm}^{-1}$]	ϵ_{4100} [$\text{L}\cdot\text{mol}^{-1}\cdot\text{cm}^{-1}$]	ϵ_{4600} [$\text{L}\cdot\text{mol}^{-1}\cdot\text{cm}^{-1}$]	ϵ_{5200} [$\text{L}\cdot\text{mol}^{-1}\cdot\text{cm}^{-1}$]
NSB10*	113.2 ± 4.9	1.39 ± 0.02	1.49 ± 0.11	0.41 ± 0.06
NSB15	99.5 ± 2.3	1.31 ± 0.07	1.34 ± 0.09	0.62 ± 0.09
NCSB15(1:1)	97.2 ± 3.7	1.38 ± 0.06	1.16 ± 0.13	0.86 ± 0.08
NCSB15(1:2)	87.4 ± 5.4	1.32 ± 0.03	1.55 ± 0.10	0.41 ± 0.09

*Notes: Water contents used for the determination of the linear molar absorption coefficients of NSB10 were estimated by the nominal water content of the glasses. Errors represent the standard deviation ($n = 3$)

2.3.4 NIR Spectroscopy

The NIR spectra of NSB10, NSB15, NCSB15(1:1) and NCSB15(1:2) containing up to 8 wt% H_2O are shown in Fig. 2.5. In the range of $6000\text{--}3700\text{ cm}^{-1}$ there are strong absorption bands at 4100 cm^{-1} and 4600 cm^{-1} . Weaker absorption bands are visible in the range of 4900 cm^{-1} and 5200 cm^{-1} . The band at 4100 cm^{-1} is attributed to the combination of OH stretching vibrations with a low frequency lattice vibration [63], analogue to silicate glasses [77, 89]. Absorption bands near 4600 cm^{-1} and 4900 cm^{-1} are related to the combination of stretching and bending of structurally bound OH groups [84, 86, 106]. As discussed in previous studies, e.g. [63, 136], the peak at 4600 cm^{-1} can be assigned to hydroxyl groups connected to tetrahedral coordinated boron while the band at 4900 cm^{-1} is due to hydroxyl groups bound to trigonal coordinated boron. These assignments are supported by MIR spectra (Fig. 2.2). The band at 4600 cm^{-1} (Fig. 2.5) results from a combination of OH stretching vibration at 3500 cm^{-1} and a BO_4 stretching vibration at approx. 1100 cm^{-1} , and the band at 4900 cm^{-1} from a combination of the OH stretching vibration at approx. 3500 cm^{-1} and the BO_3 stretching vibration at approx. 1400 cm^{-1} [63, 80, 137]. It is conspicuous that the NIR spectra do not show a band near 4500 cm^{-1} . Such band was observed in hydrated borosilicates and can be assigned

to Si-OH vibrations [77, 78, 83, 89]. Bauer et al. [89] suggest that at least half of the hydroxyl groups in sodium borosilicate glasses are bound to Si. The absence of the 4500 cm^{-1} in our glasses gives strong evidence that OH groups have strong preference for bonding to boron compared to silicon.

The band at 5200 cm^{-1} is attributed to the combination of stretching and bending modes of H_2O molecules [83-86]. The band is detectable for water contents $> 2\text{ wt}\%$ only and increases systematically towards higher water content. The position of the peak does not change noticeably with alkali/ alkaline earth contents, but slightly shift towards lower wavenumber with increasing water content (see Tab. 2.2a and 2.2b).

In order to use the NIR bands for the determination of species concentrations and total water contents of the glasses, the choice of the baseline is crucial. It is essential that the baseline has a high reproducibility as discussed in the study of Withers and Behrens on aluminosilicate glasses [87]. Following [63, 138] the baseline applied to the silicoborate glasses was defined by linear extrapolation of the shallow region in the wavenumber range of $5500\text{-}6000\text{ cm}^{-1}$ towards lower wavenumber. This approach is justified since the tail of the 3500 cm^{-1} band is very steep and does not affect the spectra beyond the maximum of the 4100 cm^{-1} band (Fig. 2.6). This baseline shows high reproducibility for both low and high-water bearing glasses. We are aware that the so obtained absorbances may have some systematic error due to superimposition of the peaks forming the complex band shape in the NIR. However, the number and the shape of the base peaks is uncertain and band deconvolution has little constraints and physical justifications. Therefore, we did not make an attempt for decomposition of spectral features in the NIR. Since band shape and position of maxima did not vary much with water content, we are convinced that our approach is suitable to estimate contents of hydrous species.

As shown in Fig. 2.7a, the absorbance of 4100 cm^{-1} band normalized to sample thickness and density is proportional to the total water content. The linear correlation indicates that both OH groups and H_2O molecules contribute to this band. It should be mentioned that the regression lines do not pass through the origin. The reason for this could be the large prolongation of the linear baseline towards low frequencies or small superimposed contribution of the fundamental OH stretching vibration. The deviation of the regression lines to the origin is very similar and marginal in glasses containing $15\text{ mol}\%$ of network modifier, while the deviation of NSB10 glasses is more obvious. The molar absorption coefficient of the 4100 cm^{-1} band is given by the slope in Fig. 2.7a. The derived values are very similar for all compositions (Table 2.3).

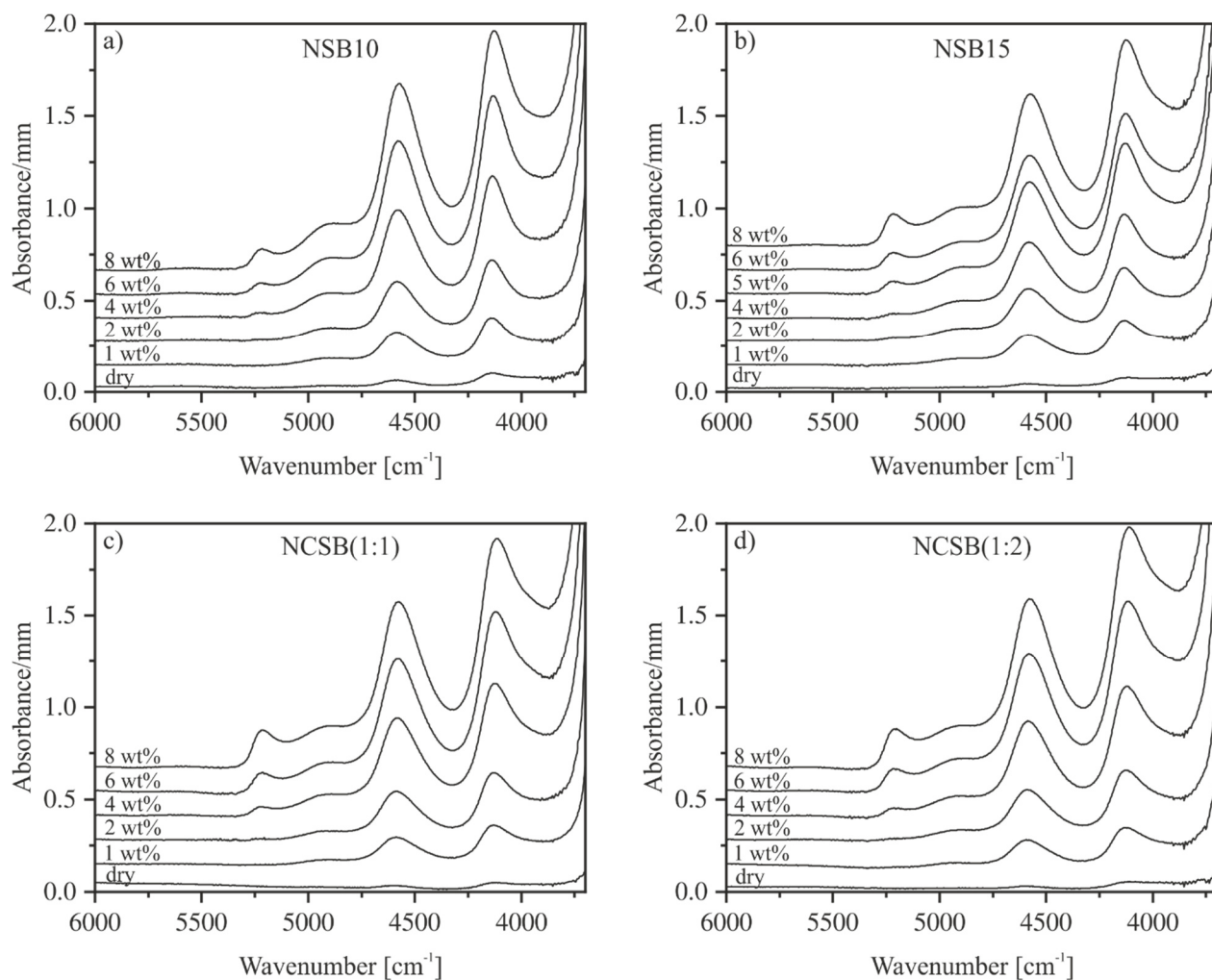


Figure 2.5: NIR spectra of NSB10 (a), NSB15 (b), NCSB15(1:1) (c) and NCSB15(1:2) (d) containing 0-8 wt% H₂O. Spectra were normalized to sample thickness and vertically shifted for clarity. Nominal water contents are indicated.

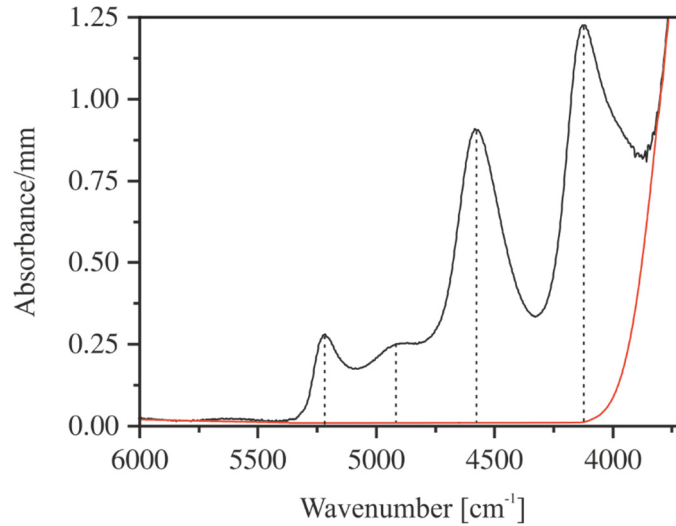


Figure 2.6: NIR spectrum of NCSB15(1:1) glass bearing 8 wt% water. Solid red curve shows the applied baseline. Dashed vertical lines represent the wavenumber of peak maxima, which were used for quantification of hydrous species.

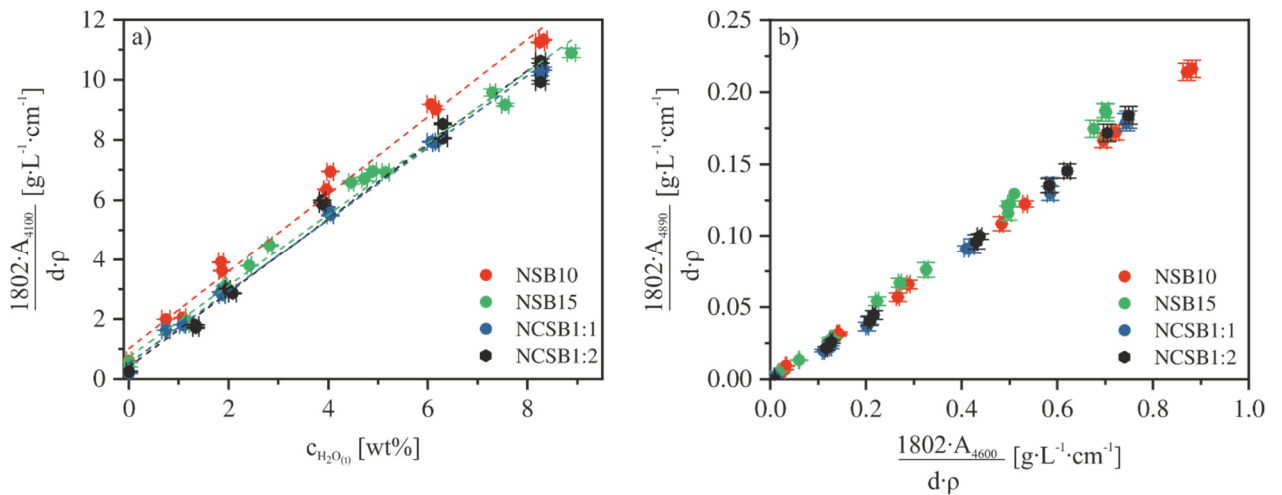


Figure 2.7: Absorbance of the 4100 cm^{-1} absorption band normalized to density and sample thickness as a function of H_2O content determined by KFT (a). Absorbance of the 4900 cm^{-1} absorption band normalized to density and sample thickness is plotted as a function of the normalized absorbance of the 4600 cm^{-1} peak (b).

Assuming that the total water content of the glasses is represented by the combination bands, a simple linear regression can be performed to determine the absorption coefficients for both bands (Eq. 2.6-2.8) [87]. A prerequisite is that the linear molar absorption coefficients are independent of the water content, and the ratio of subspecies is constant [139, 140]. Evidence for constant ratio of the OH subspecies is given by Fig. 2.7b. In the whole range of water contents the two OH bands at 4600 cm^{-1} and 4900 cm^{-1} are linearly correlated. Based on this result, we chose the 4600 cm^{-1} band to represent the total OH content of the glasses. Thus, the following equations were used to determine species contents and total water content:

$$c_{H_2O_t} = c_{OH} + c_{H_2O} \quad (2.6)$$

$$c_{OH} = \frac{1802 \cdot A_{4600}}{\rho \cdot d \cdot \varepsilon_{4600}} \quad (2.7)$$

$$c_{H_2O} = \frac{1802 \cdot A_{5200}}{\rho \cdot d \cdot \varepsilon_{5200}} \quad (2.8)$$

Here, c_{OH} represents the content of water dissolved as OH groups and c_{H_2O} the content of molecular water. Combining these three equations, the linear molar absorption coefficients ε can be derived by a linear regression

$$\frac{1802 \cdot A_{5200}}{d \cdot \rho \cdot c_{H_2O_t}} = \varepsilon_{5200} - \frac{\varepsilon_{5200}}{\varepsilon_{4600}} \cdot \frac{1802 \cdot A_{4600}}{d \cdot \rho \cdot c_{H_2O_t}} \quad (2.9)$$

The linear molar absorption coefficient of the NIR absorption bands are given as the intercepts with the corresponding axis (Fig. 2.8). This method has already been successfully applied to various glass systems such as borates [63], borosilicates [89] or aluminosilicates [61, 78, 106, 141, 142]. Following this approach, we obtain values for ε_{4600} as shown in Tab. 2.3. Consistent with findings for simple silicate glasses [78, 88], aluminosilicate glasses [61, 143] and borate glasses [63], ε_{4600} decreases with increasing alkali content. At constant network modifier content, ε_{4600} shows a minimum and ε_{5200} a maximum near a Ca/Na ratio of 1:1. However, the exact position of the extremes needs to be approved by studies on additional compositions.

The linear molar absorption coefficients are in good agreement with those for hydrous borate glasses reported by Bauer et al. [63]. For instance, they determined a ε_{4600} value of $1.47 \pm 0.08 \text{ L} \cdot \text{mol}^{-1} \cdot \text{cm}^{-1}$ and an ε_{5200} value of $0.52 \pm 0.12 \text{ L} \cdot \text{mol}^{-1} \cdot \text{cm}^{-1}$ for borate glasses containing 15 mol% network modifier [63].

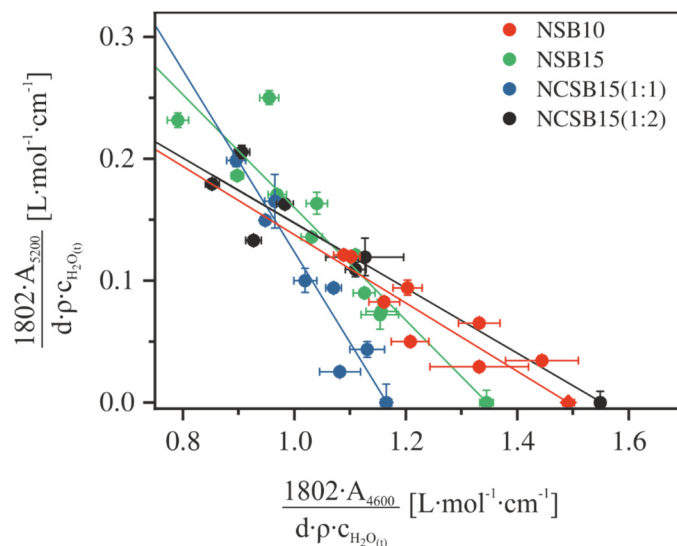


Figure 2.8: Calibration plot for the determination of the linear molar absorption coefficient of the NIR absorption band at 4600 cm^{-1} and 5200 cm^{-1} in silicoborate glasses

2.3.5 NMR Spectroscopy

^{11}B MAS-NMR spectra of NSB10, NSB15, NCSB15(1:1) and NCSB15(1:2) exhibit similar features as shown in Fig. 2.9. The main resonance is in the range of 0.5 ppm for NSB10 and NSB15 and at 0.7 ppm for NCSB15(1:1) and NCSB15(1:2). This sharp resonance is attributed to tetrahedral BO_4 [63, 144-146]. The resonance at 11 ppm is related to BO_3 groups, which causes a broad quadrupolar pattern due to second-order quadrupolar interaction [144-147]. All spectra are normalized to the BO_4 resonance to visualize changes in the lineshape caused by water. It becomes clear that the BO_3 resonance decreases as the water content increases. To determine the relative abundance of BO_4 and BO_3 units the main resonances between 25 to -20 ppm were considered. In order to deconvolute the main resonance, the program DmFit 2015 [129] was used. The resonance related to BO_4 units was fitted using Lorentzian function and the BO_3 related resonance was fitted using a quadrupolar function with a central transition only (QMAS1/2) where an infinite spinning rate is assumed. The dashed lines in Fig. 2.9a show an example of spectra deconvolution for the dry NSB10 glass.

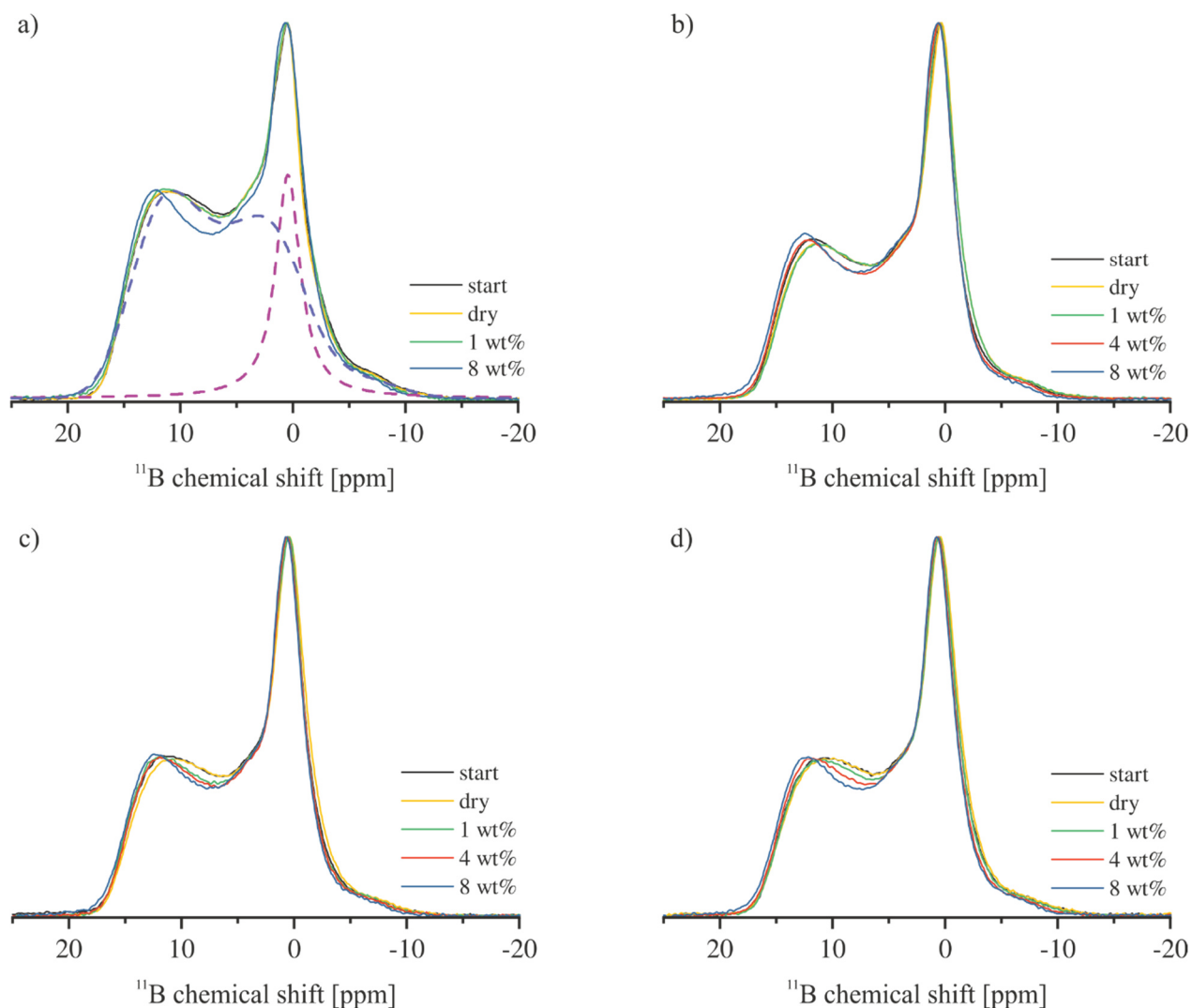


Figure 2.9: ^{11}B MAS-NMR spectra of NSB10 (a), NSB15 (b), NCSB15(1:1) (c) and NCSB15(1:2) (d). All spectra are normalized to the BO_4 resonance for comparison. Nominal water contents are indicated. Dashed lines in (a) show the applied spectra deconvolution of dry NSB10 glasses with a Lorentzian function at 0.5 ppm and a quadrupolar function at 11 ppm.

The relative abundance of tetrahedral boron in the glasses $N_4 = \text{BO}_4/(\text{BO}_3+\text{BO}_4)$ was determined by the fitted areas of the characteristic BO_3 and BO_4 resonances, respectively. It should be noted that these fits do not reflect the exact proportions of BO_3 and BO_4 in the glasses, as different quadrupolar interaction parameters of both species have influence on the signal intensities of the central transition [148]. For instance, the impulse response of a quadrupolar nucleus is strongly affected by the relationship of a quadrupolar interaction (C_Q) to the radio (rf)-frequency field. Here, BO_4 show no quadrupolar interaction with adjacent oxygens. In contrast, BO_3 shows a quadrupolar interaction. The quadrupolar parameters for BO_3 were derived from the fitted spectra and are in the range of $C_Q = 2.4 - 2.6$ MHz. In addition, quadrupolar interaction in MAS experiments leads to second-order residual effects that often affect spatial resolution. This effect depends strongly on the magnetic field [148]. At high

magnetic field strength, the resonances of BO_3 and BO_4 are separated from each other. At weaker field strengths both signals overlap and the BO_4 species can be systematically overestimated. However, the data (Fig. 2.12) show a low variance and a clear trend with increasing water content is visible. Based on internal consistency of our data, the accuracy of N_4 is better than 2%.

2.4. Discussion

4.1 Water species in silicoborate glasses

As known from literature, the relative abundance of water species depends on the glass composition. For instance, the intersection point, where the concentration of dissociated and molecular H_2O are the same, is at about 3-4 wt% total H_2O in (alumino)silicate glasses [84, 86, 106] and at about 6-7 wt% H_2O in borosilicate glasses [89, 149]. On the other hand, in borate glasses OH groups are the dominant species even at very high water content (approx. 8 wt%) [63]. Phosphate glasses are intermediate with respect to the abundance of molecular H_2O in the glasses, e.g. in lithium-magnesium-alumino phosphate glasses the intersection point is at approx. 8 wt% H_2O [110].

The compositions of our glasses are similar to a soda-lime-borate composition, studied by Bauer et al. [63], but with SiO_2 as additional component to reinforce the network. In all glass series of our study, the OH groups are the dominant species over the entire range of water content (Fig. 2.10), but compared to the borate glasses higher abundance of molecular H_2O is observed. Glasses of the NCSB15(1:2) series display the largest amount of molecular water, e.g., at 8 wt% total H_2O , 46% of dissolved water is incorporated in form of molecular water. Extrapolation of these data indicates an intersection point at 9-10 wt% total H_2O . For the other glass compositions, the point of intersection is not well constrained by the experimental data. Rough extrapolation indicates points of intersection of ~12 wt% for NSB15 and >15 wt% for NSB10 and NCSB15(1:1). In glasses with 15 mol% network modifiers, there appears to be a minimum in molecular H_2O abundance at a Na/Ca ratio close to 1:1, but data for additional compositions along the join are required to confirm this trend.

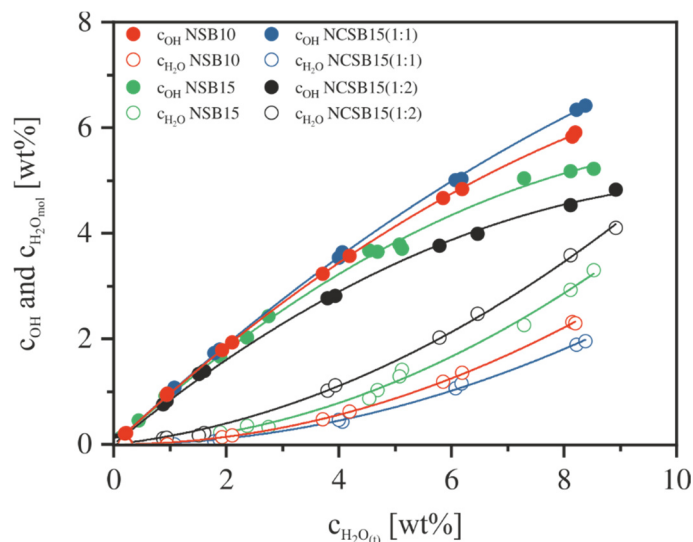


Figure 2.10: Water species concentration in silicoborate glasses as function of total water content. Error bars correspond to the size of the symbols.

Using the fictive temperatures of the glasses, trends can be established for water speciation in the melts. Studies on aluminosilicate glasses have proven the reliability of this approach [113] [112]. Fig. 2.11a shows the temperature dependence of the equilibrium constant K for water speciation in several melt compositions. Data of borates [63], silicates [127], and aluminosilicates [68, 84] are shown for comparison. Behrens and Yamashita [127] observed that K in sodium-silicates is higher than in polymerized aluminosilicates. They conclude that non-bridging oxygens charge-balanced by sodium promote the dissociation of dissolved water in silicate melts. In borate melts, which are virtually free of non-bridging oxygens, weakly bound oxygens between boron atoms support the formation of OH groups [63]. Equilibrium constants for silicoborate melts are in the range of borate melts, with the highest K values at given temperature for NCSB15(1:1) and the lowest ones for NCSB15(1:2). Comparing K values of our study with those of borate melts with similar boron contents (NCSB15(1:2) and NCB5, respectively) suggest that bridging oxygens between borate groups and silicon tetrahedra are more difficult to hydrolyze than bridging oxygens between two adjacent borate groups.

The effect of the type of network modifier on water speciation is illustrated in Fig. 2.11b for melts containing 15 mol% ($\text{Na}_2\text{O} + \text{CaO}$). The same trend is observed as for the glasses, i.e. the equilibrium constant has its minimum for a Na/Ca ratio close to 1:1. Thus, differences in water speciation in the glasses cannot be explained by differences in fictive temperatures.

The effect of CaO content on water speciation in silicoborate melts appears to be different to aluminosilicate melts. Ohlhorst et al. observed a systematic decrease of the K values by the addition of CaO for polymerized aluminosilicate melts, which was explained by a stabilization of molecular H_2O by bonding to Ca^{2+} [105]. In silicoborates, the incorporation of Ca^{2+} cations on expense of Na^+ favors the formation of OH groups until a Na/Ca ratio of 1:1 is reached. At higher Na/Ca ratio the trend reverses and the incorporation of molecular water is promoted.

Following [82, 150, 151] the standard enthalpy ΔH^0 for the water speciation reaction was calculated from the slope m of the straight line in Fig. 2.11a as $\Delta H^0 = R \cdot m$ where R is the universal gas constant. For Ca-free glasses ΔH^0 is $7.26 \pm 0.20 \text{ kJ}\cdot\text{mol}^{-1}$ (NSB10) and $2.95 \pm 0.11 \text{ kJ}\cdot\text{mol}^{-1}$ (NSB15). ΔH^0 for Ca bearing glasses is at $10.49 \pm 0.10 \text{ kJ}\cdot\text{mol}^{-1}$ (NCSB15(1:1)) and $7.29 \pm 0.12 \text{ kJ}\cdot\text{mol}^{-1}$ (NCSB15(1:2)), respectively. These values are in the range reported for borate glasses by Bauer et al. [63]. Compared to silicates and aluminosilicates ($25\text{-}35 \text{ kJ}\cdot\text{mol}^{-1}$) [68, 84, 111, 127], the reaction enthalpies are much lower. The lower reaction enthalpy for borates and silicoborates can be explained by weak B-O-B bonds, which are easily hydrolyzed.

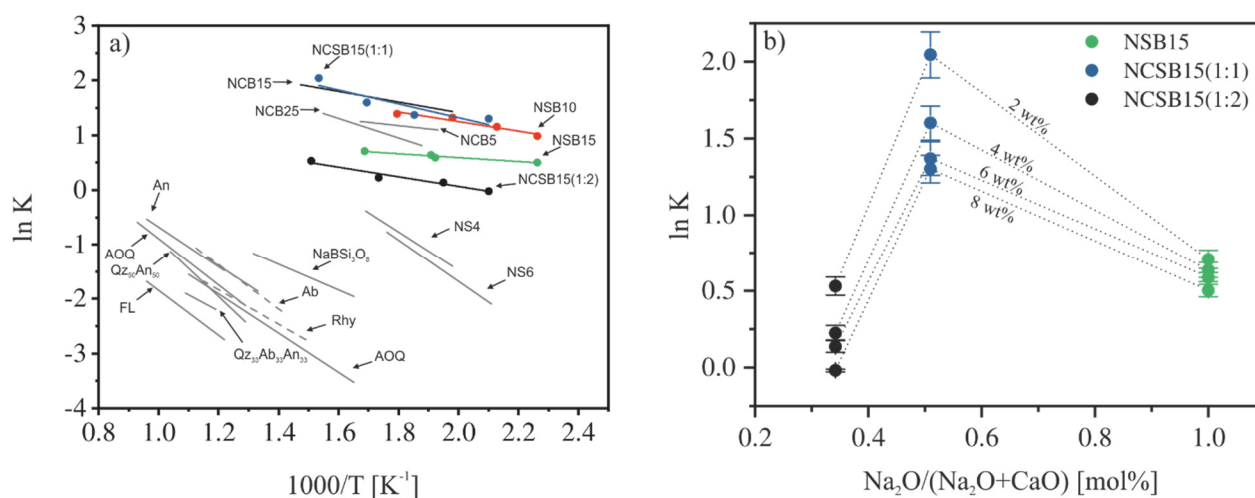


Figure 2.11: Comparison of equilibrium constants for water speciation in (alumino)-silicate, borate and silicoborate melts. Reference data marked in grey are from [63, 105, 112, 127, 138, 150-153]. Explanation of the acronyms: NCB (5, 15, 25) = $xNa_2O_{10}CaO_{90-x}B_2O_3$; NS4 = $Na_2O\text{-}4SiO_2$; NS6 = $Na_2O\text{-}6SiO_2$; Rhy = rhyolite; AOQ = $Na_{0.39}K_{0.31}Al_{0.69}Si_{3.31}O_8$; An = Andesite; Ab = $NaAlSi_3O_8$; $Qz_{33}Ab_{33}An_{33}$ = $Na_{0.5}Ca_{0.25}AlSi_3O_8$; $Qz_{50}An_{50}$ = $Ca_{0.5}AlSi_3O_8$; FL = Floatglass (a). Equilibrium constant K in dependence of alkali and alkaline earth content. Dashed lines are for guidance of the eye only (b).

2.4.2 Influence of water on boron speciation

^{11}B MAS NMR data show clear trends with increasing contents of alkali/alkaline earth oxides and water (Fig. 12). In nominally dry glasses N_4 is proportional to the sum of $\text{Na}_2\text{O} + \text{CaO}$ with negligible effect by replacing CaO for Na_2O . The effect of SiO_2 on boron coordination becomes evident when comparing our data with those reported by Bauer et al. [63] (Fig. 2.12). The slope for soda-lime borates (short-dashed line) is 1.6 whereas that of silicoborate glasses (dashed line) is 2. This means that every Na_2O (or CaO) incorporated into silicoborate glasses leads to the formation of one BO_4 tetrahedra and, according to Eq. (3), there are no non-bridging oxygens in the structure. In the case of NCSB15(1:1), this interpretation is supported by the pronounced molecular CO_2 band in MIR spectra of hydrous glasses (Fig. 2.4c). So far, molecular CO_2 has been only observed in highly polymerized silica and aluminosilicate glasses [134]. In soda lime borate glasses the formation of BO_4 tetrahedra is less efficient; each Na_2O (or CaO) produces only 0.8 BO_4 tetrahedron.

On a molar basis, the influence of water on the boron speciation is one order of magnitude lower than that of alkali and alkaline earth oxides. The slope of N_4 vs. mol H_2O in Fig. 2.12 slightly increases from 0.15 for NSB10 to 0.23 for NSB15 glasses. No significant change was observed when replacing CaO for Na_2O . As noted by Bauer et al. [63] in the study on borate glasses, the weak effect of H_2O on N_4 , indicates that protons cannot stabilize boron tetrahedra as effectively as alkalis. Due to its high ionic field strength, a proton is locally bound to one oxygen (OH-groups) and cannot form large O-polyeder.

A possible reason for the slight increase of N_4 with water content is the dramatic decrease of T_f upon hydration. Sen et al. [114] and Stebbins and Ellsworth investigated the effect of temperature on boron speciation in alkali borates, borosilicates and boroaluminate liquids. They observed that N_4 decreases at most weakly with increasing fictive temperature in glasses being nearly or totally free of NBOs. The temperature dependence is much more pronounced in glasses with high fractions of NBOs. In our glasses, the fraction of NBO is negligible and, hence, differences in fictive temperature are unlikely to explain the observed trends.

Another explanation for the increase in BO_4 on expense of BO_3 is that OH groups are incorporated between BO_3 groups, or in other words, protons are attached to bridging oxygen (B-OH-B). Such bridging OH groups have been proposed by Kohn and coworkers for hydrous sodium aluminosilicate glasses based on NMR spectroscopy [154-156]. It should be noted that the fraction of dissolved water present in form of OH bridges is small compared to terminal OH

groups (formed by hydrolysis of B-O-B bridges). In the NIR spectra, features of such species may be hidden by the broad and intensive combination bands of terminal OH groups. It is worth noting that the slope for N_4 upon hydration is similar for borate glasses and silicoborate glasses (Fig. 2.12). Therefore, we suggest that in both cases the same mechanism is responsible for the formation of tetrahedral boron and bridging OH groups may be present in hydrous borate glasses as well.

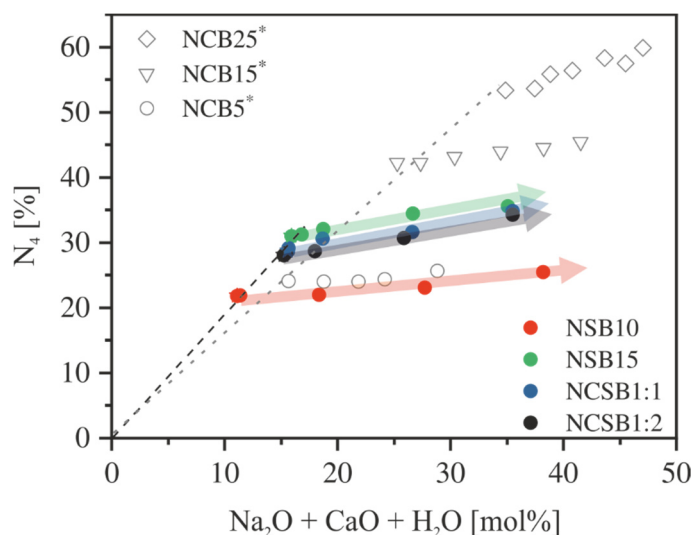


Figure 2.12: Fraction of tetrahedral coordinated boron (N_4) vs $Na_2O+CaO+H_2O$ content. Arrows show the effect of increasing water content. As a comparison, N_4 data of borate glasses are plotted in open grey symbols [63]. Explanation of the acronyms: NCB5 = $5Na_2O$ $10CaO$ $85B_2O_3$; NCB15 = $15Na_2O$ $10CaO$ $75B_2O_3$; NCB25 = $25Na_2O$ $10CaO$ $65B_2O_3$. Dashed lines refer to regression lines of anhydrous samples.

2.4.3 Compositional effects on the glass transition temperature

Consistent with other studies on borate glasses, addition of alkali oxide results in an increase of the glass transition temperature due to the increased N_4 value (Tab. 2.2) [63, 157, 158]. Substitution of Na_2O by CaO leads to a further increase of T_g due to higher ionic field strength and higher coordination number (CN) of Ca^{2+} ions compared to Na^+ ions. In oxide glasses CN is typically 7 for Ca^{2+} and 6 for Na^+ [158]. The corresponding field strength after Dietzel (defined as z/a^2 , with z = charge and a = distance between two ions) for these coordination numbers are $0.34/\text{\AA}^2$ and $0.19/\text{\AA}^2$, respectively [159]. The reinforcing effect of Ca^{2+} is visible also in silicoborate glasses, e.g. T_g increases from 704 K for NSB15 glass to 761 K for NCSB15 (1:2).

The influence of SiO₂ on T_g becomes evident by comparison of our data with soda-lime borate glasses [63, 108] and sodium borosilicate glass [89]. For anhydrous NCB5 glass Bauer et al. reported a T_g value of 697 K. The composition of this glass (5 mol% Na₂O, 10 mol% CaO, 85 mol% B₂O₃) is similar to our NCSB15(1:2) glass, except that 15 mol% B₂O₃ were replaced by SiO₂. The T_g value of dry NCSB15(1:2) glass is 761 K and thus 64 K higher than that of NCB5 glass, clearly pointing to the reinforcing effect of silicon tetrahedra in the network (Fig. 2.13a). As shown by ¹¹B MAS NMR data, the fraction of tetrahedral coordinated boron is also higher in silicoborate glasses than in borate glasses, amplifying the effect of SiO₂ incorporation. T_g values for anhydrous silicoborates are 86-198 K lower than for anhydrous sodium borosilicate. This can be explained by stronger Si-O-Si bonds compared to B-O-B bonds and by the low abundance of trigonal boron in the borosilicate.

The effect of water on the glass transition temperature is shown in Fig. 2.13a. Consistent with other studies [63, 66-68, 89], T_g decreases strongly upon hydration in particular at low water contents. The strong dependence on water content suggest that the hydrolysis of B-O-B bridges is more important for network relaxation than the slight increase of BO₄ tetrahedra.

In order to compare different glass compositions, reduced glass transition temperatures T_g^* were determined by normalization of T_g with the glass transition temperature of the nominally dry glasses. A three component model was proposed by Tomozawa et al. [160] and later on refined by Deubener et al. [161] to quantify the individual contributions of OH groups, molecular water and the dry glass on T_g using plots of T_g^* vs. water content (Fig. 2.13b). As shown by Behrens et al. [27] the contribution of molecular H₂O is very small or even negligible for oxide glasses. The effect of OH groups is in particular pronounced for polymerized aluminosilicate glasses and continuously decreases with increasing depolymerization. Data for borosilicate glasses fit nicely in the trend established for aluminosilicate and silicate glasses. On the other hand, the efficiency of OH groups in reducing T_g was found to be much smaller for borate glasses than for silica-rich glasses.

As shown in Fig. 2.13b, T_g^* values for soda-lime borates and silicoborates follows a similar trend and cover only a narrow range in plots of T_g^* vs. water content. The trend is clearly different from that of borosilicate glasses, which show a steep decrease at low water content and a lower dependence at high water content. These findings support the conclusions of Behrens et al. [27] that OH groups have much weaker effect on structural relaxation in borate glasses than in silica-dominated glasses. This is a consequence of much weaker B-O-B bonds compared to Si-O-Si bonds. For instance, the bond strength, based on the dissociation energy,

of a single B-O bond in a BO_4 tetrahedron ($89 \text{ kcal}\cdot\text{mol}^{-1}$) is weaker than the Si-O bond in a SiO_4 tetrahedron ($106 \text{ kcal}\cdot\text{mol}^{-1}$) [162]. In contrast, the B-O bond strength in a BO_3 triangle is slightly higher ($119 \text{ kcal}\cdot\text{mol}^{-1}$).

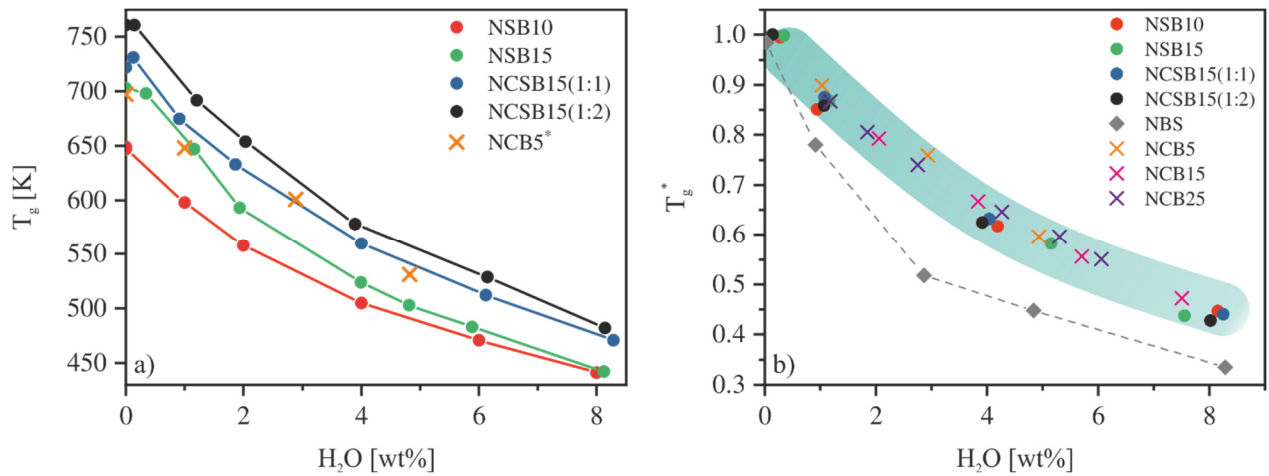


Figure 2.13: T_g values of silicoborate glasses in function of water content in comparison to borate glass NCB5 from [63] (a). Normalized T_g values for soda-lime borates [63], silicoborates and a sodium borosilicate [89]. The green area is the envelope for boron-dominated glasses (b).

2.5. Conclusion

The incorporation of SiO_2 in boron rich glasses leads to an enhanced interconnection of the network, which is further promoted by a larger fraction of BO_4 tetrahedra. The higher connectivity of the silicoborate network results in an increase of the T_g values by 50 - 60 K. While there is an effect of SiO_2 on melt relaxation, other structure-sensitive properties of silicoborate glasses resembles those of the corresponding borate glasses as four-fifths of network connection still consists of B-O-B bridges. Incorporation of water in the glass structure causes efficient breaking of such B-O-B bonds and OH groups are the predominant hydrous species in boron-rich glasses. Our findings confirm that the formed OH groups have much weaker effect on structural relaxation in borate glasses than in silica-dominated glasses. This is a consequence of much weaker B-O-B bonds compared to Si-O-Si bonds. Whereby the bond strength of a single B-O bond is higher in a BO_3 triangle compared to the B-O bond in a BO_4 tetrahedron. This implies, that fraction of N_4 has a greater impact on the relaxation mechanism compared to the fraction of BO_3 in our glasses. Considering the influence of SiO_2 and H_2O , our study improves the understanding of mechanical properties of boron-rich glasses with respect to water related fatigue.

Chapter 3

Water in alkali aluminosilicate glasses

Robert Balzer^{a,b}, Harald Behrens^{a,b}, Tina Waurischk^c, Stefan Reinsch^c, Ralf Müller^c, Philippe Kiefer^d, Joachim Deubener^d, Michael Fechtelkord^e

^a Leibniz Universität Hannover, Institute of Mineralogy, Callinstr.3, 30167 Hannover, Germany

^b ZFM-Center for Solid State Chemistry and New Materials, Leibniz Universität Hannover, Germany

^c Federal Institute for Materials and Testing (BAM), 12489 Berlin, Germany

^d Clausthal University of Technology, Institute of Non-Metallic Materials, 38678 Clausthal-Zellerfeld, Germany

^e Ruhr-Universität Bochum, Institute of Geology, Mineralogy and Geophysics, 44780 Bochum, Germany

This chapter is planned to be submitted to Journal of Non-Crystalline Solids

Abstract

In order to understand the influence of water on subaluminous aluminosilicate glasses, three glasses were synthesized, successively exchanging K₂O for Na₂O ((22.5-x)Na₂O xK₂O 22.5Al₂O₃ 55SiO₂ with $x = 0; 7.5; 11.25$). Subsequently, glasses were compacted (500 MPa) and hydrated (up to 8 wt% H₂O) using an IHPV. Densities of hydrous glasses show a linear decrease at water contents > 1wt%. NIR spectroscopy reveal that hydroxyl groups are the dominant species at low water contents (< 3 - 4 wt%), and then levels off, as the molecular water becomes the dominating species (> 3 - 4 wt%). ²⁷Al MAS-NMR shows that aluminum is exclusively four-fold coordinated (AlO₄), but also reveal local variations of the AlO₄ tetrahedra geometry, which become better arranged with increasing K₂O content. Incorporation of H₂O reinforces this effect, indicating that highly strained q⁴(4Si) species are eliminated by the formation of less polymerized q³(3Si) species. Differential thermal analysis of hydrous glasses show a significant mass loss in the regime of T_f implying that water in these glasses is highly mobile and is easily released. This is related to the bond strength of Si-O-Al and Si-O-Si, which are hard to hydrolyse.

3.1. Introduction

Ternary alkaline aluminosilicate glasses and melts make up a large and important group of materials, with a wide range of commercial applications [39, 42, 163]. The aluminum content in these glasses has a significant impact on chemical durability, hardness, tensile and compressive strength and thermal endurance [39].

Furthermore, these systems constitute more than 60% of most natural magmatic systems [163-165]. Of particularly great interest is the $\text{Na}_2\text{O}-\text{Al}_2\text{O}_3-\text{SiO}_2$ (NAS) system, since this system contains a number of geologically important minerals such as albite, jadeite and nepheline [45].

The structure and, thus the related properties of aluminosilicate glasses and melts mainly depend on the ratio between Al_2O_3 and the charge-balancing cation (M_2O or MO), as this determines the degree of polymerization of the structure [39]. For instance, in peralkaline NAS compositions ($\text{Na}/\text{Al} > 1$), all aluminum is present in tetrahedral coordination, where the charge deficit of Al^{3+} is compensated by the charge-balancing cation [45]. Excess charge-balancing cations play a network-modifying role. In subaluminous compositions ($\text{Na}/\text{Al} = 1$), all Al^{3+} is charge balanced and the structure is nearly fully polymerized forming exclusively AlO_4 tetrahedra [45, 166]. In peraluminous compositions ($\text{Na}/\text{Al} < 1$) with an excess of Al^{3+} , aluminum has a network-modifying role by forming AlO_6 octahedra [44, 45, 166]. Additionally, it has been suggested by Lacy et al. [48] and others [49, 167, 168] that the excess Al^{3+} forms triclusters by three AlO_4 tetrahedra sharing a common oxygen atom. Furthermore, it was found that the type of charge-balancing cation affects the formation of non-bridging oxygens and thus the degree of polymerization. For instance, in nearly fully polymerized subaluminous compositions it was found that the abundance of non-bridging oxygens increases in alkaline earth aluminosilicates compared to alkaline aluminosilicate glasses [39, 169]

Another important aspect that needs to be considered for the investigation of the structure of glasses and melts is the presence of water, which has dramatic effects on the structural and mechanical properties [170, 171].

Recent studies have shown that sodium silicate [23, 160, 172, 173], sodium aluminosilicate [174], soda-lime silicates [9], and commercial silicate glasses [111, 175] all exhibit changes in physical and mechanical properties together with substantial chemical effects on glass composition and micro-structural features directly influenced by the presence of water [176]. For example, water reduces the viscosity and increases the rates of structural relaxation

and phase separation of glasses [68, 177] and influences mechanical properties of glass by reducing mechanical strength and fatigue resistance [5, 17]. Moreover, the effect of water was found to be rather similar to that of alkali oxides in silicates and aluminosilicates [178, 179].

It is well known that water in glasses occurs as hydroxyl groups and as molecular water [78, 101, 111]. In melts, the interaction between molecular water and hydroxyl groups can be described by the following homogeneous reaction:



where O is an anhydrous oxygen. Assuming an ideal mixing of H₂O, O and OH species, the equilibrium constant K for the above reaction is:

$$K = \frac{[OH]^2}{[H_2O] \cdot [O]} \quad (3.2)$$

where square brackets indicate mole fractions calculated on a single oxygen basis. As a basic assumption, the measured water speciation in glasses at room temperature corresponds to the equilibrium water speciation in the melt, frozen-in at the fictive temperature (T_f) upon cooling [78, 83, 112].

Since OH and H₂O species behave differently within the structure of glasses and melts, it is clear that not only quantification of the dissolved water species but also understanding of the mechanisms of dissolution and incorporation within the silicate environment is of great importance for both material and earth sciences [106, 156]

This study is devoted to the investigation of the influence of different charge-balancing cations as well as the effect of water on the structure of aluminosilicate glasses, three different glasses (22.5- x)Na₂O x K₂O 22.5Al₂O₃ 55SiO₂ ($x = 0; 7.5; 11.25$) were prepared, wherein Na₂O was successively exchanged for K₂O. Variation of water contents of these highly polymerized glasses was achieved by high pressure- high temperature synthesis using an internally heated pressure vessel (IHPV). Fourier transformed infrared (FTIR) spectroscopy and nuclear magnetic resonance (NMR) spectroscopy were performed in order to analyze type of water speciation and the structural changes of the glass network upon hydration. Glass transition temperatures were derived from differential thermal analysis (DTA) providing information about the mobility of hydrous species in the glass structure. These findings may improve our understanding of corrosion as well as crack propagation mechanisms of glasses.

3.2. Experimental and Analytical Methods

3.2.1 Starting Materials

Three aluminosilicate glasses were prepared using Na_2CO_3 , K_2CO_3 , Al_2O_3 and SiO_2 powders. These powders were carefully mixed by hand and filled into a Pt-Rh10 crucible at 1773 K in a chamber furnace. Then temperature was raised to 1973 K (NAS glass) and 2023 K (NKAS glasses), respectively, and kept for 2 h. Afterwards the glasses were quenched by pouring out on a graphite plate. To achieve good homogeneity the glasses were re-melted under the same conditions. Clear bubble free glasses were obtained by this method.

The bulk compositions were analyzed using X-ray fluorescence spectrometry (XRF, PANalytical MagiX PRO, Almelo, Netherlands) equipped with a 4 kW Rh tube. Each measurement of bulk compositions with 20 mm and 17 mm in thickness and width, respectively, took about 10 min. For calibration, standard glasses NIST 1412, NIST 1411, NRS 93a, NBS 620 and BAM S005b were used.

In order to verify the XRF analyses, the bulk compositions were additionally analyzed using electron micro probe analyses (EMPA). Measurements were performed using a Cameca SX-100 microprobe with each glass measured 50 times at different positions to confirm homogeneity. Measurement conditions included a beam current of 15 nA, acceleration voltage of 15 kV, defocused beam of 5 μm spot size and counting times of 10 to 20 s. Both analytical methods yielded approx. the same values and revealed that all glasses are homogeneous. The nominal compositions have Na/Al and (Na+K)/Al ratios of 1 which is denoted as sub-aluminous glasses.

The measured compositions are very close to nominal compositions but all glasses show a slight excess of alkalis (Na/Al and (Na+K)/Al ratio > 1) and, thus, are denoted as peralkaline glasses Tab. 3.1.

Table 3.1: Nominal and analyzed composition of starting materials in mol% analyzed by XRF and EPMA.

	Na ₂ O	K ₂ O	Al ₂ O ₃	SiO ₂	Na/Al or (Na+K)/Al	
NAS	22.50	0.00	22.50	55.00	1.00	Nominal
	23.77 ± 0.15	0.12 ± 0.05	21.45 ± 0.08	54.67 ± 0.22	1.06	XRF
	23.14 ± 0.11	0.01 ± 0.01	21.28 ± 0.15	54.99 ± 0.18	1.08	EPMA
NKAS(2:1)	15.00	7.50	22.50	55.00	1.00	Nominal
	15.94 ± 0.21	7.70 ± 0.13	21.31 ± 0.21	55.06 ± 0.13	1.10	XRF
	15.63 ± 0.19	6.61 ± 0.09	21.71 ± 0.14	55.35 ± 0.21	1.02	EPMA
NKAS(1:1)	11.25	11.25	22.50	55.00	1.00	Nominal
	12.41 ± 0.17	11.59 ± 0.24	21.20 ± 0.11	54.80 ± 0.15	1.13	XRF
	12.21 ± 0.10	10.27 ± 0.18	21.16 ± 0.12	55.60 ± 0.10	1.06	EPMA

3.2.2 Hydrated and compressed glasses

Hydrated glasses with water content up to 8 wt% were prepared in platinum capsules. In order to achieve homogeneous initial water distribution, glass powder and distilled water were alternately added to the capsules. The powder-water mixture was compacted with a steel piston between loading steps to minimize air bubble inclusion. In order to obtain a cylindrical shape, round platinum lids were welded onto the open end of the capsules after loading. The capsules were ~25 mm in length and with inner diameter of 6 mm. Capsules were heated in a drying oven at 373 K for several hours and subsequently weighted to make sure no loss in weight occurred due to leakage.

Syntheses were performed in an internally heated pressure vessel (IHPV) at 500 MPa and 1523 - 1873 K for 20 h using Ar as pressure medium.

For experiments up to 1523 K, three capsules have been placed in the hot zone of a normal quench (NT) sample holder (controlled by K-Type thermocouples), pressurized and heated up to the desired p-T conditions. High temperature (HT) sample holder was used for experiments above 1523 K. Here, the capsule was attached to a Pt-wire and placed in the hottest zone of the sample holder (controlled by S-Type thermocouples). A detailed description of the vessel and procedures is given by Berndt et al. [60]. Samples were quenched isobarically to avoid pressure induced structural changes and to prevent water loss from hydrated glasses. The cooling rates in the regime of T_g was ~6-7 K/s for glasses performed in an HT sample holder and ~3.5 K/s for glasses synthesized in a NT sample holder.

After the experimental runs, all glass cylinders were transparent and contained neither bubbles nor crystals. To check for homogeneity of the water distribution in the glasses ~5 mm

thick slices have been cut from both ends of the cylinders. These glass pieces were subsequently analyzed by Karl-Fischer titration.

Due to the high melting temperatures of the starting glasses (1973 -2023 K), the anhydrous glasses were compacted using a cold seal pressure vessel (CSPV) with Ar as pressure medium. Therefore, cylindrical shaped samples were prepared from the starting glasses and placed in an autoclave [180]. Pressure of 500 MPa was applied to samples and externally heated furnace was pulled over the autoclave. The temperature was increased to 15 K above T_g (based on DTA measurements on starting glasses) and kept for 30 min. Afterwards the autoclave was removed from the furnace and isobarically cooled with a compressed air bell. All glass cylinders were transparent and had no visible changes to their appearance before the experiments.

3.2.3 Karl Fischer Titration

The total water content of hydrous glasses was determined by pyrolysis and subsequent by Karl-Fischer Titration (KFT). For this, ca. 10-15 mg of each glass was filled into small platinum crucibles and heated up rapidly to 1573 K. To avoid an explosive release of H₂O during heating, the crucibles were tightly bended on the top. A detailed description of the method is given by [61, 86, 126]. Results are shown in Tab 3.2a and b.

Table 3.2a: Sample characterization and spectroscopic data of NIR measurements on NAS and NKAS(2:1) glasses.

	CH ₂ O ₆ , KFT [wt%]	T _f [K]	T _g [K]	ρ [g/l]	d [mm]	Peak position [cm ⁻¹]			A ₅₂₀₀ [mm ⁻¹]	A ₄₅₀₀ [wt%]	COH [wt%]	CH ₂ O [wt%]	CH ₂ O ₆ , IR [wt%]
NAS _{start}	0.015 ± 0.002*	1003	1004	2473 ± 2	/	/	/	/	/	/	/	/	/
NAS _{dry} -I	0.015 ± 0.002*	1021	1015	2496 ± 1	0.296	/	/	4452	/	0.001	0.02	/	0.02
NAS _{dry} -II	0.014 ± 0.004*				0.305	/	/	4452	/	0.001	0.01	/	0.01
NAS 1-I	1.16 ± 0.08	967		2497 ± 2	0.295	4092	5187	4452	0.004	0.027	0.83	0.23	1.06
NAS 1-II	1.08 ± 0.07				0.298	4092	5187	4452	0.003	0.025	0.84	0.26	1.10
NAS 2-I	1.91 ± 0.09	914		2486 ± 2	0.293	4089	5187	4452	0.019	0.045	1.60	0.65	2.25
NAS 2-II	2.11 ± 0.07				0.291	4089	5187	4452	0.022	0.046	1.67	0.71	2.38
NAS 4-I	4.03 ± 0.12	787		2449 ± 3	0.293	4073	5187	4452	0.070	0.060	2.41	1.70	4.11
NAS 4-II	3.78 ± 0.09				0.293	4073	5187	4452	0.062	0.059	2.37	1.50	3.87
NAS 6-I	5.62 ± 0.09	701		2421 ± 3	0.293	4060	5187	4452	0.112	0.063	2.76	2.45	5.21
NAS 6-II	5.66 ± 0.08				0.293	4060	5187	4452	0.117	0.063	2.81	2.61	5.42
NAS 8-I	8.29 ± 0.14	651		2382 ± 3	0.296	4053	5187	4452	0.242	0.070	3.29	5.97	9.26
NAS 8-II	7.51 ± 0.09				0.301	4053	5187	4452	0.188	0.077	3.11	4.57	7.68
NKAS(2:1) _{start}	0.019 ± 0.002*	1004	996	2482 ± 2	/	/	/	/	/	/	/	/	/
NKAS(2:1) _{dry} -I	0.020 ± 0.002*	1013	1017	2500 ± 2	0.301	/	/	4447	/	0.001	0.01	/	0.01
NKAS(2:1) _{dry} -II	0.020 ± 0.003*				0.297	/	/	4447	/	0.001	0.01	/	0.01
NKAS(2:1) 1-I	1.20 ± 0.13	984		2491 ± 1	0.307	4088	5185	4447	0.006	0.033	0.64	0.30	0.94
NKAS(2:1) 1-II	0.95 ± 0.09				0.301	4088	5185	4447	0.005	0.032	0.68	0.33	1.01
NKAS(2:1) 2-I	2.08 ± 0.06	863		2477 ± 1	0.297	4074	5185	4447	0.026	0.050	1.12	0.71	1.83
NKAS(2:1) 2-II	1.88 ± 0.06				0.298	4074	5185	4447	0.021	0.049	1.19	0.80	1.99
NKAS(2:1) 4-I	3.71 ± 0.11	707		2446 ± 2	0.302	4061	5185	4447	0.088	0.065	1.79	2.33	4.12
NKAS(2:1) 4-II	4.17 ± 0.06				0.305	4061	5185	4447	0.095	0.065	1.78	2.47	4.25
NKAS(2:1) 6-I	6.11 ± 0.10	621		2411 ± 5	0.309	4049	5185	4447	0.166	0.065	2.05	4.32	6.37
NKAS(2:1) 6-II	5.61 ± 0.11				0.295	4049	5185	4447	0.152	0.068	2.05	4.21	6.26
NKAS(2:1) 8-I	7.71 ± 0.10	460		2374 ± 4	0.312	4043	5185	4447	0.219	0.064	2.15	5.63	7.78
NKAS(2:1) 8-II	8.29 ± 0.13				0.302	4043	5185	4447	0.245	0.060	2.18	6.45	8.63

Table 3.2b: Sample characterization and spectroscopic data of NIR measurements on NKAS(1:1) glasses.

	CH ₂ O ₆ , KFT [wt%]	T _f [K]	T _g [K]	ρ [g/l]	d [mm]	Peak position [cm ⁻¹]			A ₅₂₀₀ [mm ⁻¹]	A ₄₅₀₀ [wt%]	COH [wt%]	CH ₂ O [wt%]	CH ₂ O ₆ , IR [wt%]
NKAS(1:1) _{start}	0.013 ± 0.003*	1037	1038	2475 ± 3	/	/	/	/	/	/	/	/	/
NKAS(1:1) _{dry} -I	0.013 ± 0.003*	1025	1023	2493 ± 1	0.301	/	/	4445	/	0.001	0.01	/	0.01
NKAS(1:1) _{dry} -II	0.015 ± 0.002*				0.297	/	/	4445	/	0.001	0.01	/	0.01
NKAS(1:1) 1-I	1.25 ± 0.11	992		2491 ± 3	0.301	4084	5182	4445	0.004	0.027	0.65	0.25	0.90
NKAS(1:1) 1-II	1.01 ± 0.12				0.300	4084	5182	4445	0.005	0.028	0.72	0.27	0.99
NKAS(1:1) 2-I	1.93 ± 0.14	848		2475 ± 1	0.298	4068	5182	4445	0.019	0.045	1.27	0.65	1.92
NKAS(1:1) 2-II	2.23 ± 0.12				0.298	4068	5182	4445	0.022	0.045	1.24	0.71	1.95
NKAS(1:1) 4-I	3.90 ± 0.11	711		2445 ± 3	0.302	4053	5182	4445	0.082	0.059	1.99	2.18	4.17
NKAS(1:1) 4-II	4.15 ± 0.09				0.305	4053	5182	4445	0.088	0.059	1.97	2.33	4.30
NKAS(1:1) 6-I	5.79 ± 0.11	594		2405 ± 2	0.311	4046	5182	4445	0.135	0.059	2.34	3.61	5.95
NKAS(1:1) 6-II	5.81 ± 0.11				0.293	4046	5182	4445	0.135	0.056	2.35	3.83	6.18
NKAS(1:1) 8-I	7.45 ± 0.08	460		2370 ± 4	0.320	4031	5182	4445	0.208	0.065	2.44	5.45	7.89
NKAS(1:1) 8-II	8.47 ± 0.11				0.312	4031	5182	4445	0.234	0.064	2.66	6.29	8.95

Notes: I and II in the sample name refer to pieces cut from both ends of the synthesized glass body. Subscripts “start” indicate the glass melted at ambient pressure, subscript “dry” refers to the nominally dry glass after high pressure synthesis. The last number in the sample indicates the nominal water content in wt%. Water contents are measured by KFT, except for data marked by *, which were obtained by MIR spectroscopy. Fictive temperatures T_f of glasses were determined by the first upscan of DTA and glass transition temperatures T_g are averages from three following upscans of DTA. Uncertainties are ± 2K. Peak positions (± 5 cm⁻¹) and absorbances (± 0.002) of NIR combination bands were determined after linear baseline corrections, see text for detail

3.2.4 Differential thermal analysis

The fictive temperature T_f and the glass transition temperature, T_g , were determined by differential thermal analyses in air using 15-20 mg of glass pieces placed in Pt crucibles (thermobalance TAG 24 Setaram, Caluire, France). Same kind of measurement and data evaluation was applied e.g. to hydrous borate [63, 108] and phosphate [110] glasses.

For each sample, four heating and cooling cycles at 10 K min^{-1} were applied where the first cycle corresponds the fictive temperature T_f of the samples, since the sample cooling history reflects the status of quenching after the IHPV synthesis. T_g of starting and dry glasses was determined by the following three cycles. Definition of T_f and T_g is based on the onset of the endothermic step in the DTA curve according [64, 65].

It should be mentioned that T_g values could not be determined for hydrous samples, as a massive loss of water occurred when T_f was reached or this temperature was slightly exceeded by about 10 – 20 K. T_f -values and the average values of T_g (anhydrous glasses) are shown in Tab. 3.2a and 3.2b and are similar to values of albite glasses (1036 K) as reported by Arndt et al. [181]. In all samples, T_f decreases with increasing water content. This behavior is consistent with the observations made on silicate, aluminosilicate, borosilicate and borate glasses [27, 63, 67, 108, 112, 127, 128].

3.2.5 IR spectroscopy

In order to obtain information about the network structure of the glasses, MIR spectra of KBr pressed pellets in the range from 370 to 4000 cm^{-1} were collected using a Fourier Transform Infrared (FTIR) spectrometer (Bruker Vertex 80v). The spectrometer is equipped with a globar light source, a KBr beam splitter and a pyroelectric deuterated, L-alanine doped triglycerine sulfate (DLaTGS) detector. For this purpose, 1 mg glass powder and 199 mg KBr were mixed and pressed into a pellet at 100 kN. A pure KBr pellet was measured as reference to examine the contribution of contamination of KBr to the spectrum in the range of OH stretching vibrations.

Additionally, mid-infrared spectra have been measured on double-polished glass sections using a FTIR spectrometer (Bruker IFS 88). The spectrometer is linked with an IR microscope Bruker IR scope II equipped with a mercury-cadmium-tellurium (MCT) detector. Absorption spectra in the mid-infrared (MIR) were recorded to investigate the fundamental OH stretching

vibrations. The spectra were measured in a range between 600 and 6000 cm^{-1} using a KBr beam splitter and a globar light source with a spectral resolution of 2 cm^{-1} . For each sample and background (air) measurement 50 scans were accumulated.

Near-infrared (NIR) spectra were recorded to determine the water speciation in the glasses. Here, the same set-up was used as for MIR measurements on thin sections except that a tungsten light source and a CaF_2 beam splitter have been used. The spectral resolution was 4 cm^{-1} , and for each spectrum, 100 scans were accumulated. In order to guarantee good reproducibility and homogeneous water distribution, pieces of each glass cylinder were cut off from the top and bottom, and each sample was analyzed at least three times at different positions. Sample thickness was determined using a digital micrometer (Mitutoyo Absolute) with a precision of $\pm 2 \mu\text{m}$.

3.2.6 ^{27}Al MAS-NMR spectroscopy

In order to analyze the distribution of the Al coordination in our glasses, ^{27}Al MAS-NMR spectra were acquired on selected samples (anhydrous and 8wt% H_2O) at room temperature using a Bruker ASX 400 WB spectrometer. Measurements were performed at a Larmor frequency of 104.27 MHz using a standard Bruker 4 mm probe with a spinning of 12.5 kHz. AlCl_3 (1M) was processed as secondary reference standard. To ensure homogeneous excitation a single pulse duration of 0.6 μs was applied. The recycle delay was 0.1 s and 16000 scans were accumulated. ^{27}Al spectra were processed using DMFit 2015 program [129].

3.3. Results

3.3.1 Water distribution in the glasses

The first column of Table 3.2a, b lists total water content data measured by KFT on both ends of the sample (I and II). The average water content of the respective samples of NAS, NKAS(2:1) and NKAS(1:1) corresponds to the calculated water content, indicated by the sample code. The deviation between the top and the bottom pieces of the samples is not significant for glasses with $< 4 \text{ wt}\% \text{ H}_2\text{O}$ and is within the range of analytical error. In contrast, the deviation is more distinct in samples with water contents above 4 wt%. These deviations could be the result of an initial inhomogeneous water distribution during the sample preparation. And as reported by Zhang et al. [113], the water diffusion in oxide melts is too slow to achieve

a homogeneous water distribution over the entire glass body by diffusion within the synthesis process [130].

In the following we refer to the average of KFT data for analytical bulk methods (e.g. density). For local methods (e.g. IR), we used KFT measurements on pieces taken just next to the analysis points.

3.3.2 Density

Densities of anhydrous glasses compacted at 500 MPa (diamond) are increased by approx. 1% compared to glasses melted at ambient pressure (star). (Fig. 3.1a). The increase in density upon compression in anhydrous glasses is similar to values for silicate and aluminosilicate glasses as reported e.g. by Wondraczek et al. [69, 70]. Addition of < 1 wt% water shows no significant change in densities of NAS and NKAS(1:1) glasses, while the decrease in density in NKAS(2:1) is more evident. The linear behavior at water contents > 1 wt% is consistent with ideal mixing of oxide glass and water, as also found for silicate glasses [71]. According to Richet [71] and Bouhifd [72], partial molar volume of water is directly obtained by the intercepts of tangents fitted to our data (Fig. 3.1b). Molar volumes of our glasses (NAS: $11.8 \pm 0.1 \text{ cm}^3 \cdot \text{mol}^{-1}$; NKAS(2:1): $12.0 \pm 0.1 \text{ cm}^3 \cdot \text{mol}^{-1}$; NKAS(1:1): $12.1 \pm 0.2 \text{ cm}^3 \cdot \text{mol}^{-1}$) are constant over the studied range of water contents and in good agreement with values reported for silicate and aluminosilicate glasses ($11.5 - 12.5 \text{ cm}^3 \cdot \text{mol}^{-1}$) [71].

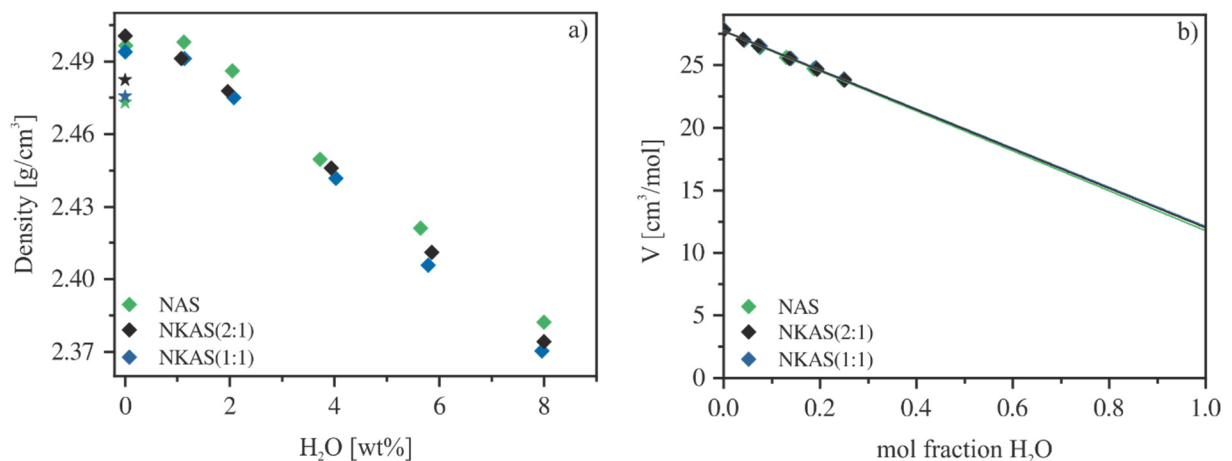


Figure 3.1: Density of aluminosilicate glasses. Densities of starting glasses (1 atm) are marked with a star symbol. Compacted glasses (500 MPa) are marked with diamond symbols (a). Partial molar volume of hydrous glasses. Differences in the respective mole fractions are smaller than symbol size (b). Errors are smaller than symbol size.

3.3.3 MIR spectroscopy

MIR spectra of aluminosilicate glasses (NAS; NKAS(2:1) and NKAS(1:1)) in KBr pressed pellets in the frequency range between 400 and 4000 cm^{-1} are shown in Fig 3.2. The spectra can be divided into two areas. First area comprises, lattice vibrations in the range between 400 and 1250 cm^{-1} while the second comprises, the OH-related stretching vibration in the range between 3250 and 3700 cm^{-1} [77, 78].

In the first area with lattice vibrations, three main bands are clearly visible. The absorption band at $\sim 450 \text{ cm}^{-1}$ is related to bending vibration of Si-O-Si and Si-O-Al linkages [182, 183]. The $\sim 700 \text{ cm}^{-1}$ band is associated with the symmetric stretching vibration of Si-O-Al bonds between SiO_4 and AlO_4 tetrahedra [182-185] while the band at $\sim 998 \text{ cm}^{-1}$ corresponds to the asymmetric stretching vibration of Si-O-Al bonds [182, 183, 185, 186].

A closer look at the band structures in this region reveals some differences in peak position and shape, caused by different content of network modifier and water. For instance, the bands at $\sim 450 \text{ cm}^{-1}$ and $\sim 700 \text{ cm}^{-1}$ in anhydrous glasses shift slightly to lower wavenumbers as the K_2O content is increased on expense of Na_2O . The peak position of the 998 cm^{-1} band is the same in all three anhydrous glasses.

The addition of water results in some changes in the structure of the MIR bands. In pure sodium aluminosilicate glasses (Fig 3.2a), the peak at 458 cm^{-1} (dry glass) shifts to 448 cm^{-1} (8 wt%) and its intensity decreases, while the peak at 702 cm^{-1} (dry glass) shifts to 708 cm^{-1} (8 wt%). The intensity of the latter remains unchanged. Peak position and intensity of the 996 cm^{-1} band is constant, but at water contents above 4 wt% a shoulder at $\sim 854 \text{ cm}^{-1}$ is formed that is related to SiOH groups. In addition, a small peak at 575 cm^{-1} evolves at water contents above 4 wt%. According to [183-185], this peak is related to stretching vibrations of four and six-membered rings systems of Si-O and Al-O tetrahedra.

Similar trends upon hydration are visible in NKAS(2:1) and NKAS(1:1) glasses (Fig. 3.2b and c). Addition of water results in a peak shift and decrease of intensity of the 456 cm^{-1} band (dry glass) to 446 cm^{-1} (8 wt%) (NKAS(2:1)) and from 454 cm^{-1} to 444 cm^{-1} (NKAS(1:1)), respectively. In NKAS(2:1) glasses, the band of the symmetric stretching vibration of Si-O-Al bonds shifts from 698 cm^{-1} (dry glass) to 706 cm^{-1} (8 wt%). In NKAS(1:1) glasses this peak shifts from 696 cm^{-1} (dry glass) to 704 cm^{-1} (8wt%). At 4 wt% the formation of the SiOH shoulder is visible at 852 cm^{-1} (NKAS(2:1)) and 850 cm^{-1} (NKAS(1:1)), respectively, while the peak position and intensity of the main absorption band at 996 cm^{-1} does not change. As in NAS

glasses the peak at 575 cm^{-1} becomes visible. However, these features are more pronounced in the mixed alkali glasses (Fig. 3.2b and c) than in the sodium aluminosilicate glasses (Fig. 3.2a).

As water content is increased a small peak in the range of 1650 cm^{-1} appears which becomes more visible at water contents above 4 wt%. According to [83, 101] this peak is caused by the bending vibration of H_2O . In the high wavenumber range broad bands between 3250 cm^{-1} and 3700 cm^{-1} are visible in all glasses with a maximum at 3400 cm^{-1} and a small shoulder towards lower wavenumbers. These bands are related to OH stretching vibrations of weakly to moderately H-bound hydrous species [77, 78, 101] and become more pronounced with increasing water content. These broad bands indicate that the KBr pressed pellets are sensitive to water adsorption during sample preparation, thus, we cannot obtain reliable information of water bands using this method.

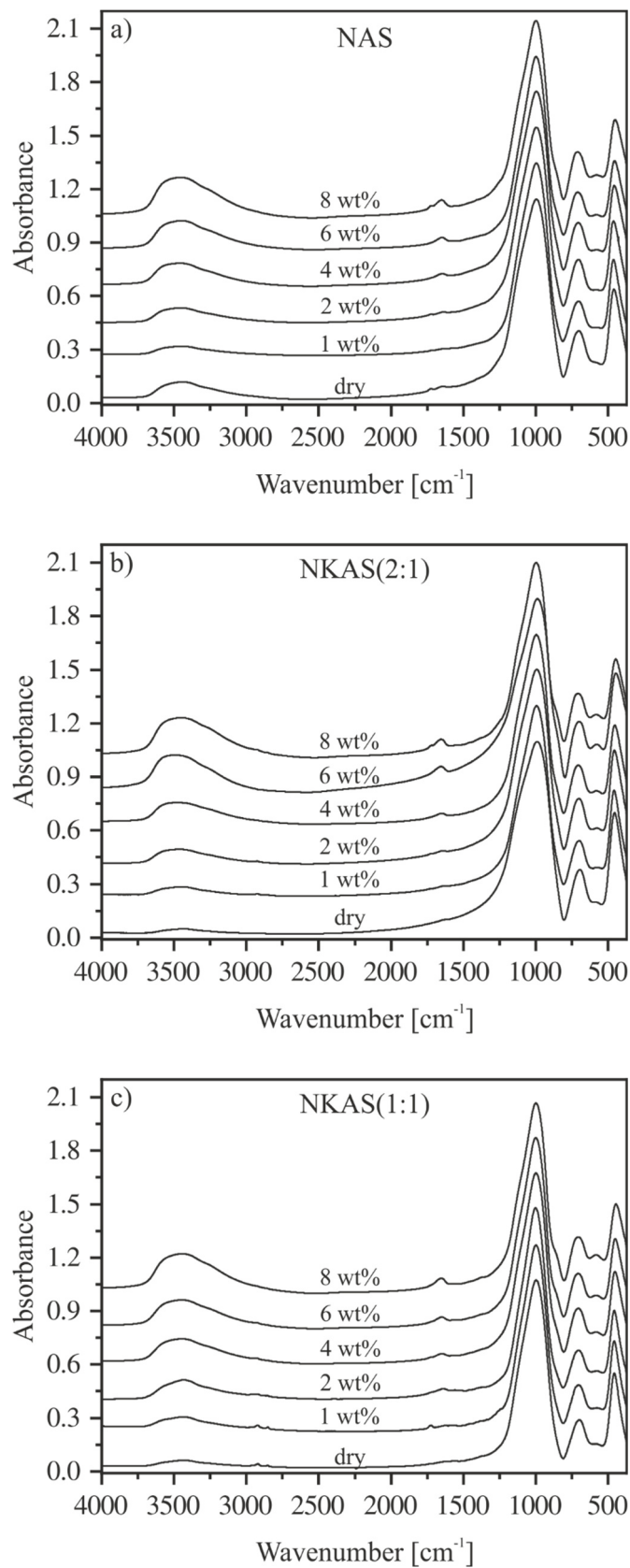


Figure 3.2: MIR spectra of KBR pressed pellets of NAS (a), NKAS(2:1) (b) and NKAS(1:1) (c). Spectra were normalized to absorption peak of $\sim 996 \text{ cm}^{-1}$ and shifted vertically for clarity. Nominal water contents are indicated.

In order to get more detailed information of structural incorporation of water in the glass structure, MIR spectra of thin sections (approx. 80 μm) for glasses containing < 2 wt% H_2O were recorded. Fig. 3.3 show examples of these MIR measurements on NAS glasses.

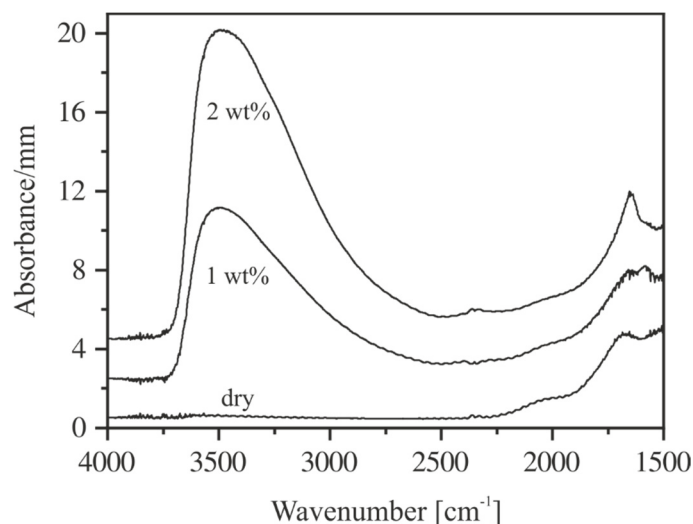


Figure 3.3: MIR spectra of thin section of NAS containing 0-2 wt% H_2O . Irregularities at 2350 cm^{-1} are due to differences in CO_2 during background and sample measurements. Spectra are shifted vertically for clarity. Nominal water contents are indicated.

In the range of OH stretching vibrations, the absorption spectra of hydrous NAS glasses resemble spectra of other aluminosilicate glasses, e.g. [77, 135, 176, 187, 188] with the peak near 3500 cm^{-1} and an asymmetric tailing towards lower wavenumber. These features are characteristic for weakly H-bonded hydrous species in glasses [78, 101, 111, 133]. At water contents above 1 wt% the sharp bend of bending vibrations of H_2O molecules develops at 1650 cm^{-1} which is superimposed by a wide broad band system originating for glass network vibrations [77, 78, 83, 86, 140]. MIR spectra of NKAS(2:1) and NKAS(1:1) glasses are similar to NAS glasses. In order to separate the water-related peaks from the network vibration features, the spectrum of each dry glass was subtracted from the spectra of water bearing glasses, as shown in Fig. 3.4. After subtraction, the bands at 3500 cm^{-1} and 1650 cm^{-1} remain and become better resolved. In NAS glasses containing 1 wt% H_2O the peak at 1650 cm^{-1} peak is most pronounced (Fig. 3.4a) while the intensity of this peak decreases with increasing K_2O content (Fig. 3.4b and 3.4c). In glasses containing 2 wt% H_2O the intensity of this peak is similar in all glasses.

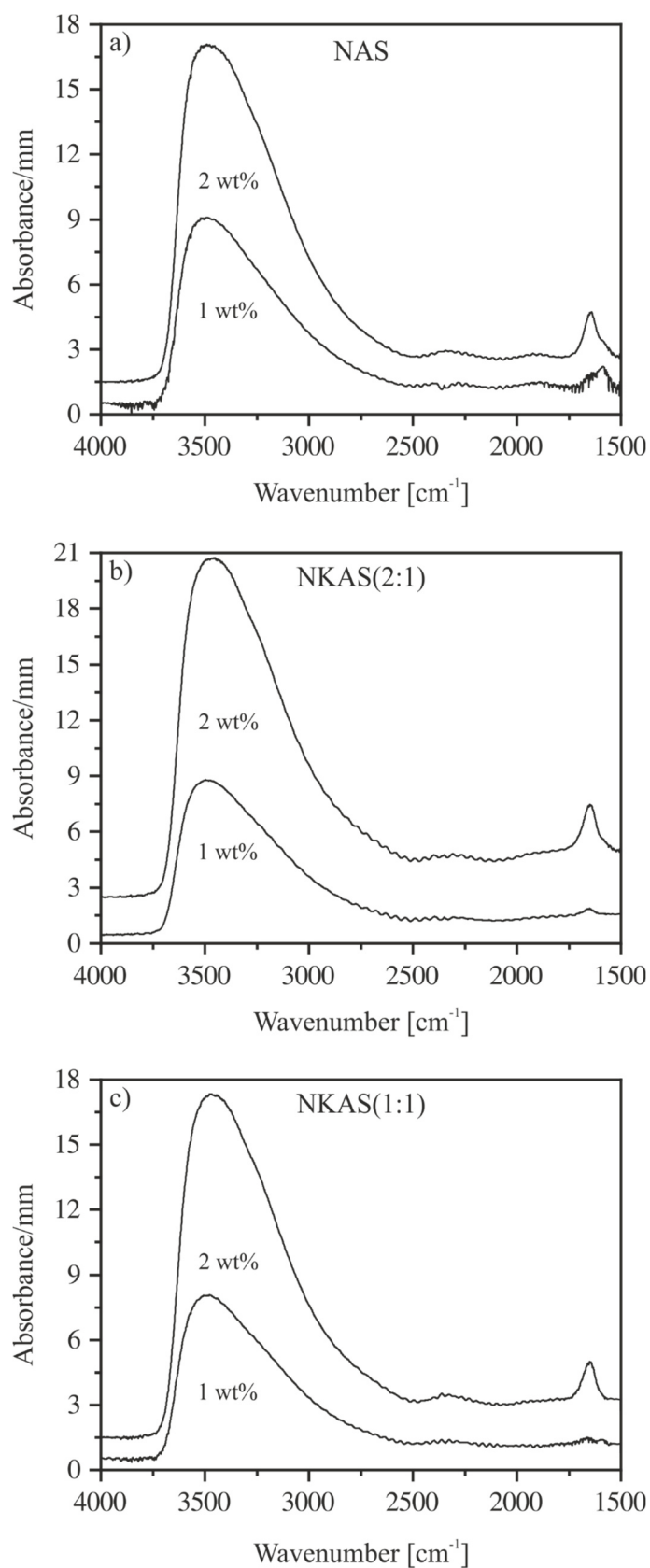


Figure 3.4: Subtraction spectra of NAS (a), NKAS(2:1) (b) and NKAS(1:1) (c) demonstrate the water related peaks at 3500cm^{-1} and 1650cm^{-1} . Spectra were normalized to sample thickness and shifted for clarity.

In order to quantify water contents of nominally dry glasses (Tab. 3.2a and b), linear molar absorption coefficients for glasses containing up to 2 wt% were determined for the band at 3500 cm^{-1} (Tab. 3.3). The absorbance at the peak maximum is related to the total water content measured by KFT. This approach is justified since the intensity ratio of the water-related bands is mainly constant. The total water content of $\text{c}_{\text{H}_2\text{O}_t}$ is given as

$$c_{\text{H}_2\text{O}_t} = \frac{1802 \cdot A_i}{\rho \cdot d \cdot \varepsilon} \quad (3)$$

where A_i refers to the absorbance of the band at 3500 cm^{-1} , ρ to the density in $\text{g} \cdot \text{L}^{-1}$, and d to the sample thickness in cm. The values of the linear molar absorption coefficient are decreasing in our glasses when Na_2O is substituted for K_2O . Compared to other aluminosilicate glasses the linear molar absorption coefficient of ε_{3500} are relatively low. For instance, in fully polymerized albite glasses, Silver et al. [189] and Yamashita et al. [190] determined a value for ε_{3500} of 70 $\text{L} \cdot \text{mol}^{-1} \cdot \text{cm}^{-1}$. In rhyolite compositions, ε_{3500} values between 88 $\text{L} \cdot \text{mol}^{-1} \cdot \text{cm}^{-1}$ and 100 $\text{L} \cdot \text{mol}^{-1} \cdot \text{cm}^{-1}$ [140, 190] and in basaltic compositions 65 $\text{L} \cdot \text{mol}^{-1} \cdot \text{cm}^{-1}$ [190, 191] were obtained. ε_{3500} values of our glasses are similar to values reported for float glasses ($\sim 40 \text{ L} \cdot \text{mol}^{-1} \cdot \text{cm}^{-1}$) as determined by Harder et al. [111] and others [192]. These variations in ε_{3500} can be caused by different degrees of polymerization, e.g. between rhyolite and basalt glasses where ε decreases with increasing depolymerization [135], or by different SiO_2 contents [90]. But, since the degree of polymerization of our glasses is comparable with that of albite glasses, our values are only lower due to the higher alkali content.

Table 3.3: Average values of the linear molar absorption coefficient ε for water related bands in aluminosilicate glasses.

	MIR		NIR	
	ε_{3500} [$\text{L} \cdot \text{mol}^{-1} \cdot \text{cm}^{-1}$]	ε_{4050} [$\text{L} \cdot \text{mol}^{-1} \cdot \text{cm}^{-1}$]	ε_{4450} [$\text{L} \cdot \text{mol}^{-1} \cdot \text{cm}^{-1}$]	ε_{5200} [$\text{L} \cdot \text{mol}^{-1} \cdot \text{cm}^{-1}$]
NAS	52.7 ± 2.7	0.20 ± 0.02	0.62 ± 0.15	1.03 ± 0.07
NKAS(2:1)	50.7 ± 1.9	0.18 ± 0.04	0.88 ± 0.09	0.91 ± 0.09
NKAS(1:1)	41.9 ± 3.1	0.15 ± 0.03	0.72 ± 0.06	0.90 ± 0.05

Notes: Errors represent the standard deviation ($n=3$)

Nominally dry glasses contain a small amount of water, whereas the content is the same for starting (1 atm) and compacted glasses (500 MPa). We obtained a water content of $0.015 \pm 0.002 \text{ wt}\%$ (NAS), $0.019 \pm 0.005 \text{ wt}\%$ NKAS(2:1) and $0.0013 \pm 0.03 \text{ wt}\%$ NKAS(1:1), respectively (Tab. 3.2a,b). These values are typical for aluminosilicate glasses melted at air [101].

3.3.4 NIR spectroscopy

NIR spectra of NAS, NKAS(2:1) and NKAS(1:1) containing up to 8 wt% H₂O are shown in Fig. 3.5. Strong absorption bands at ~5200 cm⁻¹, ~4450 cm⁻¹ and ~4050 cm⁻¹ are visible in the range between 6000 and 3700 cm⁻¹. Analogue to silica glasses, the band at 4050 cm⁻¹ is attributed to the combination of OH stretching vibration with a lower frequency lattice vibration [63, 77, 89, 193]. The absorption band near 4500 cm⁻¹ is related to the combination of stretching and bending of hydroxyl groups connected to tetrahedrally coordinated silicon (Si-OH) [61, 77, 82, 193]. This assignment is supported by MIR spectra (Fig. 3.4). As the band at 4500 cm⁻¹ results from a combination of OH stretching vibration at 3500 cm⁻¹ and the Si-O stretching vibration at 1000 cm⁻¹ (Fig. 3.4).

The absorption band at 5200 cm⁻¹ is related to the combination of stretching and bending modes of H₂O molecules [83-86]. All these bands are visible at water contents > 1 wt%, whereby their intensities increase with increasing water content. The peaks of ~4050 cm⁻¹, ~4500 cm⁻¹ and ~5200 cm⁻¹ are shifting towards lower wavenumber when the K₂O content is increased at expense of Na₂O. A peak shift upon hydration is not observed in any peak (Tab. 3.2a and b).

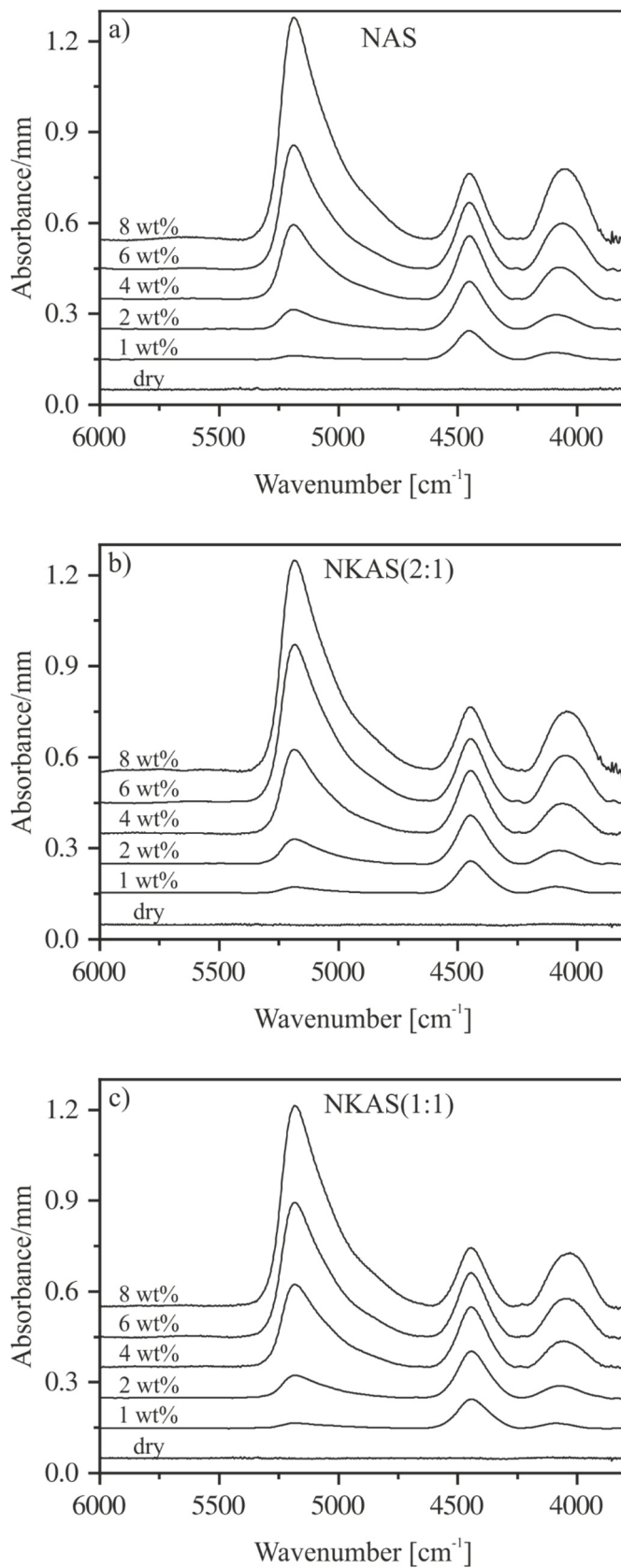


Figure 3.5: Baseline corrected NIR spectra of NAS (a), NKAS(2:1) (b) and NKAS(1:1) (c) containing 0-8 wt% H₂O. Spectra were normalized to sample thickness and vertically shifted for clarity. Nominal water contents are indicated.

In order to use NIR bands for the determination of species concentrations and the total water contents of the glasses, the choice of baseline is crucial. As discussed by Withers and Behrens on aluminosilicate glasses, it is mandatory that the baseline has a high reproducibility [87]. The highest reproducibility for our glasses was found for tangential baselines as illustrated in Fig. 3.6.

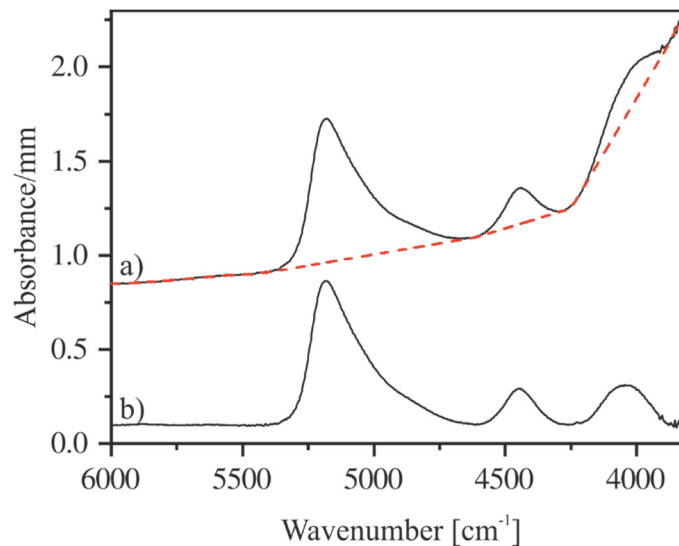


Figure 3.7: Measured NIR spectrum of NKAS(2:1) 8-I with the applied tangential baseline (red dashed line) (a). Corresponding baseline corrected spectrum (b). Spectra are shifted for clarity.

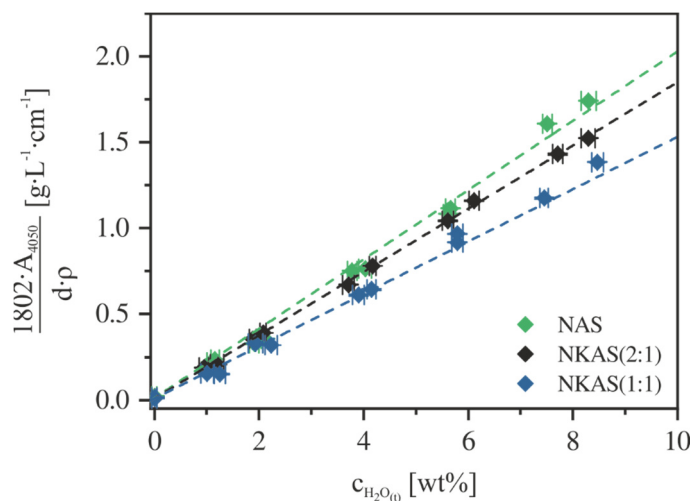


Figure 3.6: Absorbance of the 4050 cm⁻¹ absorption band normalized to density and sample thickness as a function of H₂O content analyzed by KFT.

As shown in Fig. 3.7, the absorbance of the $\sim 4100 \text{ cm}^{-1}$ band, normalized to sample thickness and density, is proportional to the total water content. This linear correlation indicates that both OH groups and H_2O molecules contribute to this band. The linear molar absorption coefficient (ϵ_{4100}) of this band was derived by the slope of data points and decreases when Na_2O is replaced by K_2O (NAS: $0.20 \pm 0.02 \text{ L}\cdot\text{mol}^{-1}\cdot\text{cm}^{-1}$; NKAS(2:1): $0.18 \pm 0.04 \text{ L}\cdot\text{mol}^{-1}\cdot\text{cm}^{-1}$; NKAS(1:1): $0.15 \pm 0.03 \text{ L}\cdot\text{mol}^{-1}\cdot\text{cm}^{-1}$) (Tab. 3.3). These values are much lower than those determined for rhyolite ($0.68 \text{ L}\cdot\text{mol}^{-1}\cdot\text{cm}^{-1}$), basalt ($0.51 \text{ L}\cdot\text{mol}^{-1}\cdot\text{cm}^{-1}$) and albite ($0.94 \text{ L}\cdot\text{mol}^{-1}\cdot\text{cm}^{-1}$) glasses [77, 87]. On the one hand this is due to the different degrees of polymerization between our glasses and rhyolite and basalt glasses. On the other hand due to the higher alkali content compared to albite glasses [87].

Assuming that the combination bands at $\sim 4500 \text{ cm}^{-1}$ and $\sim 5200 \text{ cm}^{-1}$ represent the total water content and that the absorption coefficients are independent on the water content, a simple calibration can be performed to determine the linear molar absorption coefficient for both bands (Eq. 4-6)[61, 87, 110, 140]:

$$c_{\text{H}_2\text{O}_t} = c_{\text{OH}} + c_{\text{H}_2\text{O}} \quad (3.4)$$

$$c_{\text{OH}} = \frac{1802 \cdot A_{4450}}{\rho \cdot d \cdot \epsilon_{4450}} \quad (3.5)$$

$$c_{\text{H}_2\text{O}} = \frac{1802 \cdot A_{5200}}{\rho \cdot d \cdot \epsilon_{5200}} \quad (3.6)$$

where c_{OH} denotes the content of water dissolved as OH groups and $c_{\text{H}_2\text{O}}$ the content of molecular H_2O . The linear molar absorption coefficients ϵ can be derived by a linear regression, resulting from the combination of the equation above:

$$\frac{1802 \cdot A_{5200}}{d \cdot \rho \cdot c_{\text{H}_2\text{O}_t}} = \epsilon_{5200} - \frac{\epsilon_{5200}}{\epsilon_{4450}} \cdot \frac{1802 \cdot A_{4450}}{d \cdot \rho \cdot c_{\text{H}_2\text{O}_t}} \quad (3.7)$$

The linear molar absorption coefficient of the NIR absorption bands can be derived by a regression analysis by the intercepts with the corresponding axis (Fig. 3.8). This approach was successfully applied to a variety of different glass systems, e.g. silicates [77, 78, 88, 102], aluminosilicate [61, 82, 105, 106, 153], borosilicates [89], borates [63] and phosphates [109, 110]. Values of ϵ_{4500} and ϵ_{5200} resulting from this approach, are shown in Tab. 3.3.

On the one hand, the linear molar absorption coefficient ϵ_{4600} increases when 7.5 mol% K_2O are incorporated at the expense of 7.5 mol% Na_2O . This behavior is consistent with findings on aluminosilicate glasses [61]. A further increase of K_2O content and a simultaneous decrease in the Na_2O content in turn lead to a decrease of ϵ_{4450} . On the other hand, a decrease of ϵ_{5200} is observed, when the K_2O content increases.

Linear molar absorption coefficients of ϵ_{4450} and ϵ_{5200} in our glasses are much lower compared to other aluminosilicate glasses, e.g. albite glasses as reported by Withers et al. [87]. They obtained values of $1.21 \text{ L}\cdot\text{mol}^{-1}\cdot\text{cm}^{-1}$ (ϵ_{4450}) and $1.46 \text{ L}\cdot\text{mol}^{-1}\cdot\text{cm}^{-1}$ (ϵ_{5200}) respectively, choosing the same baseline correction for their spectra. This comparison shows that higher alkali contents in polymerized aluminosilicate glasses lead to lower absorption coefficient. These findings are consistent with investigations on sodium silicate glasses made by Yamashita et al. where a decrease of the molar absorption coefficient with depolymerization of the glasses was observed [90].

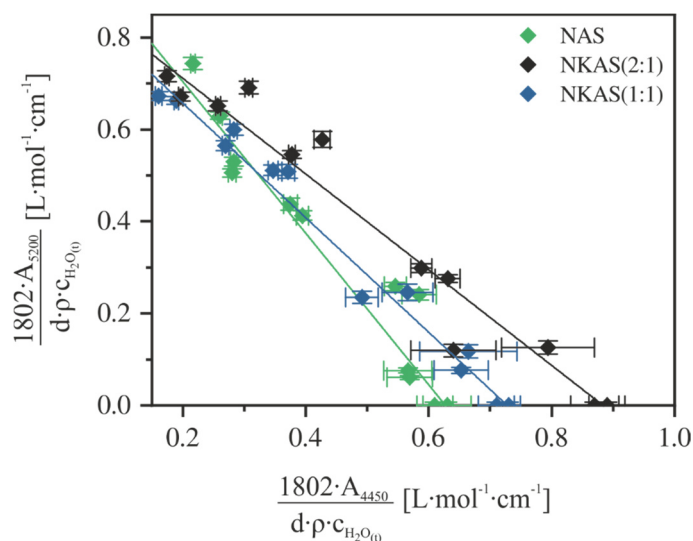


Figure 8: Calibration plot for the determination of the linear molar absorption coefficient of the NIR bands at 4450 cm^{-1} and 5200 cm^{-1} in aluminosilicate glasses.

3.3.5 ^{27}Al NMR Spectroscopy

^{27}Al MAS-NMR spectra of NAS, NKAS(2:1) and NKAS(1:1) exhibit similar features (Fig. 3.9). The main resonance in spectra of nominally dry NAS glass is centered at 55.9 ppm with the typical asymmetric form with tails extending towards lower frequency resulting from distributions of quadrupolar parameters for ^{27}Al , arising from the disordered nature of the glass [169, 194] (Fig. 3.9a and c). According to previous studies [40, 42, 45, 46, 114, 167-169, 195-197], this peak is assigned to tetrahedral coordinated Al (Al^{IV}). In the range of 13 ppm a weakly pronounced shoulder is visible, Typically, this resonance is caused by octahedral coordinated Al (Al^{VI}). The spinning sidebands of the main resonance are located at 178 and - 62 ppm.

In anhydrous mixed alkali glasses (NKAS(2:1) and NKAS(1:1)) the main resonance shifts by 0.4 ppm to a higher chemical shift and is located at 56.3 ppm for both nominally dry glasses (Fig. 3.9a and c). This shift is caused by the larger size and the lower electronegativity of K^+ and possibly from increasing angles between T-O-T tetrahedra [197]. As observed in anhydrous NAS glasses, a shoulder that can be assigned to Al^{VI} is observed at 13 ppm that becomes more pronounced when Na_2O is exchanged for K_2O . However this shoulder is weakly pronounced in all three compositions and due to the quadrupolar broadening of the peaks, it is not possible to quantify the relative proportion in of the Al^{VI} species spectra of dry glasses. With increasing K_2O content on expense of Na_2O we observed a decrease of the Full Width at Half Maximum (FWHM) (Tab 3.4).

According to e.g. Stebbins et al. [46, 197] and others [47, 167-169], five-fold coordinated aluminum (Al^{V}) was observed in several aluminosilicate glasses with a peak located around 30 - 40 ppm. This high Al coordination was mostly observed in glasses with divalent modifier cations like CAS ($\text{CaO-Al}_2\text{O}_3\text{-SiO}_2$) [50] and MAS ($\text{MgO-Al}_2\text{O}_3\text{-SiO}_2$) [167] but also in binary $\text{Al}_2\text{O}_3\text{-SiO}_2$ glasses [197]. In addition, this species was found in NAS ($\text{Na}_2\text{O-Al}_2\text{O}_3\text{-SiO}_2$) and KAS ($\text{K}_2\text{O-Al}_2\text{O}_3\text{-SiO}_2$) glasses that were quenched from melts at pressures above 10 GPa [46].

We do not observe such species in our data, but the presence of this species cannot be ruled out in our glasses as the broad tail of the Al^{IV} peak could hide it.

The peaks of the hydrous glasses containing 8 wt% H_2O (Fig. 3.9b and d) are more symmetric and significantly narrower compared to the peaks of the anhydrous glasses as shown by the FWHM (Tab. 3.4). The main resonance in all three compositions, attributed to Al^{IV} , is slightly shifted to higher frequencies and is located at 58 ppm. By narrowing the main

resonance, the broad tail in the range of 30 – 40 ppm disappears and the shoulder, which was observed in dry glasses at 13 ppm (Al^{IV}), becomes better resolved at the same chemical shift but the intensity does not seem to change.

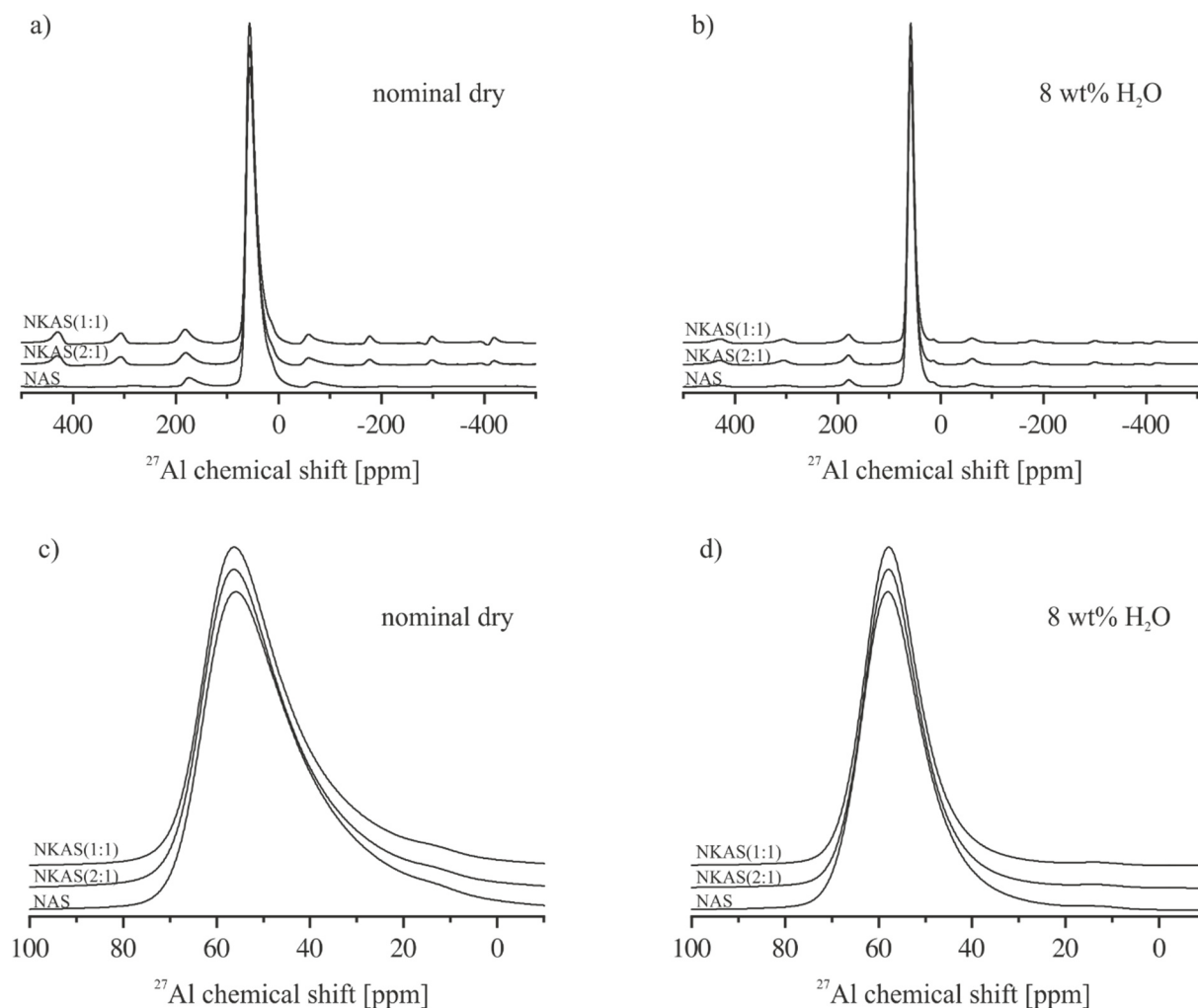


Figure 9: ^{27}Al MAS NMR spectra of anhydrous glasses (a) and magnification of the main resonance between 100 and -10 ppm (c). ^{27}Al MAS NMR spectra of hydrous glasses bearing 8 wt% (b) and magnification of the main resonance between 100 and -10 ppm (d). All spectra are normalized to the Al^{IV} resonance (~55 ppm) and shifted vertically for comparison.

Table 3.4: FWHM of anhydrous and hydrous ^{27}Al MAS NMR spectra in ppm and Hz.

	Nominally dry		8wt% H ₂ O	
	ppm	FWHM (Hz)	ppm	FWHM (Hz)
NAS	21.8	2273	14.6	1526
NKAS(2:1)	20.8	2115	13.6	1418
NKAS(1:1)	19.6	2048	13.2	1376

3.3.6 T_g/DTA

Fig. 3.10 show T_g/DTA measurements of the NKAS(1:1) glasses between 1-8 wt% H₂O. The fictive temperatures of these glasses were determined from the crossover temperature of two tangents aligned to the decreasing flank and base lines of the endotherm [65, 108]. As mentioned above, only the fictive temperatures could be determined for hydrous glasses. Background of this issue is that the samples show a dramatic decrease in the thermal gravimetric signal (TG) in the regime of T_f or shortly above it. For instance, for the NKAS(1:1) samples bearing 1 wt% H₂O (Fig 3.10a), a T_f value of ~ 992 K was determined (green line). Already 10 K (1003 K) above this values we observed a significant decrease in TG (red line) which occurs in a very short temperature range (1003 K – 1050 K). At 2 wt% H₂O T_f was found to be at ~ 848 K and the massive decrease of TG starts a ~ 866 K (Fig. 3.10b). At 4 wt% (Fig 3.10c) and 8 wt% H₂O (Fig. 3.10e), respectively, T_f is at 711 K and 460 K, respectively, and the loss of mass is at 733 K and 483 K, respectively. TG of NKAS(1:1) 6 wt% (Fig. 3.10d) deviates about ~90 K from the observed trend, possibly related to errors during measurements. Similar trends were observed in the other hydrous glasses (NAS and NKAS(2:1)).

Another problem, which makes it difficult to evaluate the T_f values are the unrrregular shapes of the DTA, curves (especially at high water contents), since they affect the application of the tangents.

Regarding these problems, T_f values can only determined approximately, but we are also aware that there might be already a small loss of water during the heating process, but this loss can be neglected compared to the massive loss in the regime of T_f.

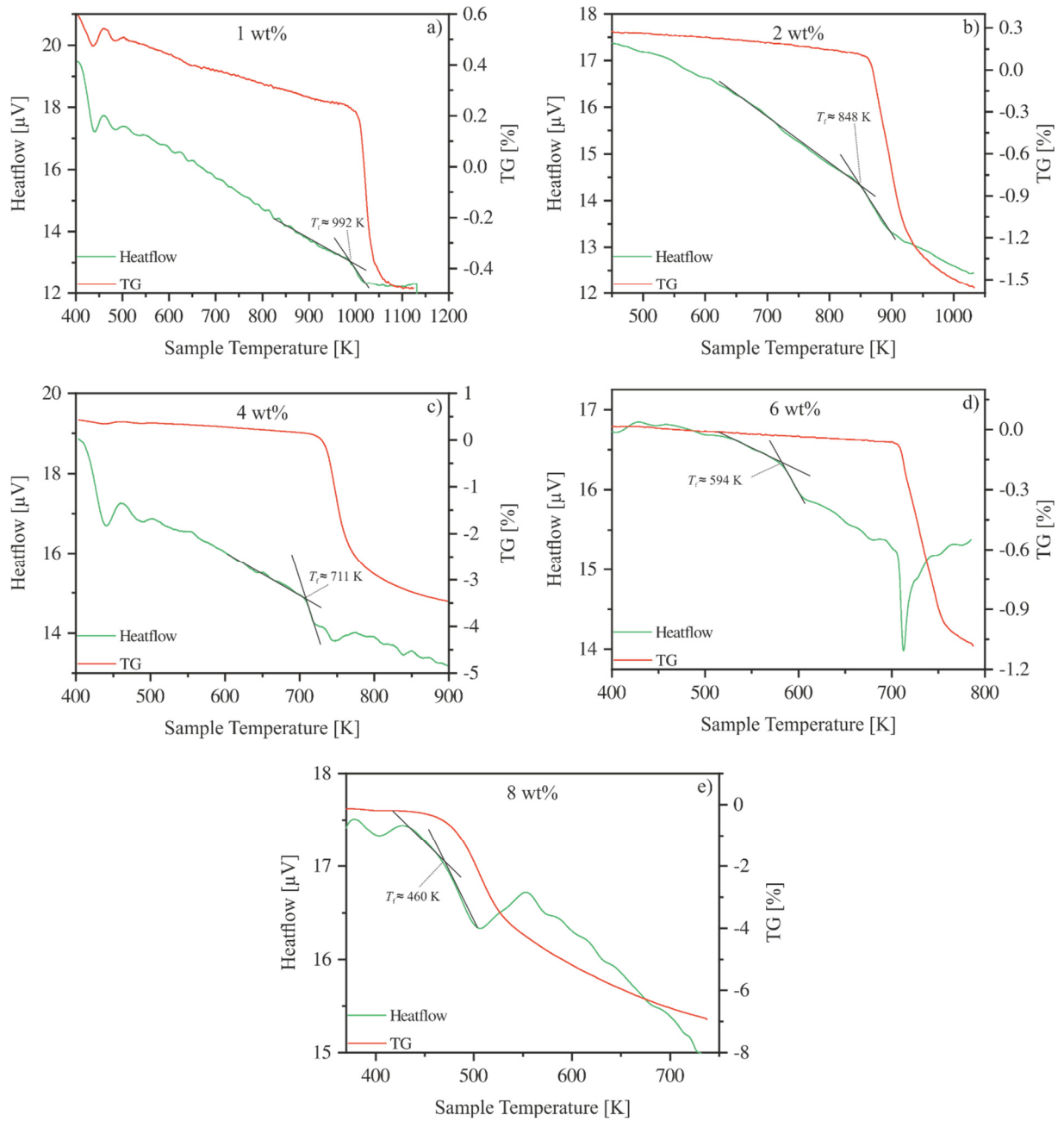


Figure 3.10: First upscan of T_g /DTA analysis of hydrous NKAS(1:1) glasses with DTA curves (green solid lines) and corresponding mass loss (red solid lines).

3.4. Discussion

3.4.1 Structure of aluminosilicate glasses

The nominal composition of our glasses is denoted as subaluminous compositions with $\text{Na}/\text{Al} = 1$ and $(\text{Na}+\text{K})/\text{Al} = 1$, respectively. As known from literature, these compositions are extremely sensitive to slight variations in the ratio of charge-balancing cation vs. Al^{3+} [39, 45]. For instance, an excess of charge-balancing cations (e.g. Na^+ , K^+) shifts the melt into the peralkaline region. If there is an excess of Al^{3+} , the melt is referred to a peraluminous melt [39, 42, 43, 45, 198]. Variations in this ratio have extreme effects on the structural properties of melts, as it influences the degree of polymerization and the associated change in viscosity of the melt. According to literature, melts with a $\text{Na}/\text{Al} = 1$ ratio are fully polymerized by the formation of AlO_4 tetrahedra that are cross-linked to SiO_4 tetrahedra which is evidenced by a pronounced peak between 50 – 70 ppm in ^{27}Al AS NMR measurements [39, 40, 43, 50, 154, 168, 169]. ^{27}Al MAS NMR spectra of our anhydrous glasses show the same characteristic features with a pronounced resonance around 55 ppm that is attributed to AlO_4 tetrahedra and an asymmetric tail toward lower chemical shift (Fig 3.9) resulting from distributions in quadrupolar coupling constants [169]. Meaning there are variations in the local geometry of the AlO_4 tetrahedra.

In order to describe the degree of polymerization, the $Q^i(m\text{Al})$ and $q^i(m\text{Si})$ notation is commonly used, with Q represents an Si atom and q an Al atom, bonded to four oxygen atoms forming a tetrahedron. The superscript i indicates the connectivity, i.e. the number of other Q units attached to the tetrahedron [40]. m is denoted as number of equal tetrahedra (SiO_4 or AlO_4) cross-linked to the central atom Q or q. respectively [40].

The Al/Si ratio in our glasses is 0.82, i.e. the distribution between Al and Si tetrahedra is not ideal. For instance, at a ratio of $\text{Al}/\text{Si} = 1$, one would expect a $Q^4(4\text{Al})$ or $q^4(4\text{Si})$ speciation, respectively, which would be reflected in a sharp pronounced peak located in the range of the AlO_4 coordination since the closest neighbor of the AlO_4 tetrahedron is always a SiO_4 [40, 46]. This means, that the Al avoidance rule (Loewenstein rule) is completely obeyed [163, 199].

Since the Al/Si ratio in our glasses is slightly lower, there is no ideal distribution between SiO_4 and AlO_4 tetrahedra. As a result, we also expect Si-O-Si linkages in addition to the dominating $Q^4(4\text{Al})$ species, but no Al-O-Al linkages. I.e. the direct neighbors of an AlO_4 tetrahedra are always 4 SiO_4 tetrahedra ($q^4(4\text{Si})$), but there are also $Q^4(3\text{Al})$ and $Q^4(4\text{Al})$ species

in our glasses. Based on this ratio, however, we can rule out the possibility that even lower species like $Q^4(2Al)$ and $Q^4(1Al)$ may exist in our glass structure.

As a result of the different Q-species, there are also variations in bonding-angles and bonding lengths in the network, which also contribute to the asymmetric form of the AlO_4 resonance. For instance, the cation-oxygen distance of an SiO_4 tetrahedra is 1.62 Å while the bond lengths of an $Al-O$ tetrahedra is slightly extended to 1.71 Å [200-202]. In addition, the T-O-T angles varies regarding the terminal cation between $\sim 130^\circ$ (Si-O-Al) and $\sim 150^\circ$ (Si-O-Si) [200-204]. Furthermore, we observed a decrease in FWHM (Tab. 3.4) of the AlO_4 resonance, when Na_2O is exchanged for K_2O . This effect is related to the higher cation field strength of Na^+ compared to K^+ . The corresponding cation field strength after Dietzel (defined as z/a^2 , with z = charge and a = distance between two ions) of Na^+ is 0.19 Å² and 0.13 Å² for K^+ , respectively [4]. The higher cation field strength of Na^+ in NAS glasses causes a higher degree of disorder than in mixed alkali glasses [201, 205]. The reason for this is that Na^+ has a higher attraction on the T-O-T tetrahedra which have therefore less possibilities to arrange than in the mixed alkali glasses (NKAS(2:1) and NKAS(1:1)) [197, 201].

To summarize this: the different local environmental variations of the AlO_4 tetrahedra and the resulting differences in bonding angles between AlO_4 and SiO_4 as well as the field strength of cations in the network cause variations of the local structure.

The high Al coordination at 13 ppm observed in all anhydrous glasses is attributed to Al^{VI} and possibly results from reaction with atmospheric moisture during sample preparation for ^{27}Al MAS NMR measurements. Similar observations were made by Zeng et al. [194]. If the Al^{VI} resonance is not caused by atmospheric moisture, this would imply that the anhydrous glasses would have a certain amount of NBO in the structure and therefore are not fully polymerized. The NBO/T ratio based on our bulk analysis show that the anhydrous glasses have a minor proportion of NBO (NAS: 0.039 ± 0.001 ; NKAS(2:1): 0.052 ± 0.002 ; NKAS(1:1): 0.027 ± 0.002), but this proportion is so low that it is already within the analytical error.

Similar to anhydrous spectra, we observed the small shoulder in the region of Al^{VI} in hydrous glasses. In order to estimate the contribution of the AlO_6 species to the total peak area, spectra of anhydrous and hydrous glasses were fitted with two Gauss curves according to [206]. Unfortunately, it was not possible to achieve a reasonable fit for the Al^{IV} site. In order to make a rough estimation of the contribution of these species to the total spectrum, the peak areas of

the two fitted curves were subtracted from the total peak area and the difference was assigned as contribution of the Al^{VI} site. Following this, we determined a contribution of $0.90\% \pm 0.06$ of the Al^{VI} species to the total peak area in all anhydrous and hydrous glasses.

Due to the similar proportion of the AlO₆ species in anhydrous and hydrous glasses bearing 8 wt% H₂O, it can be expected that this species is just an artefact coming from the adsorbed water from the atmosphere. Otherwise, one would expect clear differences in the abundances between the two glasses as the AlO₆ site in hydrous glasses would be much more pronounced. Furthermore, the incorporation of water seems to have only a minor role on the depolymerization in our glasses. For instance, the incorporation of water into lithium aluminophosphate glasses causes pronounced decrease of the AlO₄ tetrahedra and a significant increase of the AlO₆ octahedra, i.e. a dramatic depolymerization of the phosphate network [207]. In our aluminosilicate glasses, however, the proportion of the AlO₄ species seems to be similar in anhydrous and hydrous glasses. Also, the NBO/T values of glasses bearing 8 wt% H₂O are quite low with 0.31 ± 0.1 (NAS); 0.21 ± 0.2 (NKAS(2:1)) and 0.27 ± 0.1 (NKAS(1:1)).

But, the slight peakshift towards higher chemical shift indicates that the q⁴ species is depolymerized into q³ species. Zeng et al. [194] described a similar trend on hydrous sodium aluminosilicate glasses. As well as in our glasses, only the AlO₄ species was found in both anhydrous and hydrous glasses and the observed peakshift between the glasses was attributed to a depolymerization from q⁴ species to q³ species.

Next to the slight peakshift, the addition of 8 wt% H₂O into the glass structure shows a significant decrease in line width of the Al NMR signal (Tab 3.4). In order to determine the relative shift of parts of the Al species between 100 and -30 ppm, integral peak areas of anhydrous and hydrous glasses were normalized to the same area (Fig. 3.11). The narrowing of the AlO₄ resonance in hydrous glasses, and the more symmetric shape indicate a smaller distribution of the AlO₄ sites thus a more uniform bond angle between the T-O-T tetrahedra. As a result, a more ordered structure can be formed that is less tensed. Similar features were observed in hydrous albite glasses by Kohn et al. [154, 155] and later in hydrous sodium aluminosilicate glasses by Zeng et al. [194].

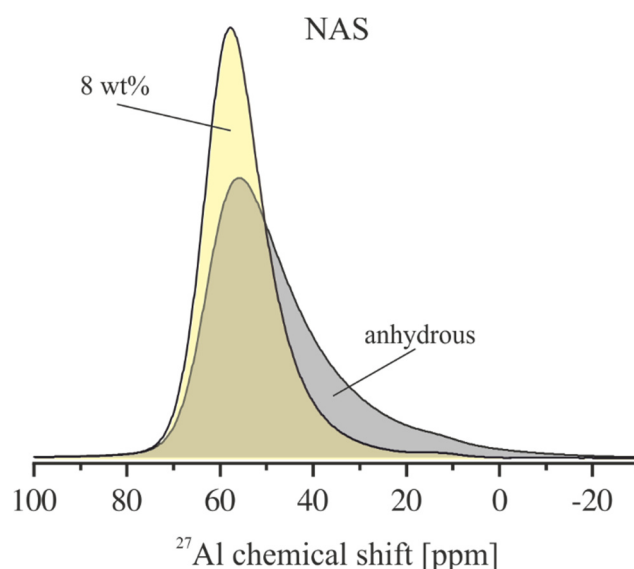


Figure 3.11: Normalized peak area of the main resonance of the ²⁷Al MAS NMR spectra of anhydrous (grey area) and hydrous glasses (yellow areas) NAS glasses.

3.4.2 Water speciation in aluminosilicate glasses

As known from literature, the relative abundance of water species depends on the glass composition. For instance, in soda-lime borate glasses OH groups are the dominant species even at very high water content (approx. 8 wt%) [63]. In borosilicate glasses, the intersection point, where the concentration of dissociated water and molecular H₂O are at the same level is at about 6-7 wt% H₂O [89]. In (alumino)silicate glasses this intersection point was found between 3 and 4 wt% H₂O [84, 86, 88, 106].

Water speciation data of our glasses are in good agreement with values reported for various aluminosilicate glasses (Fig. 3.12), e.g. [88]. For all compositions, the OH groups are dominating at low water contents and then levels off at high water contents when the respective intersection point is reached. In NAS glasses the intersection point is at 5.9 wt% total H₂O. In albite glasses, this intersection point was found at ~ 4 wt% H₂O e.g. [189]

When K₂O is incorporated into the structure on expense of Na₂O, the intersection point shift to 3.0 wt% H₂O (NKAS2:1). At the same contents of Na₂O and K₂O, the intersection point shifts slightly to higher concentration of total water and is located at 3.8 wt%.

As mentioned above, the species concentration is dependent on the glass composition. Studies on calcium-aluminosilicate (CAS), albite, i.e. sodium-aluminosilicate glasses (NAS), potassium-aluminosilicates (KAS) and rhyolite glasses reveal that the intersection point shifts to lower concentrations of total water when the SiO₂ content is increased [88, 90, 153, 189]. The trend in our glasses cannot be explained by this, because the SiO₂ content is constant. Rather, the trend seems to be related to the type of charge balancing cations in the glasses [88] as the concentration of OH groups in NAS glasses is higher compared to the mixed alkali glasses.

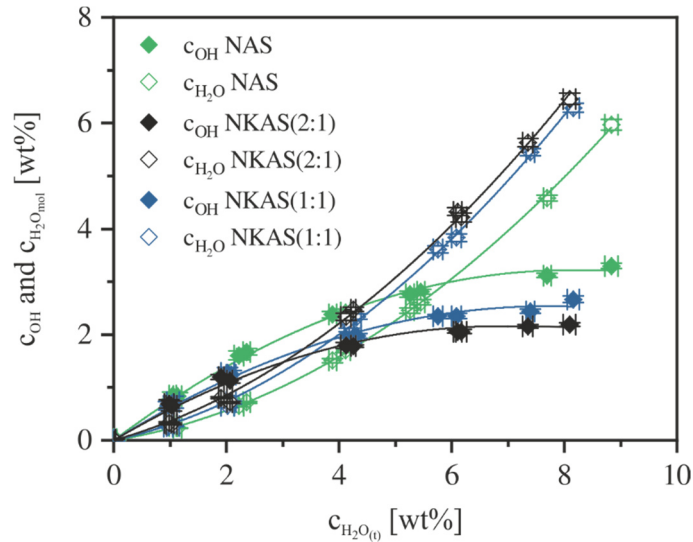


Figure 3.12: Water species concentration of aluminosilicate glasses (NAS, NKAS(2:1) and NKAS(1:1)).

Using the fictive temperatures of glasses, trends can be established for water speciation in the melt. Previous studies on aluminosilicate glasses have proven this approach [112, 113]. The temperature dependence of the equilibrium constant K for water speciation in several melt compositions is shown in Fig. 3.13. Behrens et al. [127] observed that K in sodium silicate glasses is higher than in polymerized aluminosilicate glasses, which indicates that non-bridging oxygens charged-balanced by Na^+ promote the dissociation of dissolved water in silicate melts. On the other hand, boron melts which are virtually free of non-bridging oxygens support the formation of OH groups.

Equilibrium constants of our melts are slightly increased compared to other aluminosilicate melts, e.g. rhyolites, andesites and albites, with the highest K value at given temperatures for NAS and the lowest one for NKAS(2:1). Values for NKAS(1:1) are in between. On the one hand, the lower SiO_2 and the higher network modifier content of our glasses can explain this. For instance, the equilibrium constant for an albite glass is lower compared to our NAS glass, although the glass components are similar (Na_2O , Al_2O_3 , SiO_2). Difference in between this glasses is the higher content of Na_2O and the lower content of SiO_2 in our NAS glasses compared to albite glasses e.g. [105]. This indicates that incorporation of OH groups is promoted in melts with lower SiO_2 and higher network modifier content [127]. On the other hand, the slope of our glasses towards higher $1000/K$ values, i.e. lower T_f values,

is very shallow compared to albite and other aluminosilicate glasses. This shallow slope may be a result of the issue to determine T_f values in our glasses.

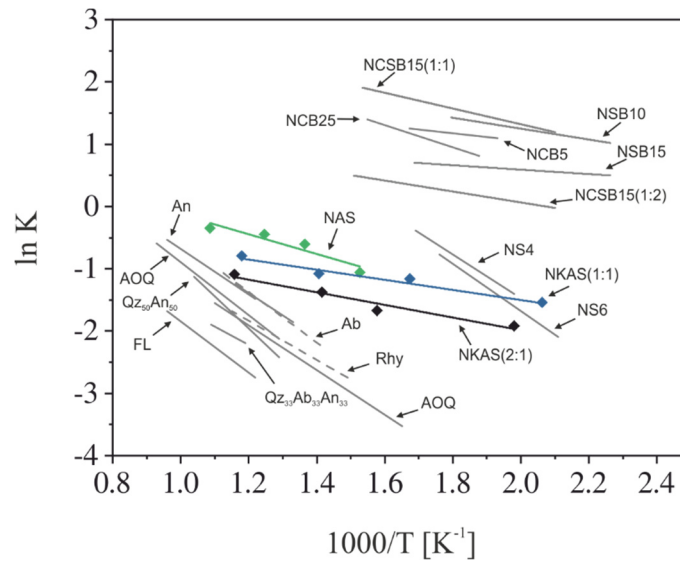


Figure 3.13: Comparison of equilibrium constants for water speciation in (alumino)-silicate, borate and silicoborate melts. Reference data are marked in grey and are collected from [63, 105, 112, 127, 138, 150 – 153]. Explanation of the acronyms: NCB (5, 15, 25) = $x\text{Na}_2\text{O}_{10}\text{CaO}_{90-x}\text{B}_2\text{O}_3$; NS4 = $\text{Na}_2\text{O}-4\text{SiO}_2$; NS6 = $\text{Na}_2\text{O}-6\text{SiO}_2$; Rhy = rhyolite; AOQ = $\text{Na}_{0.39}\text{K}_{0.31}\text{Al}_{0.69}\text{Si}_{3.31}\text{O}_8$; An = Andesite; Ab = $\text{NaAlSi}_3\text{O}_8$; $\text{Qz}_{33}\text{Ab}_{33}\text{An}_{33}$ = $\text{Na}_{0.5}\text{Ca}_{0.25}\text{AlSi}_3\text{O}_8$; $\text{Qz}_{50}\text{An}_{50}$ = $\text{Ca}_{0.5}\text{AlSi}_3\text{O}_8$; FL = Floatglass.

The standard enthalpy ΔH^0 for water speciation reaction was calculated from the slope m of the straight line in Fig. 3.13 as $\Delta H^0 = R \cdot m$ where R is the universal gas constant [82, 150, 151]. For NAS glasses ΔH^0 is $13.26 \pm 0.15 \text{ kJ} \cdot \text{mol}^{-1}$. For mixed alkali glasses ΔH^0 decreases with increasing K_2O content, e.g. $8.4 \pm 0.11 \text{ kJ} \cdot \text{mol}^{-1}$ (NKAS(2:1)) and $6.7 \pm 0.19 \text{ kJ} \cdot \text{mol}^{-1}$ (NKAS(1:1)). These values are decreased compared to e.g. sodium-silicates glasses ($28.5 - 31.0 \text{ kJ} \cdot \text{mol}^{-1}$) [127], albites glasses ($19.9 \text{ kJ} \cdot \text{mol}^{-1}$) [138] and rhyolite glasses ($25.2 \text{ kJ} \cdot \text{mol}^{-1}$) [150]. This results from the different Si/Al ratios of the glasses and different abundance of Si-O-Si and Si-O-Al linkages. For instance, a high Si/Al ratio results in higher standard enthalpies due to the stronger bonding between Si-O-Si compared to the weaker bonding of Si-O-Al, which are more easily hydrolyzed. The differences between NAS NKAS(2:1) and NAKS(1:1) can be attributed to the higher cation field strength of Na^+ compared to K^+ , where Na^+ ensures that the network is more closely connected and thus more rigid. This interpretation is supported by the Al-MAS NMR results on our glasses as FWHM (Tab. 3.4) of the NAS spectra are broader compared to NKAS glasses indicating that the structure in NAS is more tensed ad rigid (Fig. 3.9).

3.4.3 Effect of water on the glass fictive temperature

The effect of water on the fictive temperature is shown in Fig. 3.14. Values of anhydrous glasses are very similar. For the anhydrous NAS glass we obtained a T_f value of approx. 1020 K. Incorporation of K_2O on expense of Na_2O reduces T_f to 1013 K (NKAS(2:1)). A further increase of K_2O content and subsequent decrease of the Na_2O content leads to an increase of T_f to 1025 K (NKAS(1:1)). The decrease in T_f when at a Na/K ratio close to 2:1 can be originated to the higher ionic field strength of Na^+ ($0.19/\text{\AA}^2$) compared to K^+ ($0.12/\text{\AA}^2$) [4]. However, it is unclear why there is an increase of T_f in glasses with the highest K_2O content, although there are much more K^+ cations with a lower ionic field strength compared to NAS glasses. T_g values of anhydrous glasses are similar to T_f values, e.g. 1015 K (NAS); 1017 K (NKAS(2:1)) and 1038 K (NKAS(1:1)). Compared to albite glasses ($T_g = 1050$ K) [205] T_g and T_f values of our anhydrous glasses are slightly lower, which is caused by the increased network modifier content. Upon hydration the fictive temperature decreases, which is consistent with literature on other aluminosilicate glasses [66-68].

But, it should be mentioned that, compared to other studies on various glass systems [67, 205], the decrease of T_f upon hydration in our glasses is much steeper. In general, a more pronounced decrease of the fictive temperature in the range of low water contents is reported which gets progressively shallower with increasing water content. The trend upon hydration between our three glasses show some differences. For instance, T_f values of NAS glasses are higher compared to NKAS(2:1) and NKAS(1:1) and seem to level off at 5 wt% H_2O . K_2O bearing samples, on the other hand, show a more or less continuous decrease even at high water contents.

In addition, T_f values of our hydrous glasses are higher than values reported for hydrous albite glasses. For instance, Romano et al. [205] determined T_g values for glasses bearing ~ 2 wt% H_2O at ~ 720 K. T_f in our NAS glass bearing 2 wt% H_2O is at 914 K (i.e. increased by approx. 190 K). These significant differences must be related to the massive water loss in our glasses in the regime of T_f , as T_f values of anhydrous glasses are consistent with values for albite glasses [205]. In order to improve the understanding of this issue, viscosity measurements are necessary, which however could not be carried out due to lack of sample material in this study.

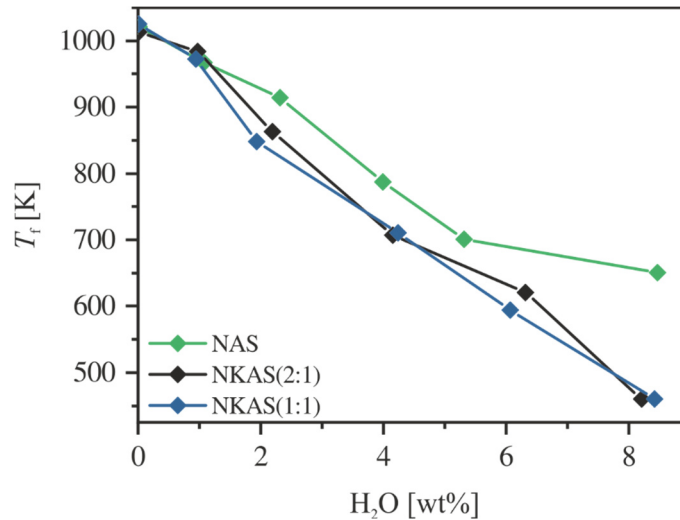


Figure 14: Values of the fictive temperature (T_f) as a function of the total water content.

3.5. Conclusion

Aluminosilicate glass in this study reveal a fully polymerized network as only AlO_4 species was found in ^{27}Al MAS NMR although a slight excess of network modifier cations was analyzed. The Al/Si ratio of 0.82 avoids that the SiO_4 and AlO_4 tetrahedra are ideally arranged. Instead, there seem to be local variations of $\text{Q}^4(4\text{Al})$, $\text{Q}^4(3\text{Al})$ and $\text{q}^4(4\text{Si})$ which indicate a tensed network which is reflected in the asymmetric peak of the AlO_4 resonance. The successive exchange of Na_2O for K_2O provides a slightly more relaxed structure of the AlO_4 species in the anhydrous glasses. Incorporation of up to 8 wt% H_2O reinforces this effect, indicating that dissolution of water eliminates the highly strained $\text{q}^4(4\text{Si})$ species and promotes the slightly depolymerized $\text{q}^3(3\text{Si})$ species [194]. However, since only 2-3 % of the incorporated water (depending on the glass composition) is present as OH groups which have a depolymerizing effect on the glass structure, the degree of polymerization is still high. In addition, water in these structures appears to be highly mobile which is evidenced by a significant loss of mass in the range of T_f . Possible diffusion mechanism in polymerized silicate melts were discussed by Behrens et al. [208]. The reaction of water molecules with bridging oxygens by formation of OH group pairs is considered the most probable variant, whereby also direct jumps of water molecules without reaction to the network could not be ruled out. If the direct jumps of water molecules play a role in the water release, the water is probably more easily in the mixed alkali glasses, since the caverns are larger than in NAS glasses due to the larger size of the K^+ . Knowledge of water content and its behavior in these glasses may be helpful to understand the mechanical properties of water rich glasses with respect to water related fatigue mechanism.

General conclusions

In this thesis, different network formers (P_2O_5 , B_2O_3 , and SiO_2), intermediates (Al_2O_3), and network modifier (Li_2O , MgO , Na_2O , K_2O and H_2O) were investigated with respect to their structural properties in glasses. For instance, the incorporation or successive exchange of alkaline and alkaline earth cations have different impacts on the glass structure. In anhydrous phosphate glasses the incorporation of 5 mol% Al_2O_3 on expense of 5 mol% MgO results in an increase of Q^3 species by about 10% at the simultaneous decrease of Q^2 species. This implies that small amounts of Al_2O_3 have a reinforcing effect on the structure, wherein the majority of Al_2O_3 is present in the form of AlO_6 octahedra. Incorporation of water in these structures leads to a dramatic depolymerization by complete elimination of Q^3 species at moderate water contents (~ 4 wt%) and preferential formation of diphosphate groups (Q^1). The presence of Al_2O_3 slightly compensates this behavior. In silicoborate glasses, on the other hand, increasing Na_2O content of 5 mol% on expense of 5 mol% B_2O_3 results in a preferential formation of BO_4 units (N_4) by approx. 8%, i.e. a higher polymerization of the network, whereby the successive exchange of Na_2O for CaO is only slightly noticeable. However, the incorporation of SiO_2 into the structure ensures a stronger interconnection of the network and a more efficient formation of BO_4 groups compared to pure borate systems [63]. The incorporation of water into these structures only results in a decreased formation of N_4 compared to alkalis and is similar to pure borate glasses. In slightly peralkaline but highly polymerized aluminosilicate glasses, the successive exchange of Na_2O for K_2O provides a slight decrease of the highly strained AlO_4 tetrahedra, which is related to the lower field strength of K^+ in contrast to Na^+ . The incorporation of water further enhances this effect by converting $q^4(4Si)$ species to $q^3(3Si)$ species.

In addition, water is incorporated differently in glasses, depending on the glass structure. In aluminum-free phosphates, water is predominantly incorporated in the form of OH groups and molecular water is only observed at water contents above of 4 wt%. The presence of Al_2O_3 provides the incorporation of molecular water, but hydroxyl groups remain the dominant hydrous species. In silicoborate glasses, OH groups are the predominant species, similar to phosphate glasses, whereby glasses with the highest CaO contents can incorporate the largest amount of molecular water. The incorporation of water in aluminosilicate glasses, on the other hand, is completely different. Here, molecular water is the predominant species at water contents higher than 3-4 wt% and the formation of hydroxyl groups levels off.

We have shown, that the incorporation of dissociated water and dissolved water strongly depend on the glass structure. Here, the bond strength of the T-O-T tetrahedra is particularly of importance. For instance, the bond strength of P-O-P and B-O-B in phosphate and silicoborate glasses, respectively, are much weaker compared to Si-O-Si and Si-O-Al bonds in aluminosilicate glasses. The bonding energy of a single B-O bond is $\sim 89 \text{ kcal}\cdot\text{mol}^{-1}$ and that of a single P-O bond is $\sim 90 \text{ kcal}\cdot\text{mol}^{-1}$ [162]. In contrast, the bonding energy of a single Si-O bond is $\sim 106 \text{ kcal}\cdot\text{mol}^{-1}$ and that of a single Al-O is $\sim 101 \text{ kcal}\cdot\text{mol}^{-1}$ [162]. Thus, a weaker bonding energy implies that water can hydrolyze these bonds more easily, as evidenced by the higher abundance of OH species in phosphate and silicoborate glasses compared to their abundance in aluminosilicate glasses. This in turn means, that higher bond strengths promote the formation of molecular water as evidenced in our investigated aluminosilicate glasses. T_g data of silicates [66], aluminosilicates [67], borates [63], silicoborates [209] and phosphates [207] show that higher polymerized glasses (silicates and aluminosilicates) are much more sensitive to depolymerization upon hydration which is reflected in a strong decrease of T_g , even at low water contents. In contrast, glasses that are not fully polymerized and already contain some amounts of non-bridging oxygens (e.g. phosphate glasses) show a more continuous decrease in T_g upon hydration. This implies that water speciation, but especially water molecules, are important for relaxation mechanisms in glass structure.

Recent study on hydrous soda-lime silicate glasses showed that water strongly affects the microchemical properties [210]. Kiefer et al. observed the occurrence of a time-dependent softening effect in these hydrous glasses under environmental moisture. They suggested that water species, and most probably molecular water, which is preferentially incorporated in these glasses, is capable to relax stressed Si-O bonds effectively and, thus, may promote crack propagation [210]. Studies on crack growth in glass systems investigated in this study are currently being carried out. However, it seems reasonable to assume a similar effect of molecular water on the micromechanical properties, e.g. SCCG, of our investigated glasses as observed for hydrous soda-lime glasses.

References

1. Angell, C.A., *Formation of Glasses from Liquids and Biopolymers*. Science, 1995. **267**: p. 1924-1935.
2. Freiman, S.W., S.M. Wiederhorn, and J.J.J. Mecholsky, *Environmentally Enhanced Fracture of Glass: A Historical Perspective*. Journal of the American Ceramic Society, 2009. **92**(7): p. 1371-1382.
3. Schula, S., *Mechanik, Werkstoffe und Konstruktion im Bauwesen*. Charakterisierung der Kratzanfälligkeit von Gläsern im Bauwesen. Vol. 43. 2015, Darmstadt: Springer Vieweg.
4. Scholze, H., *Glas-Natur, Struktur, Eigenschaften* Vol. 3. 1988: Springer Verlag.
5. Wiederhorn, S.M., *Strength of glass-A Fracture Mechanics Approach*. 1974.
6. Pavelchek, E.K. and R.H. Doremus, *Fracture strength of soda-lime glass after etching*. Journal of Material Science, 1974. **9**(11): p. 1803-1808.
7. Lower, N., R. Brow, and C. Kurkjian, *Inert Failure Strain Studies of Sodium Silicate Glass Fibers*. Vol. 349. 2004. 168-172.
8. Wiederhorn, S.M. and L.H. Bolz, *Stress Corrosion and Static Fatigue of Glass*. Journal of the American Ceramic Society, 1970. **53**(10): p. 543-548.
9. Wiederhorn, S.M., *Influence of Water Vapor on Crack Propagation in Soda-Lime Glass*. Journal of the American Ceramic Society, 1967. **50**(8): p. 407-414.
10. Wiederhorn, S.M., et al., *Fracture of glass in vacuum*. Journal of the American Ceramic Society, 1974. **57**(8).
11. L. Glathart, J. and F. W. Preston, *The Fatigue Modulus of Glass*. Vol. 17. 1946. 189-195.
12. C. Baker, T. and F. W. Preston, *Fatigue of Glass Under Static Loads*. Vol. 17. 1946. 170-178.
13. Kurkjian, C.R., *Mechanical properties of phosphate glasses*. Journal of Non-Crystalline Solids, 2000. **263 & 264**: p. 207-212.
14. Pallares, G., et al., *Crack opening profile in DCDC specimen*. International Journal of Fracture, 2009. **156**(1): p. 11-20.
15. Ciccotti, M., et al., *Dynamic condensation of water at crack tips in fused silica glass*. Journal of Non-Crystalline Solids, 2008. **354**(2-9): p. 564-568.
16. Koike, A. and M. Tomozawa, *Fictive temperature dependence of subcritical crack growth rate of normal and anomalous glass*. Journal of Non-Crystalline Solids, 2006. **352**: p. 5522-5530.
17. Lee, Y.-K. and M. Tomozawa, *Effect of water content in phosphate glasses on slow crack growth rate*. Journal of Non-Crystalline Solids, 1999. **248**: p. 203-210.
18. Salomson, J., K. Zeng, and D. Rowcliffe, *Decay of Residual Stresses at Indentation Cracks During Slow Crack Growth in Soda-Lime Glass*. Acta mater., 1996. **44**(2): p. 543-546.
19. Suratwala, T.I., et al., *Effects of OH content, water vapor pressure, and temperature on sub-critical crack growth in phosphate glass*. Journal of Non-Crystalline Solids, 2000. **263**: p. 213-227.
20. Michalske, T.A. and S.W. Freiman, *A molecular interpretation of stress corrosion in silica*. Nature, 1982. **295**(5849): p. 511-512.
21. Michalske, T.A. and S.W. Freiman, *A molecular mechanism for stress corrosion in vitreous silica*. Journal of the American Ceramic Society, 1983. **66**(4): p. 284-288.
22. Michalske, T.A. and B.C. Bunker, *Steric Effects in stress corrosion fraction of glass*. Journal of the American Ceramic Society, 1987. **70**(10): p. 780-784.
23. Ito, S. and M. Tomazawa, *Dynamic Fatigue of Sodium-Silicate Glasses with High Water Content*. Le Journal de Physique Colloques, 1982. **43**(C9): p. C9-611-C9-614.

24. Bunker, B.C., *Molecular mechanisms for corrosion of silica and silicate glasses*. Journal of Non-Crystalline Solids, 1994. **179**: p. 300-308.
25. Nogami, M. and M. Tomozawa, *Effect of Stress on Water Diffusion in Silica Glass*. Journal of the American Ceramic Society, 1984. **67**(2): p. 151-154.
26. Day, D.E., *Internal friction of glasses with low water content*. Journal of the American Ceramic Society, 1974. **57**(12): p. 530-533.
27. Behrens, H., et al., *Structural relaxation mechanisms in hydrous sodium borosilicate glasses*. Journal of Non-Crystalline Solids, 2018. **497**: p. 30-39.
28. Han, W.-T. and M. Tomozawa, *Effect of residual water in silica glass on static fatigue*. Journal of Non-Crystalline Solids, 1991. **127**(1): p. 97-104.
29. Le Parc, R., et al., *Influence of fictive temperature and composition of silica glass on anomalous elastic behaviour*. Journal of Physics Condensed Matter, 2006. **18**(32): p. 7507-7527.
30. Van Wazer, J.R., *Phosphorus and its Compounds*. Interscience Publishers, 1958. **1**.
31. Hope, U., et al., *The P-O bond lengths in vitreous P₂O₅ probed by neutron diffraction with high real-space resolution*. Journal of Physics: Condensed Matter, 1998. **10**: p. 261-270.
32. Suzuya, K., et al., *Structure of vitreous P₂O₅ and alkali phosphate glasses*. Journal of Non-Crystalline Solids, 1998. **232-234**: p. 650-657.
33. Brow, R.K., *Review :The structure of simple phosphate glasses* Journal of Non-Crystalline Solids, 2000. **263 & 264**: p. 1-28.
34. Wright, A.C., et al., *The structure of some simple amorphous network solids revisited*. Journal of Non-Crystalline Solids, 1991. **129**(1): p. 213-232.
35. Nelson, B.N. and G.J. Exarhos, *Vibrational spectroscopy of cation-site interactions in phosphate glasses*. The Journal of Chemical Physics, 1979. **71**(7).
36. Warren, B.E. and J. Bischof, *The structure of Silica glass by X-Ray diffraction studies*. Journal of the American Ceramic Society, 1938. **21**(2): p. 49-54.
37. Vogel, W., *Glas Chemie*. Vol. 3. 1992: Springer-Verlag Berlin Heidelberg GmbH.
38. Richter, H., G. Breitling, and F. Herre, *Struktur des glasigen B₂O₃*. Naturforschung, 1963. **9a**: p. 390-402.
39. Mysen, B.O. and P. Richet, *Silicate Glasses and Melts-Property and Structure*. Vol. 10. 2005. 111-112.
40. Engelhardt, G. and D. Michel, *High-Resolution Solid-State NMR of Silicates and Zeolites*. 1987.
41. Prescher, C., et al., *Beyond sixfold coordinated Si in SiO₂ glass at ultrahigh pressures*. Proceedings of the National Academy of Sciences, 2017. **114**(38): p. 10041.
42. Merzbacher, C.I., *A high-resolution ²⁹Si and ²⁷Al NMR study of alkaline earth aluminosilicate glasses*. Journal of Non-Crystalline Solids, 1990. **124**: p. 194-206.
43. Mysen, B.O., *Role of Al in depolymerized, peralkaline aluminosilicate melts in the systems Li₂O-Al₂O₃-SiO₂, Na₂O-Al₂O₃-SiO₂, K₂O-Al₂O₃-SiO₂*. American Mineralogist, 1990. **75**: p. 120-134.
44. Mysen, B.O., D. Virgo, and I. Kushiro, *The structural role of aluminum in silicate melts—a Raman spectroscopic study at 1 atmosphere*. American Mineralogist, 1981. **66**(7-8): p. 678-701.
45. Toplis, M.J., D.B. Dingwell, and T. Lenci, *Peraluminous viscosity maxima in Na₂O-Al₂O₃-SiO₂ liquids - The role of triclusters in tectosilicate melts*. Geochimica et Cosmochimica Acta, 1997. **61**(13): p. 2605-2612.
46. Stebbins, J.F., J. Wu, and L.M. Thompson, *Interactions between network cation coordination and non-bridging oxygen abundance in oxide glasses and melts Insights from NMR spectroscopy*. Chemical Geology, 2013. **346**: p. 34-46.

47. Neuville, D.R., L. Cormier, and D. Massiot, *Al coordination and speciation in calcium aluminosilicate glasses: Effects of composition determined by ^{27}Al MQ-MAS NMR and Raman spectroscopy*. Chemical Geology, 2006. **229**(1-3): p. 173-185.
48. Lacy, E.D., *Aluminum in glasses and melts*. Physical Chemistry of Glasses, 1963. **4**: p. 234-238.
49. Kuryaeva, R.G., *Degree of Polymerization of Aluminosilicate Glasses and Melts*. Glass Physics and Chemistry, 2004. **30**(2): p. 157-166.
50. Neuville, D.R., L. Cormier, and D. Massiot, *Al environment in tectosilicate and peraluminous glasses: A ^{27}Al MQ-MAS NMR, Raman, and XANES investigation*. Geochimica et Cosmochimica Acta, 2004. **68**(24): p. 5071-5079.
51. Weber, M.J., *Science and technology of laser glass*. Journal of Non-Crystalline Solids, 1990. **123**(1): p. 208-222.
52. Campbell, J.H. and T.I. Suratwala, *Nd-doped phosphate glasses for high-energy high-peak-power lasers*. Journal of Non-Crystalline Solids, 2000. **263 & 264**.
53. Day, D.E., et al., *Chemically durable iron phosphate glass wasteforms*. Journal of Non-Crystalline Solids, 1998. **241**: p. 1-12.
54. Brow, R.K., et al., *Spectroscopic Studies on the Structures of Phosphate Sealing Glasses*. MRS Bulletin, 2013. **23**(11): p. 63-67.
55. Alam, T.M., et al., *^6Li , ^7Li nuclear magnetic resonance investigation of lithium coordination in binary phosphate glasses*. Journal of Non-Crystalline Solids, 1999. **258**: p. 140-154.
56. Sharmin, N. and C.D. Rudd, *Structure, thermal properties, dissolution behaviour and biomedical applications of phosphate glasses and fibres: a review*. Journal of Materials Science, 2017. **52**(15): p. 8733-8760.
57. Christie, J.K., et al., *Structures and properties of phosphate-based bioactive glasses from computer simulation: a review*. J. Mater. Chem. B, 2017. **5**(27): p. 5297-5306.
58. Knowles, J.C., *Phosphate based glasses for biomedical applications*. Journal of Materials Chemistry, 2003. **13**(10).
59. Sglavo, V.M., et al., *Mechanical Properties of Phosphate Glass Optical Fibers*. International Journal of Applied Glass Science, 2014. **5**(1): p. 57-64.
60. Berndt, J., et al., *A combined rapid-quench and H_2 -membrane setup for internally heated pressure vessels-Description and application for water solubility in basaltic melts*. American Mineralogist, 2002. **87**: p. 1717-1726.
61. Behrens, H., et al., *Near-infrared spectroscopic determination of water species in glasses of the system MAlSi_3O_8 ($\text{M}=\text{Li, Na, K}$)-an intralaboratory study*. Chemical Geology, 1996. **128**: p. 41-63.
62. Leschik, M., G. Heide, and G.H. Frischat, *Determination of H_2O and D_2O contents in rhyolitic glasses*. Physical Chemistry of Glasses, 2004. **45**(4): p. 238-251.
63. Bauer, U., et al., *Water- and boron speciation in hydrous soda-lime-borate glasses*. Journal of Non-Crystalline Solids, 2015. **423-424**: p. 58-67.
64. Mazurin, O.V. and Y.V. Gankin, *Glass transition temperature-problems of measurement and analysis of the existing data*. 2007.
65. Mazurin, O.V., *Problems of Compatibility of the values of Glass Transition Temperatures Published in the World Literature*. Glass Physics and Chemistry, 2007. **33**(1): p. 22-36.
66. Zhang, Y., Z. Xu, and Y. Liu, *Viscosity of hydrous rhyolitic melts inferred from kinetic experiments, and a new viscosity model*. American Mineralogist, 2003. **88**: p. 1741-1752.
67. Bouhifd, M.A., et al., *Effect of water on the heat capacity of polymerized aluminosilicate glasses and melts*. Geochimica et Cosmochimica Acta, 2006. **70**(3): p. 711-722.
68. Del Gaudio, P., H. Behrens, and J. Deubener, *Viscosity and glass transition temperature of hydrous float glass*. Journal of Non-Crystalline Solids, 2007. **353**(3): p. 223-236.

69. Wondraczek, L. and H. Behrens, *Molar volume, excess enthalpy, and Prigogine-Defay ratio of some silicate glasses with different (P,T) histories*. Journal of Chemical Physics, 2007. **127**.
70. Wondraczek, L., S. Krolikowski, and H. Behrens, *Relaxation and Prigogine-Defay ratio of compressed glasses with negative viscosity-pressure dependence*. Journal of Chemical Physics, 2009. **130**.
71. Richet, P., et al., *Water and the density of silicate glasses*. Contributions to Mineralogy and Petrology, 2000. **138**: p. 337-347.
72. Bouhifd, A.M., A. Whittington, and P. Richet, *Partial molar volume of water in phonolitic glasses and liquids*. Contributions to Mineralogy and Petrology, 2001. **142**(2): p. 235-243.
73. Lai, Y.M., et al., *Raman and FTIR spectra of iron phosphate glasses containing cerium*. Journal of Molecular Structure, 2011. **992**(1-3): p. 84-88.
74. Ivascu, C., et al., *FT-IR, Raman and thermoluminescence investigation of P2O5–BaO–Li2O glass system*. Journal of Molecular Structure, 2011. **993**(1-3): p. 249-253.
75. Bengisu, M., et al., *Aluminoborate and aluminoborosilicate glasses with high chemical durability and the effect of P2O5 additions on the properties*. Journal of Non-Crystalline Solids, 2006. **352**(32-35): p. 3668-3676.
76. Velli, L.L., et al., *Structural investigation of metaphosphate glasses*. Physics and Chemistry of Glasses, 2005. **46**(2): p. 178-181.
77. Stolper, E., *Water in silicate glasses- An infrared Spectroscopic Study*. Contributions to Mineralogy and Petrology, 1982. **81**: p. 1-17.
78. Stolper, E., *The speciation of water in silicate melts*. Geochimica et Cosmochimica Acta, 1982. **46**: p. 2609-2620.
79. Karmakar, B., et al., *Effect of hydroxyl content on the physical properties of calcium metaphosphate glasses*. Bulletin of Materials Science, 1999. **22**(2): p. 115-119.
80. Zarubin, D.P., *Infrared spectra of hydrogen bonded hydroxyl groups in silicate glasses. A re-interpretation*. Physics and Chemistry of Glasses, 1999. **40**(4): p. 184-192.
81. Ebendorff-Heidepriem, H., W. Seeber, and D. Ehrt, *Dehydration of phosphate glasses*. Journal of Non-Crystalline Solids, 1993. **163**: p. 74-80.
82. Nowak, M. and H. Behrens, *The speciation of water in haplogranitic glasses and melts determined by in situ near-infrared spectroscopy*. Geochimica et Cosmochimica Acta, 1995. **59**(16): p. 3445-3450.
83. Bartholomew, R.F., et al., *Infrared spectra of a water-containing glass*. Journal of the American Ceramic Society, 1980. **63**(9-10): p. 481-485.
84. Stuke, A., et al., *H2O speciation in float glass and soda lime silica glass*. Chemical Geology, 2006. **229**(1-3): p. 64-77.
85. Nowak, M. and H. Behrens, *An experimental investigation of diffusion of water in haplogranitic melts*. Contributions to Mineralogy and Petrology, 1997. **126**: p. 365-376.
86. Behrens, H. and A. Stuke, *Quantification of H2O contents in silicate glasses using IR spectroscopy - a calibration based on hydrous glasses analyzed by Karl-Fischer titration*. Glass Science Technology, 2003. **76**(4): p. 176-189.
87. Withers, A.C. and H. Behrens, *Temperature-induced changes in the NIR spectra of hydrous albitic and rhyolitic glasses between 300 and 100 K*. Physics and Chemistry of Minerals, 1999. **27**: p. 119-132.
88. Silver, L.A., P.D. Ihinger, and E. Stolper, *The influence of bulk composition on the speciation of water in silicate glasses*. Contributions to Mineralogy and Petrology, 1990. **104**: p. 142-162.
89. Bauer, U., et al., *Structural investigation of hydrous sodium borosilicate glasses*. Journal of Non-Crystalline Solids, 2017. **465**: p. 39-48.

90. Yamashita, S., et al., *Water speciation in sodium silicate glasses based on NIR and NMR spectroscopy*. Chemical Geology, 2008. **256**(3-4): p. 231-241.
91. Mascaraque, N., A. Durán, and F. Muñoz, *Effect of alumina on the structure and properties of Li₂O–B₂O₃–P₂O₅ glasses*. Journal of Non-Crystalline Solids, 2011. **357**(16-17): p. 3212-3220.
92. Abe, Y. and M. Grayson, *Topics in Phosphorus Chemistry*, ed. E.J. Griffith. Vol. 11. 1983.
93. Uchino, T. and T. Yoko, *Sodium and Lithium Environments in Single- and Mixed-Alkali Silicate Glasses. An ab Initio Molecular Orbital Study* Journal of Physical Chemistry B, 1999. **109**: p. 1854-1858.
94. Alam, T.M., J.-J. Liang, and R.T. Cygan, *Molecular dynamics simulations of the lithium coordination environment in phosphate glasses*. Physical Chemistry Chemical Physics, 2000. **2**(19): p. 4427-4432.
95. Alam, T.M. and R.K. Brow, *Local structure and connectivity in lithium phosphate glasses*. Journal of Non-Crystalline Solids, 1998. **223**: p. 1-20.
96. Brow, R.K., C.A. Click, and T.M. Alam, *Modifier coordination and phosphate glass networks*. Journal of Non-Crystalline Solids, 2000. **274**: p. 9-16.
97. Metwalli, E. and R.K. Brwo, *Modifier effects on the properties and structures of aluminophosphate glasses* Journal of Non-Crystalline Solids, 2001. **289**: p. 113-122.
98. Brow, R.K., J.R. Kirkpatrick, and G.L. Turner, *Nature of Alumina in Phosphate Glasses II, Structure of Sodium Aluminophosphate Glass* Journal of the American Ceramic Society, 1993. **76**(4): p. 919-928.
99. Metwalli, E. and R.K. Brow, *Cation Effects on Anion Distributions in Aluminophosphate Glasses* Journal of the American Ceramic Society, 2001. **84**(5): p. 1025-32.
100. Brow, R.K., R.J. Kirkpatrick, and G.L. Turner, *The short range structure of sodium phosphate glasses I. MAS NMR studies*. Journal of Non-Crystalline Solids, 1990. **116**(1): p. 39-45.
101. Scholze, H., *Der Einbau des Wassers in Gläsern* Zeitschrift für Glaskunde, 1959. **32**(3).
102. Bartholomew, R.F., *Water in Glass* Treatise on Materials Science and Technology, 1982. **22**: p. 76-127.
103. Acocella, J., M. Tomozawa, and E.B. Watson, *The Nature of dissolved water in sodium silicate glasses and its effect on various properties*. Journal of Non-Crystalline Solids, 1984. **65**: p. 355-372.
104. Davis, K.M. and M. Tomazawa, *An infrared spectroscopic study of water-related species in silica glasses* Journal of Non-Crystalline Solids, 1996. **201**: p. 177-198.
105. Ohlhorst, S., et al., *Water speciation in aluminosilicate glasses and melts*. Applied Mineralogy, 2000: p. 193-196.
106. Schmidt, B.C., et al., *Quantitative determination of water speciation in aluminosilicate glasses- a comparative NMR and IR spectroscopic study*. Chemical Geology, 2001. **174**: p. 195-208.
107. Shelby, J.E., *Diffusion and solubility of water in alkali borate melts*. Physical Chemistry of Glasses, 2003. **44**(2): p. 106-112.
108. Reinsch, S., et al., *Water the other network modifier in borate glasses*. Journal of Non-Crystalline Solids, 2016. **432**: p. 208-217.
109. Efimov, A.M. and V.G. Pogareva, *Water-related IR absorption spectra for some phosphate and silicate glasses*. Journal of Non-Crystalline Solids, 2000. **275**: p. 189-198.
110. Balzer, R., et al., *Structural investigation of hydrous phosphate glasses*. Phys. Chem. Glasses: Eur. J. Glass Sci. Technol. B, 2019. **60**(2): p. 49-61.

111. Harder, U., et al., *Determination of the water content of alkali lime silica glasses by IR spectroscopy using nuclear reaction analysis for calibration* Glass Science Technology, 1998. **71**(1): p. 12-18.
112. Behrens, H. and M. Nowak, *Quantification of H₂O Speciation in Silicate Glasses and Melts by IR Spectroscopy -in situ versus Quench Techniques*. Phase Transitions, 2003. **76**(1-2): p. 45-61.
113. Zhang, Y., J. Jenkins, and Z. Xu, *Kinetics of the reaction H₂O + O = 2OH in rhyolitic glasses upon cooling - Geospeedometry and comparison with glass transition* Geochimica et Cosmochimica Acta, 1997. **61**(11): p. 2167-2173.
114. Sen, S., Z. Xu, and J.F. Stebbins, *Temperature dependent structural changes in borate, borosilicate and Boroaluminate liquids high resolution ¹¹B, ²⁹Si, ²⁷Al NMR studies*. Journal of Non-Crystalline Solids, 1998. **226**: p. 29-40.
115. Bunker, B.C., J.R. Kirkpatrick, and R.K. Brow, *Local structure of Alkaline-Earth Boroaluminate Crystals and Glasses I, Crystals Chemical Concepts-Structural Predicts and Comparison to known structures*. Journal of the American Ceramic Society, 1991. **74**(6): p. 1425-1429.
116. Pye, L.D., V.D. Fréchet, and N.J. Kreidl, *Borate glasses - Structure, Properties, Applications*. Vol. 12. 1978: Plenum Press, New York.
117. Vogel, W., *Struktur und Kristallisation der Gläser* 1971.
118. Y. D. Yiannopoulos, Y.D., G.D. Chryssikos, and E.I. Kamitsos, *Structure and properties of alkaline earth borate glasses*. Physics and Chemistry of Glasses, 2001. **42**(3): p. 164-172.
119. Michaelis, V.K., P.M. Aguiar, and S. Kroeker, *Probing alkali coordination environments in alkali borate glasses by multinuclear magnetic resonance*. Journal of Non-Crystalline Solids, 2007. **353**: p. 2582-2590.
120. Franz, H., *Solubility of Water Vapor in Alkali Borate Melts*. Journal of the American Ceramic Society, 1966. **49**(9): p. 473-477.
121. Oeser, M., et al., *High-Precision Fe and Mg Isotope Ratios of Silicate Reference Glasses Determined In Situ by Femtosecond LA-MC-ICP-MS and by Solution Nebulisation MC-ICP-MS*. Geostandards and Geoanalytical Research, 2014. **38**(3): p. 311-328.
122. Oeser, M., et al., *Processes and time scales of magmatic evolution as revealed by Fe-Mg chemical and isotopic zoning in natural olivines*. Geochimica et Cosmochimica Acta, 2015. **154**: p. 130-150.
123. Lazarov, M. and I. Horn, *Matrix and energy effects during in-situ determination of Cu isotope ratios by ultraviolet-femtosecond laser ablation multicollector inductively coupled plasma mass spectrometry*. Spectrochimica Acta Part B: Atomic Spectroscopy, 2015. **111**: p. 64-73.
124. Pearce, N.J.G., et al., *A Compilation of New and Published Major and Trace Element Data for NIST SRM 610 and NIST SRM 612 Glass Reference Materials* The Journal of Geostandards and Geoanalysis, 1997. **21**(1): p. 115-144.
125. Liu, Y., et al., *In situ analysis of major and trace elements of anhydrous minerals by LA-ICP-MSLA-ICP-MS without applying an internal standard*. Chemical Geology, 2008. **257**(1-2): p. 34-43.
126. Behrens, H., *Determination of water solubilities in high-viscosity melts- An experimental study on NaAlSi₃O₈ and KAlSi₃O₈ melts*. European Journal of Mineralogy, 1995. **7**: p. 905-920.
127. Behrens, H. and S. Yamashita, *Water speciation in hydrous sodium tetrasilicate and hexasilicate melts: Constraint from high temperature NIR spectroscopy*. Chemical Geology, 2008. **256**(3-4): p. 306-315.
128. Reinsch, S., et al., *Internal friction of hydrated soda-lime-silicate glasses*. Journal of Chemical Physics, 2013. **139**: p. 1-7.

129. Massiot, D., et al., *Modelling one- and two-dimensional solid-state NMR spectra*. Magnetic Resonance in Chemistry, 2002. **40**(1): p. 70-76.
130. Zhang, Y. and H. Ni, *Diffusion of H, C, and O Components in Silicate Melts*. Reviews in Mineralogy and Geochemistry, 2010. **72**(1): p. 171-225.
131. Balachander, L., et al., *IR analysis of borate glasses containing three alkali oxides*. ScienceAsia, 2013. **39**(3).
132. Kamitsos, E.I. and G.D. Chryssikos, *Borate glass structure by Raman and infrared spectroscopies*. Journal of Molecular Structure, 1991. **247**: p. 1-16.
133. Franz, H. and T. Kelen, *Erkenntnisse über die Struktur von Alkalisilicatgläsern und -schmelzen aus dem Einbau von OH-Gruppen*. Glastechnischer Bericht 1966. **40**(4): p. 141-148.
134. Behrens, H., *Noble Gas Diffusion in Silicate Glasses and Melts*. Reviews in Mineralogy and Geochemistry, 2010. **72**(1): p. 227-267.
135. Behrens, H., N. Tamic, and F. Holtz, *Determination of the molar absorption for the infrared absorption band of CO₂ in rhyolitic glasses*. American Mineralogist, 2004. **89**: p. 301-306.
136. Nemilov, S., *The Review of Possible Interrelations Between Ionic Conductivity, Internal Friction and the Viscosity of Glasses and Glass Forming Melts Within the Framework of Maxwell Equations*. Journal of Non-Crystalline Solids, 2011. **357**: p. 1243-1263.
137. Efimov, A.M. and V.G. Pogareva, *IR absorption spectra of vitreous silica and silicate glasses: The nature of bands in the 1300 to 5000 cm⁻¹ region*. Chemical Geology, 2006. **229**(1-3): p. 198-217.
138. Schmidt, B., C., *Effect of boron on the water speciation in (alumino)silicate melts and glasses*. Geochimica et Cosmochimica Acta, 2004. **68**(24): p. 5013-5025.
139. Behrens, H., et al., *Near-infrared spectroscopic determination of water species in glasses of the system MAlSi₃O₈ (M= Li, Na, K)- an interlaboratory study*. Chemical Material, 1996. **128**: p. 41-63.
140. Newman, S., E.M. Stolper, and S. Epstein, *Measurement of water in rhyolitic glasses Calibration of an infrared spectroscopic technique*. American Mineralogist, 1986. **71**: p. 1527-1541.
141. Romano, C., D.B. Dingwell, and K.U. Hess, *The effect of boron on the speciation of water in haplogranite melts*. Per. Mineral., 1995. **64**: p. 413-431.
142. Zotov, N. and H. Keppler, *The influence of water on the structure of hydrous sodium tetrasilicate glasses*. American Mineralogist, 1998. **83**: p. 823-834.
143. Ohlhorst, S., H. Behrens, and F. Holtz, *Compositional dependence of molar absorptivities of near-infrared OH- and H₂O bands in rhyolitic to basaltic glasses*. Chemical Geology, 2001. **174**: p. 5-20.
144. Smedskjaer, M.M., et al., *Irreversibility of Pressure Induced Boron Speciation Change in Glass*. Scientific Report, 2013. **4**.
145. Du, L.-S. and J.F. Stebbins, *Nature of Silicon-Boron Mixing in Sodium Borosilicate Glasses: A High-Resolution ¹¹B and ¹⁷O NMR study*. Journal of Physical Chemistry B, 2003. **107**: p. 10063-10076.
146. Du, L.-S., et al., *Pressure-induced structural changes in a borosilicate glass-forming liquid-Boron coordination, non-bridging oxygens, and network ordering*. Journal of Non-Crystalline Solids, 2004. **337**: p. 196-200.
147. Wu, J. and J.F. Stebbins, *Quench rate and Temperature effects on the boron coordination in aluminoborosilicate melts*. Journal of non-Crystalline Solids, 2010. **356**: p. 2097-2108.
148. Alemany, L.B., et al., *Observation and accurate quantification of ²⁷Al MAS NMR spectra of some Al₂SiO₅ polymorphs containing sites with large*

- quadrupole interactions. *Chemical Physics Letters*, 1991. **177**(3).
149. Zotov, N. and H. Keppler, *The structure of sodium tetrasilicate glass from neutron diffraction reverse Monte Carlo simulations and Raman spectroscopy*. *Physics and Chemistry of Minerals*, 1998. **25**: p. 259-267.
150. Sowerby, J.R. and H. Keppler, *Water speciation in rhyolitic melt determined by in-situ infrared spectroscopy*. *American Mineralogist*, 1999. **84**: p. 1843-1849.
151. Nowak, M. and H. Behrens, *Water in rhyolitic magmas - getting a grip on a slippery problem*. *Earth and Planetary Science Letters*, 2001. **184**: p. 515-522.
152. Liu, Y., Y. Zhang, and H. Behrens, *H₂O diffusion in dacitic melts*. *Chemical Geology*, 2004. **209**(3-4): p. 327-340.
153. Ihinger, P.D., Y. Zhang, and E.M. Stolper, *The speciation of dissolved water in rhyolitic melt*. *Geochimica et Cosmochimica Acta*, 1999. **63**(21): p. 3567-3578.
154. Kohn, S.C., R. Dupree, and M.E. Smith, *A multinuclear magnetic resonance study of the structure of hydrous albite glasses*. *Geochimica et Cosmochimica Acta*, 1989. **53**: p. 2925-2935.
155. Kohn, S.C., R. Dupree, and M. Golam Mortuza, *The interaction between water and aluminosilicate magmas*. *Chemical Geology*, 1992. **96**: p. 399-409.
156. Kohn, S.C., et al., *Sodium environments in dry and hydrous albite glasses - Improved ²³Na solid state NMR data and their implications for water dissolution mechanisms*. *Geochimica et Cosmochimica Acta*, 1998. **61**(1): p. 79-87.
157. Mauro, J.C., P.K. Gupta, and R.J. Loucks, *Composition dependence of glass transition temperature and fragility. II. A topological model of alkali borate liquids*. *Journal of Chemical Physics*, 2009. **130**(23): p. 234503.
158. Zheng, Q., et al., *Glass-forming ability of soda lime borate liquids*. *Journal of Non-Crystalline Solids*, 2012. **358**: p. 658-665.
159. Behrens, H., *Ar, CO₂ and H₂O diffusion in silica glasses at 2kbar pressure*. *Chemical Geology*, 2010. **272**(1-4): p. 40-48.
160. Tomozawa, M., et al., *Thermal Properties of Na₂O-2SiO₂ Glasses with High Water Content*. *Journal of Non-Crystalline Solids*, 1983. **56**: p. 343-348.
161. Deubener, J., et al., *Water and the glass transition temperature of silicate melts*. *Journal of Non-Crystalline Solids*, 2003. **330**(1-3): p. 268-273.
162. Sun, K.-H., *Fundamental conditions of glass formation*. *Journal of the American Ceramic Society*, 1947. **30**: p. 277-281.
163. Yildirim, E. and R. Dupree, *Investigation of Al-O-Al sites in an Na-aluminosilicate glass*. *Bulletin of Materials Science*, 2004. **27**(3): p. 269-272.
164. Merzbacher, C.I. and W.B. White, *The structure of alkaline earth aluminosilicate glasses as determined by vibrational spectroscopy*. *Journal of Non-Crystalline Solids*, 1991. **130**: p. 18-34.
165. Neuville, D.R. and B.O. Mysen, *Role of aluminium on silicate network: In situ, high-temperature study of glasses and melts on the join SiO₂-NaAlO₂*. *Geochimica et Cosmochimica Acta*, 1996. **60**(10): p. 1727-1737.
166. Doweidar, H., *Density - structure correlations in Na₂O-Al₂O₃-SiO₂ glasses*. *Journal of Non-Crystalline Solids*, 1998. **240**: p. 55-65.
167. Toplis, M.J., et al., *Fivefold-coordinated aluminum in tectosilicate glasses observed by triple quantum MAS NMR*. *American Mineralogist*, 2000. **85**: p. 1556-1560.
168. Xue, X. and M. Kanzaki, *Al coordination and water speciation in hydrous aluminosilicate glasses: direct evidence from high-resolution heteronuclear ¹H-²⁷Al correlation NMR*. *Solid State Nucl Magn Reson*, 2007. **31**(1): p. 10-27.

169. Wu, J. and J.F. Stebbins, *Effects of cation field strength on the structure of aluminoborosilicate glasses: High-resolution ^{11}B , ^{27}Al and ^{23}Na MAS NMR*. Journal of Non-Crystalline Solids, 2009. **355**(9): p. 556-562.
170. Riemer, T., et al., *H₂O-OH ratio determination in hydrous aluminosilicate glasses by static proton NMR and the effect of chemical shift anisotropy*. Solid State Nuclear Magnetic Resonance, 2000. **15**: p. 201-207.
171. Frischat, G.H., M. Leschik, and G. Heide, *Hydration and corrosion of polymerised aluminosilicate glasses*. European Journal of Glass Science and Technology Part B, 2010. **51**(2): p. 107-116.
172. Takata, M., M. Tomozawa, and E.B. Watson, *Effect of Water Content on Mechanical Properties of Na₂O-SiO₂*. Communication of the American Ceramic Society, 1982: p. C156-C157.
173. Han, W.-T. and M. Tomozawa, *Indentation Creep of Na-Trisilicate glasses with various water contents*. Journal of the American Ceramic Society, 1990. **73**(12).
174. Striepe, S., et al., *Relaxation kinetics of the mechanical properties of an aluminosilicate glass*. Journal of Non-Crystalline Solids, 2013. **362**: p. 40-46.
175. Tomozawa, M., *The role of water in the mechanical fatigue of glasses*. 1989.
176. Jewell, J.M., C.M. Shaw, and J.E. Shelby, *Effects of water content on aluminosilicate glasses and the relation to strong-fragile liquid theory*. Journal of Non-Crystalline Solids, 1993. **152**: p. 32-41.
177. Zietka, S. and J. Deubener, *Glass transition and viscosity of hydrated silica glasses*. Physical Chemistry of Glasses, 2007. **48**(6): p. 380-387.
178. Shaw, H.R., *Obsidian-H₂O Viscosities at 1000 and 2000 Bars in the Temperature Range 700°C to 900°C*. Journal of Geophysical Research, 1963. **68**(23): p. 6337-6343.
179. Dingwell, D.B., C. Romano, and K.U. Hess, *The effect of water on the viscosity of a haplogranitic melt under P-T-X conditions relevant to silicic volcanism*. Contributions to Mineralogy and Petrology, 1996. **124**: p. 19-28.
180. Kuschel, L., *Pre-eruptive conditions of the Cougar Point Tuff rhyolites, Snake River Plain, USA*, in *Institut für Mineralogie*. 2008, Leibniz Universität Hannover.
181. Arndt, J. and F. Häberle, *Thermal Expansion And Glass Transition Temperatures of Synthetic glasses of Plagioclase-Like Compositions*. Contributions to Mineralogy and Petrology, 1973. **39**: p. 175-183.
182. Handke, M. and W. Mozgawa, *Vibrational spectroscopy of the amorphous silicates*. Vibrational Spectroscopy, 1993. **5**: p. 75-84.
183. Środa, M. and C. Paluszkiwicz, *The structural role of alkaline earth ions in oxyfluoride aluminosilicate glasses—Infrared spectroscopy study*. Vibrational Spectroscopy, 2008. **48**(2): p. 246-250.
184. Tarte, P., *Infra-red spectra of inorganic aluminates and characteristic vibrational frequencies of AlO₄ tetrahedra and AlO₆ octahedra*. Spectrochimica Acta 1967. **23A**: p. 2127-2143.
185. Handke, M., W. Mozgawa, and M. Nocun, *Specific features of the IR spectra of silicate glasses*. Journal of Molecular Structure, 1994. **325**: p. 129-136.
186. Stoch, L. and M. Sroda, *Infrared spectroscopy in the investigation of oxide glasses structure*. Journal of Molecular Structure, 1999. **511–512**: p. 77-84.
187. Robert, G., et al., *The effect of water on the viscosity of a synthetic calc-alkaline basaltic andesite*. Chemical Geology, 2013. **346**: p. 135-148.
188. Tamic, N., H. Behrens, and F. Holtz, *The solubility of H₂O and CO₂ in rhyolitic melts in equilibrium with a mixed CO₂-H₂O fluid phase*. Chemical Geology, 2001. **174**: p. 333-347.

189. Silver, L.A. and E. Stolper, *Water in Albitic glasses*. Journal of Petrology, 1989. **30**(3): p. 667-709.
190. Yamashita, S., T. Kitamura, and M. Kusakabe, *Infrared spectroscopy of hydrous glasses of arc magma compositions*. Geochemical Journal, 1997. **31**: p. 169-174.
191. Shishkina, T.A., et al., *Solubility of H₂O- and CO₂-bearing fluids in tholeiitic basalts at pressures up to 500MPa*. Chemical Geology, 2010. **277**(1-2): p. 115-125.
192. Suzuki, T., et al., *IR Practical Extinction Coefficients of Water in Alkali Lime Silicate Glasses Determined by Nuclear Reaction Analysis*. Journal of the American Ceramic Society, 2015. **98**(6): p. 1794-1798.
193. Wu, C.-K., *Nature of Incorporated Water in Hydrated Silicate Glasses*. Journal of the American Ceramic Society, 1980. **63**(7-8): p. 453-457.
194. Zeng, Q., H. Nekvasil, and C.P. Grey, *In support of a depolymerization model for water in sodium aluminosilicate glasses: Information from NMR spectroscopy*. Geochimica et Cosmochimica Acta, 2000. **64**(5): p. 883-896.
195. Sukenaga, S., et al., *Reconsideration of Al coordination in CaO-SiO₂-Al₂O₃-(R₂O or RO) Glasses by using High Field Solid State ²⁷Al NMR Spectroscopy*. ISIJ International, 2010. **51**(2): p. 333-335.
196. Schmidt, B.C., et al., *Different water solubility mechanisms in hydrous glasses along the Qz-Ab Join-Evidence from NMR spectroscopy*. Geochimica et Cosmochimica Acta, 2000. **64**(3): p. 513-526.
197. Stebbins, J.F. and I. Farnan, *Effects of High Temperature on Silicate Liquid Structure - A Multinuclear NMR Study*. Science. **255**: p. 586-589.
198. Mysen, B., *Structure of H₂O-saturated peralkaline aluminosilicate melt and coexisting aluminosilicate-saturated aqueous fluid determined in-situ to 800°C and ~800MPa*. Geochimica et Cosmochimica Acta, 2010. **74**(14): p. 4123-4139.
199. Loewenstein, W., *The Distribution of Aluminum in the Tetrahedra of Silicates and Aluminates*. American Mineralogist, 1954. **39**: p. 92-96.
200. Liu, Y., H. Nekvasil, and J. Tossel, *Explaining the effects of T-O-T Bond Angles on NMR Chemical Shifts in Aluminosilicates - A Natural Bonding Orbital (NBO) and Natural Chemical Shielding (NCS)* Journal of Physical Chemistry A, 2005. **109**: p. 3060-3066.
201. Navrotsky, A., et al., *The Tetrahedral Framework in Glass and Melts - Inferences from Molecular Orbital Calculations and Implications for Structure, Thermodynamics, and Physical Properties*. Physics and Chemistry of Minerals, 1985. **11**: p. 284-298.
202. Taylor, M. and G.E.J. Brown, *Structure of mineral glasses -II. The SiO₂-NaAlSiO₄ join*. Geochimica et Cosmochimica Acta, 1979. **43**: p. 1467-1473.
203. Okhotnikov, K., B. Stevansson, and M. Eden, *New interatomic potential parameters for molecular dynamics simulations of rare-earth (RE = La, Y, Lu, Sc) aluminosilicate glass structures: exploration of RE³⁺ field-strength effects*. Phys Chem Chem Phys, 2013. **15**(36): p. 15041-55.
204. Yuan, X. and A.N. Cormack, *Si-O-Si bond angle and torsion angle distribution in vitreous silica and sodium silicate glasses*. Journal of Non-Crystalline Solids, 2003. **319**(1-2): p. 31-43.
205. Romano, C., et al., *The viscosities of dry and anhydrous XAlSi₃O₈ (X = Li, Na, K, Ca_{0.5}, Mg_{0.5}) melts*. Chemical Geology, 2001. **174**: p. 115-132.
206. Du, L.-S. and J.F. Stebbins, *Network connectivity in aluminoborosilicate glasses: A high-resolution ¹¹B, ²⁷Al and ¹⁷O NMR study*. Journal of Non-Crystalline Solids, 2005. **351**(43-45): p. 3508-3520.
207. Balzer, R., et al., *Structural investigation on hydrous Phosphate Glasses* Phys. Chem. Glasses: Eur. J. Glass Sci. Technol. B, 2019. **60**(2): p. 49-61.

208. Behrens, H. and M. Nowak, *The mechanisms of water diffusion in polymerized silicate melts*. Contributions to Mineralogy and Petrology, 1997. **126**: p. 377-385.
209. Balzer, R., et al., *The influence of H₂O and SiO₂ on the structure of silicoborate glasses*. Journal of Non-Crystalline Solids, 2019. **519**.
210. Kiefer, P., et al., *Density, elastic constants and indentation hardness of hydrous soda-lime-silica glasses*. Journal of Non-Crystalline Solids, 2019. **521**.

Appendix

Curriculum Vitae

Personal Details

Robert Balzer
23.08.1987 in Forst, German citizenship

Work Experience

05/2015 – 05/2019	Research assistant Institut für Mineralogie, Leibniz Universität Hannover, Germany Student assistant, workgroup petrology
01/2011 – 04/2015	Institut für Mineralogie, Leibniz Universität Hannover, Germany Student assistant, workgroup crystallography
02/2009 – 07/2012	Institut für Mineralogie, Leibniz Universität Hannover, Germany

Education

01/2016 - today	PhD student Leibniz Universität Hannover, Germany Thesis: "Interaction of water with oxide glass structures"
10/2013 – 04/2015	Master's studies in Earthscience with focus in Mineralogy/Geochemistry Leibniz Universität Hannover Thesis: "Structural investigation on hydrous phosphate glasses"
10/2008 – 06/2013	Bachelor's studies in Earthscience Leibniz Universität Hannover Thesis: "Untersuchung der thermischen Eigenschaften von $\text{Bi}_2(\text{Al}_x\text{Fe}_{1-x})_4\text{O}_9$ -Verbindungen (Mullittyp) mittels Infrarot- und Raman-Spektroskopie"
08/2000 – 06/2008	Abitur Theodor-Heuss-Gymnasium, Wolfenbüttel, Germany

List of Publications

2019

Kiefer, P., **Balzer, R.**, Deubener J., Behrens, H., Waurischk, T., Reinsch, S., Müller, R. (2019): Density, elastic constants and indentation hardness of hydrous soda-lime-silica glasses, *Journal of Non-Crystalline Solids*, Vol. 521, pp. 119480

Balzer, R., Behrens, H., Schuth, S., Waurischk, T., Reinsch, S., Müller, R., Fechtelkord, M., Deubener, J. (2019): The influence of H₂O and SiO₂ on the structure of silicoborate glasses, *Journal of Non-Crystalline Solids*, Vol. 519, pp. 119454

Balzer, R., Behrens, H., Reinsch, S., Fechtelkord, M. (2019): Structural investigation of hydrous phosphate glasses, *Phys. Chem. Glasses: Eur. J. Glass Sci. Technol. B*, 2019, Vol. 60 (2), pp. 49-61

2018

Hughes, EC., Buse, B., Kearns, SL., Blundy, JD., Kilgour, G., Mader, HM., Brooker, RA, **Balzer, R.**, Botcharnikov, RE., Di Genova, D., Almeev, RR & Riker, JM, (2018): High spatial resolution analysis of the iron oxidation state in silicate glasses using the electron probe. *American Mineralogist*, Vol 103, pp. 1473-1486

Conference Abstracts

2018

Waurischk, T., **Balzer, R.**, Kiefer, P., Müller, R., Behrens, H., Deubener, J. (2018): The influence of volatile constituents on mechanical properties of glasses. Annual meeting of the Priority Project SPP1594, Jena, Germany

2017

Balzer, R., Welsch, Anna-Maria, Kiefer, P., Reinsch, S., Fechtelkord, M., Behrens, H. (2017): The effect of water on the structure of phosphate glasses. International Conference on Phosphate Glasses, Crystals and Melts, Oxford, UK

Balzer, R., Welsch, Anna-Maria, Bauer, U., Behrens, H., Fechtelkord, M. (2017): Structural investigation on hydrous phosphate glasses. 12th Pacific Rim Conference on Ceramic and Glass Technology, Hilo, Big Island Hawaii

Kiefer, P., **Balzer, R.**, Bauer, U., Behrens, H., Waurisch, T., Müller, R., Reinsch, S., Deubener, J.: Viscosity of water bearing glasses in the glass transition range – phosphates vs. silicates and borates. 91. Glastechnische Tagung der DGG, Weimar, Germany

Waurisch, T., **Balzer, R.**, Kiefer, P., Reinsch, S., Behrens, H., Deubener, J.: New devices for inert sub-critical crack growth: measurements in crystallized glasses. 91. Glastechnische Tagung der DGG, Weimar, Germany